Title
The Breathing of Halogenated Volatile Organic Compounds (HVOCs) from Human-impacted Ecosystems

Author
Jiao, Yi

Publication Date
2021

Peer reviewed|Thesis/dissertation

The Breathing of Halogenated Volatile Organic Compounds (HVOCs) from Human-impacted Ecosystems

by

Yi Jiao

A dissertation submitted in partial satisfaction of the
requirements for the degree of
Doctor of Philosophy
in
Geography
in the
Graduate Division
of the
University of California, Berkeley

Committee in charge:

Professor Robert C. Rhew, Chair
Professor Dennis D. Baldocchi
Professor John C. H. Chiang
Professor Allen H. Goldstein

Spring 2021

The Breathing of Halogenated Volatile Organic Compounds (HVOCs) from Human-impacted Ecosystems

by

Yi Jiao

Abstract

The Breathing of Halogenated Volatile Organic Compounds (HVOCs) from Human-impacted Ecosystems

by

Yi Jiao

Doctor of Philosophy in Geography

University of California, Berkeley

Professor Robert C. Rhew, Chair

Atmospheric methyl chloride (CH_3Cl) and methyl bromide (CH_3Br) are the largest natural gaseous carriers of reactive chlorine and bromine, which contribute to stratospheric ozone depletion. Chloroform ($CHCl_3$) also contributes to total stratospheric chlorine load and ozone destruction, with a much smaller impact. This dissertation investigates and quantifies emissions of these halogenated volatile organic compounds (HVOCs) from some natural ecosystems impacted by human activities.

Chapter two describes a study on HVOCs flux measurements at an intermediate zone of coastal ecosystems in South Carolina, which are subject to seawater intrusion induced by storm surges combined with sea level rise. The degraded forested wetland showed significant $CHCl_3$ emission rates and remained a net CH_3Cl sink and a negligible CH_3Br source/sink, unlike the saltmarsh which was a significant source for both. This study suggested that sea level rise and frequent storm surges derived from global climate change, in the long term, may increase $CHCl_3$ emissions from coastal degraded forested wetlands and of methyl halides if salt marshes expand, with potential impacts for stratospheric ozone depletion.

Chapter three describes a project that measured life-cycle fluxes of CH_3Cl, CH_3Br and CH_3I from rapeseed (*Brassica napus* "Empire"). The results showed that rapeseed emitted 5.3 ± 1.3 Gg CH_3Cl $year^{-1}$, 2.8 ± 0.7 Gg CH_3Br $year^{-1}$, and 4.0 ± 0.8 Gg CH_3I $year^{-1}$ as of 2018. Assuming the future global rapeseed production follows the same rate of increase as the past 60 years, the atmospheric sources of CH_3Cl, CH_3Br and CH_3I may

increase to 13.1 Gg $year^{-1}$, 7.0 Gg $year^{-1}$, and 9.8 Gg $year^{-1}$, respectively by 2050, becoming an ever-larger global source.

Chapter four describes a study which showed that $CuSO_4$, in conjunction with either hydrogen peroxide (H_2O_2) or solar radiation, significantly enhanced CH_3Cl and CH_3Br production from organic matter in soil or seawater. This study identified a new abiotic pathway of methyl halide production occurring in agricultural fields and water bodies facilitated by the widespread application of Cu (II) based pesticides, herbicides and fungicides. A rough quantification suggested this mechanism had the potential to account for a significant part of the missing sources of CH_3Cl and CH_3Br.

These aforementioned studies highlight the increasing contribution from natural sources of ozone depleting substances (ODSs) influenced by human activities, which may offset some of the ODSs reductions achieved by the Montreal Protocol.

To my parents

焦丙同&才颖英

TABLE OF CONTENTS

LIST OF FIGURES

LIST OF TABLES

LIST OF PEER-REVIEWED PUBLICATIONS

Jiao, Y., Zhang, W., Kim, J. Y., Deventer, M. J., Vollering, J., & Rhew, R. C. (2021). Copper-mediated production of CH_3Cl and CH_3Br from organic matter in soil and seawater. ***Under review***.

Jiao, Y., Acdan, J., Xu, R., Deventer, M. J., Zhang, W., & Rhew, R. C. (2020). Global methyl halide emissions from rapeseed (*Brassica napus*) using life cycle measurements. *Geophysical Research Letters*, 47 (19), e2020GL089373. DOI: 10.1029/2020GL089373

Jiao, Y., Rücker, A., Deventer, M. J., Chow, A. T., & Rhew, R. C. (2018). Halocarbon emissions from a degraded forested wetland in coastal South Carolina impacted by sea level rise. *ACS Earth & Space Chemistry*, 2 (10), 955-967. DOI: 10.1021/acsearthspacechem.8b00044

Zhang, W.[=], Jiao, Y.[=], Zhu, R., Rhew, R. C., Sun, B., and Dai, H. (2021). Biogenic chloroform ($CHCl_3$) emission from coastal Antarctic tundra enhanced by the coupling of penguin activities and climate change. ***Under review***.

Zhang, W., Jiao, Y., Zhu, R., & Rhew, R. C. (2020). Methyl chloride and methyl bromide production and consumption in coastal Antarctic tundra soils subject to sea animal activities. *Environmental Science & Technology*, 54 (20), 13354-1336. DOI: 10.1021/acs.est.0c04257

Deventer, M. J., Jiao, Y., Knox, S. H., Anderson, F., Ferner, M. C., Lewis, J. A., & Rhew, R. C. (2018), Ecosystem scale measurements of methyl halide fluxes from a brackish tidal marsh invaded with perennial pepperweed (*Lepidium latifolium*). *Journal of Geophysical Research: Biogeosciences*, 123, 2104-2120. DOI: 10.1029/2018JG004536

Wang, J. J., Jiao, Y., Rhew, R. C., & Chow, A. T. (2016). Haloform formation in coastal wetlands along a salinity gradient at South Carolina, United States. *Environmental Chemistry*, 13 (4), 745-756. DOI: 10.1071/EN15145

ACKNOWLEDGEMENTS

I would like to express the foremost gratitude to my Ph.D. supervisor, Professor Robert C. Rhew, for his consistent support and gracious shepherding throughout my graduate study, intellectually and mentally. His decision to admit me to his group many years ago has literally changed my life. His wise foresight and rigorous approach to scholarly research is contagious and has shaped my understanding of science, my way of conducting research.

Many thanks go to my excellent committee on qualifying examination and dissertation, which include (in alphabetical order by last names) Professors Dennis D. Baldocchi, John C. H. Chiang, and Allen H. Goldstein, for their insightful ideas, inspiration and guidance.

I am indebted to Dr. Malte Julian Deventer, who has helped me a lot during my graduate study, such as mentoring me on preparing conference presentations and manuscripts, hands-on tutorials on the relaxed eddy accumulation method and MATLAB coding skills.

Of the many professors and colleagues who have assisted me in laboratory and field work, presentations and publications, and curriculum teaching, I would like to thank Prof. Alex T. Chow, Dr. Alexander Rücker, Prof. Jun-Jian Justin Wang, Hunter Robinson (Clemson University); Prof. Renbin Zhu, Dr. Wanying Zhang (University of Science and Technology of China); Dr. Wenwen Kong, Prof. Kurt M. Cuffey, Prof. Laurel G. Larsen, Prof. Jeffery Q. Chambers (Berkeley Geography); Prof. Timothy M. Bowles (Berkeley ESPM); Dr. Rong Yu (University of Wisconsin-Milwaukee); and Dr. Dennis Zellmann (TU Braunschweig).

The Rhew group has hosted many undergraduate researchers, who have also contributed to my research and are hereby earnestly appreciated. They are Janna Abad, Jerrold Acdan, Andrew Beecher, Ryan Bowers, Rory French, Phoebe Gross, Jae Yun Robin Kim, Bernard Koh, Charles Li, Anya Mikheicheva, Sanjeevi Nagalingam, Metta Nicholson, Celine Payne, Sancialita Sathiyamoorthy, Steve Shen, Kai Kristy Sheng, Connor Shingai, Parker Stow, Yujia Tao, Julien Vollering, Ross Ward, Jiaxuan Flora Xu, Rong Xu, and many others.

I also would like to thank the friendly staff members for their help on administrative affairs, IT support, lab safety management and research facility access, which include Eron Budi, Marjorie A. Ensor, Bobby Ewing, Joshua Mandel, Daniel S. Plumlee, Sarah Varner, Natalia Vonnegut (Berkeley Geography); Christina M. Wistrom (Oxford Tract); and Jeff Brown, Faerthen Felix (Sagehen Creek Field Station).

Last but not least, exceedingly gratitude goes to my parents, who are my lifetime unconditional inexhaustible sources of love and support, especially during the period of this difficult and labyrinthine endeavor.

Specifically, the text of chapter two, in full, has been peer-reviewed and published in *ACS Earth and Space Chemistry* (DOI: 10.1021/acsearthspacechem.8b00044), with contributions from co-authors Alexander Rücker, Malte Julian Deventer, Alex T. Chow, and Robert C. Rhew. The co-authors and I would like to thank the National Science Foundation (EAR-1529927; EAR-1530375) for financial support for this publication. We are also grateful to Samuel Lin, Wenchen Liu for assistance on the access to the field, Junjian Wang, Dennis Zellmann, David Miller and Hunter Robinson for the assistance on fieldwork, and Jerrold Acdan, Rory French, Bernard Koh, Anya Mikheicheva and Connor Shingai for assistance on laboratory analysis. This part incorporated the constructive comments from three anonymous reviewers.

The text of chapter three, in full, has been peer-reviewed and published in *Geophysical Research Letters* (DOI: 10.1029/2020GL089373), with contributions from co-authors Jerrold Acdan, Rong Xu, Malte Julian Deventer, Wanying Zhang and Robert C. Rhew. We would like to thank the National Science Foundation (ATM-1258365) for financial support; the Brassica breeding and research group at the University of Idaho for providing the canola seeds; Christina M. Wistrom for coordinating field work at the Oxford Tract; Wenchen Liu, Yujia Tao and Connor Shingai for assistance on sampling; Bernard Koh, Anya Mikheicheva and Ross Ward for GC/MS measurements; Dennis Zellmann for producing rapeseed drawings. This part incorporated the constructive comments from two anonymous reviewers.

The text of chapter four, in full, has just been submitted to a journal for peer-review, with contributions from co-authors Wanying Zhang, Robin Kim, Malte Julian Deventer, Jullien Vollering, and Robert C. Rhew. This work was funded by the Natural Science Foundation (EAR-1530375). The coauthors and I are grateful to Andrew Beecher and Flora Xu for assistance with soil sample preparation and some of the GC/MS analysis; Christina M. Wistrom for coordinating field work at the Oxford Tract, Professors Garrison Sposito and Timothy M. Bowles for information and discussion. I would also like to thank the Carol Baird Award from the University of California Natural Reserves for financial support.

Post note: I started my Ph.D. program when atmospheric CO_2 at Mauna Loa was 397 ppm (https://twitter.com/Keeling_curve/status/501039882731417601); by the time I file this dissertation to complete my Ph.D. program, it has increased to 418 ppm (https://twitter.com/Keeling_curve/status/1385681537828458496).

Chapter 1. Natural sources of halogenated volatile organic carbons (HVOCs) influenced by human activities

1.1 Stratospheric ozone depletion and current challenges

In the 1970s, atmospheric chemists first predicted the potential effects of chlorofluorocarbons (CFCs) for causing destruction on the stratospheric ozone layer (Cicerone et al., 1974; Donahue et al., 1976; Molina & Rowland, 1974; Rowland, 1996; Stolarski & Cicerone, 1974). However, global production of CFCs continued to grow rapidly as new uses were found for these chemicals in refrigeration and fire suppression. (Howard & Hanchett, 1975). Since the 1980s, the ozone hole over Antarctica has been observed every austral spring (Farman et al., 1985; Solomon, 1988; Solomon et al., 1986). The depletion of the stratospheric ozone layer has raised worldwide concern and interest from scientists, the public and policymakers because stratospheric ozone protects life on Earth's surface from biologically damaging ultraviolet radiation. The scientific and political communities worked together to create and then ratify *The Montreal Protocol on Substances That Deplete the Ozone Layer* in 1987 following the 1985 Vienna Convention for the Protection of the Ozone Layer.

The Montreal Protocol, first signed in 1987 and ratified by 198 countries so far, aims to protect the stratospheric ozone layer by phasing out the production and consumption of substances that are responsible for ozone depletion, such as CFCs, halons, and other chlorine- or bromine-containing compounds. It is considered by many the most successful environmental global action by far. Ronald Reagan, the 40th president of the United States, appraised it as "a model of cooperation" and "a monumental achievement".

The Global Monitoring Laboratory of the National Oceanic & Atmospheric Administration (NOAA) reported that atmospheric concentrations of CFC-11 (CCl_3F), CFC-12 (CCl_2F_2), methyl chloroform (CH_3CCl_3), carbon tetrachloride (CCl_4), and CH_3Br and their contributions to stratospheric halogen radicals have declined steadily since the late 1990s due to the phasing out the anthropogenic halocarbons as mandated by the Montreal Protocol (Figure 1.1).

As a consequence, the beginning of the ozone layer recovery has been observed in the upper stratosphere since the first decade of the 21st century (Kuttippurath et al., 2018; Newchurch et al., 2003; Solomon et al., 2016; Strahan et al., 2019; Yang et al., 2008). Assuming the compliance with the controls in the Montreal Protocol continues in the coming decades, stratospheric ozone is projected to return to 1980 levels around the years 2040-2060 (Dhomse et al., 2018; Oman et al., 2010). However, while the long-term ozone layer recovery from the ozone-depleting substances (ODSs) phase-out is predicted to be underway, it still faces some obstacles in the coming decades that could affect the extent

and timing of ozone recovery. For example, during the austral spring of 2020 (September-October), NASA observed a peak ozone hole area of 23 million km^2, almost the same size as North America, and almost the same level as in 1993-1994 (Figure 1.2).

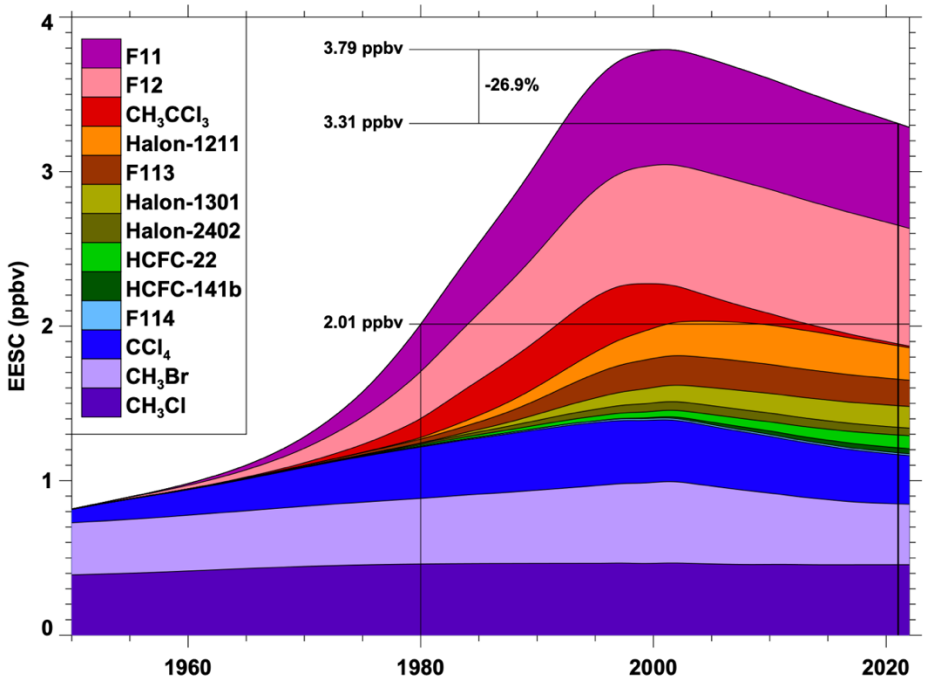

Figure 1.1 The contributions of various halogen source gases to the total EESC. Equivalent effective stratospheric chlorine (EESC) is a convenient parameter to estimate the amount of stratospheric ozone depletion due to these chlorine- or bromine- containing compounds. The units of EESC are in parts per billion by volume (ppbv). This figure was from https://ozonewatch.gsfc.nasa.gov/.

The variability of stratospheric ozone and its recovery is subject to several factors, such as the development of polar stratospheric clouds (PSCs) and the polar vortex which are influenced by meteorological variability, long term climate change, atmospheric dynamical variability and solar proton events (SPEs) (Chipperfield et al., 2017; Stone et al., 2018). In addition, there are at least three possible challenges with regard to ODS emissions, which could delay the return of stratospheric ozone levels to historical values by up to decades (Chipperfield et al., 2020; Fang et al., 2019; Liang et al., 2017).

1.1.1 Emissions of short-lived ODSs, such as $CHCl_3$

The typical transport time scale from the troposphere to the stratosphere is longer than 0.5 years. Therefore, halogenated compounds of tropospheric lifetime less than 0.5 years, categorized as very short-lived halogenated substances (VSLSs), are less likely to

get into the stratosphere to contribute to ozone depletion (Carpenter et al., 2014; Engel et al., 2018). VSLSs, such as chloroform ($CHCl_3$), dichloromethane (CH_2Cl_2), bromoform ($CHBr_3$), are not regulated by the Montreal Protocol.

However, concern has been raised as the atmospheric concentrations of $CHCl_3$ and CH_2Cl_2 have been increasing steadily in the past 1-2 decades (Fang et al., 2019; Hossaini et al., 2015, 2017; Oram et al., 2017). For example, observations showed $CHCl_3$ atmospheric molar fractions have been steadily increasing at a rate of 2.6-6.3% each year over the past decade, which is likely attributable to industrial activities (Engel et al., 2018; Fang et al., 2019). Numerical model simulations also indicate that these increasing VSLSs can influence ozone destruction in the lower stratosphere, and the recovery of stratospheric ozone may be significantly delayed if atmospheric concentrations of VSLSs, including $CHCl_3$, continue to grow (Claxton et al., 2019; Fernandez et al., 2017).

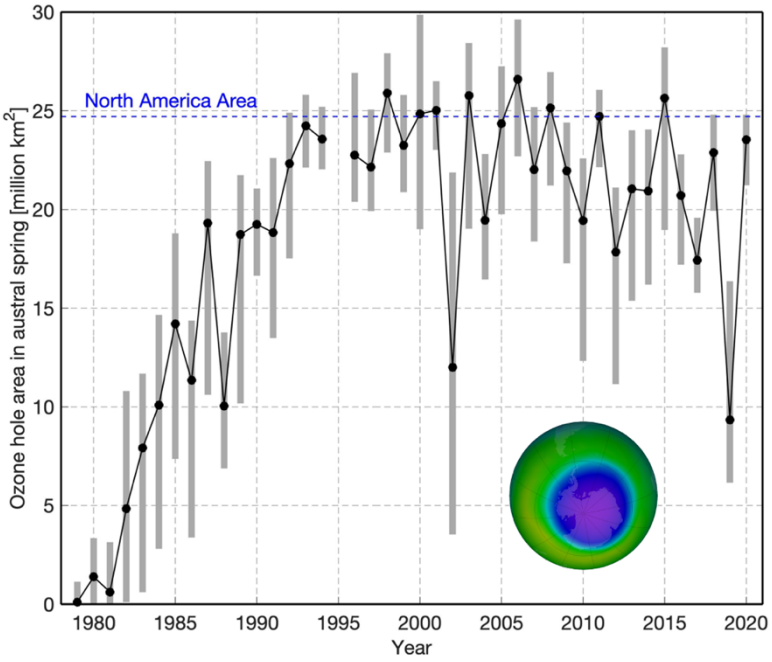

Figure 1.2 The ozone hole area over Antarctica in early austral spring season (7th September – 13th October) from 1979 to 2020. The ozone hole area is determined from total ozone satellite measurements and is defined to be that region of ozone values below 220 Dobson Units (DU) located south of 40°S. The inserted ozone map is the monthly-averaged total ozone over the Antarctic pole in October 2020; the blue and purple colors are where there is the least ozone, and the yellows and reds are where there is more ozone. The data and the inserted map were retrieved from the Ozone Watch website of the National Aeronautics and Space Administration.

1.1.2 Potential emission increases in natural ODSs, such as methyl halides, induced by anthropogenic activities

Methyl chloride (CH_3Cl) and methyl bromide (CH_3Br) are the largest natural gaseous carriers of chlorine and bromine, contributing to the reactive chlorine and bromine burden and halogen radical driven ozone destruction in the stratosphere (Carpenter et al., 2014; Engel et al., 2018). However, current estimates of CH_3Cl and CH_3Br sources cannot be balanced by their sinks, with discrepancies at about -430 Gg year^{-1} and -43 Gg year^{-1}, respectively (Table 1.1). Though part of the imbalance may be attributed to the uncertainties associated with the quantification of these sources and sinks, it still indicated the existence of missing sources and/or underestimation on some current sources. Some natural sources are increasing, induced by global warming or anthropogenic activities, such as land use change, which may offset some of gains introduced by the Montreal Protocol (Andreae & Merlet, 2001; Jiao et al., 2020; Westerling et al., 2006). Therefore, periodic re-quantification of these evolving sources of methyl halide may be needed.

1.1.3 Noncompliant emissions of controlled anthropogenic ODSs such as CFC-11, CCl_4.

As mandated by the Montreal Protocol, all contracting parties should have phased out the production and consumption of CFCs, e. g., CFC-11, CFC-12, CFC-113 (Cl_2FC-CF_2Cl), CFC-114 (ClF_2C-CF_2Cl) and CFC-115 (F_3C-CF_2Cl), commencing on January 1, 2010 (for non-article 5 countries, this date was on January 1, 1996), with exemptions for only a few essential uses. However, studies have reported slowdown in the diminishing of atmospheric CFC-11 and increase in the hemispheric differences since 2012, indicating an increase in CFC-11 emissions likely coming from unreported industrial production (Montzka et al., 2018; Rigby et al., 2019). Though recent studies in 2021 found that the noncompliant emissions of CFC-11 were declining in 2018-2019, before the economic slowdown due to the COVID-19 pandemic (Montzka et al., 2021; Park et al., 2021), this observed fugitive emission probably meant much more CFC-11 may be evaporated into the atmosphere eventually (up to six times larger than the observed increase) if the noncompliant production was for closed-cell foam use, a long-term CFC-11 reservoir. Such an increase of CFC-11 emissions would delay the restoration of the stratospheric ozone layer, although there are large uncertainties in the extent and time of this potential CFC-11 leak (Dhomse et al., 2019).

Dispersive use of CCl_4 has the same phasing-out timeline as CFCs' as scheduled by the Montreal Protocol. Nevertheless, in addition to the fugitive emission derived from legal feedstock usage of CCl_4 (2 Gg year^{-1}, Engel et al., 2018), non-compliant production and emissions of CCl_4 also exist across the globe at a rate of ~13 Gg year^{-1} (Liang et al., 2016; Sherry et al., 2018). For example, CCl_4 emissions were inferred at 2.2 ± 0.8 Gg year^{-1} from Europe (Graziosi et al., 2016), 4 (2.0-6.5) Gg year^{-1} from the United States (Hu et al., 2016)

and 4-24 Gg year^{-1} from Eastern Asia, especially China (Bie et al., 2017; Lunt et al., 2018; Park et al., 2018).

All these noncompliant industrial sources of ODSs, together with newly discovered anthropogenic emissions of some CFC/HCFC species (Laube et al., 2014; Vollmer et al., 2021), contributed to the stratospheric chlorine/bromine load and induced potential delay in stratospheric ozone recovery.

1.2 Current understanding on some natural halocarbons

1.2.1 Chloroform ($CHCl_3$)

$CHCl_3$ is the second largest natural carrier of chlorine in the atmosphere. Natural sources of $CHCl_3$ are believed to predominate, and account for 50-90% of its global emissions (McCulloch, 2003; Worton et al., 2006). AGAGE measurements show stable global mean mole fractions of $CHCl_3$ in the range of 7.3–7.7 ppt with a stable inter-hemispheric difference (IHD, 4.3 ppt) over 1997–2010 (Figure 1.3), suggesting that atmospheric $CHCl_3$ was dominated by natural sources during this period. It is noted, however, as discussed above, this stable period was followed by a subsequent increase in both atmospheric molar fractions and IHD (6.3 ppt as of 2016) of $CHCl_3$ since 2010, suggesting an increase in Northern Hemisphere anthropogenic emissions in the past decade.

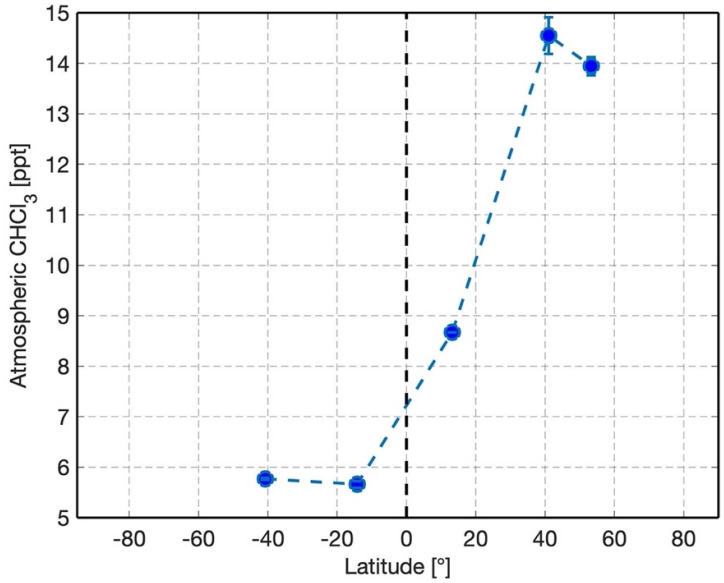

Figure 1.3 Latitudinal profile of atmospheric $CHCl_3$ molar fraction in 2018. Each data point represents the annual averaged $CHCl_3$ molar fraction and the error bars represent the standard deviation of the annual molar fractions. Positive latitude values represent Northern Hemisphere latitudes, negative latitude values represent

Southern Hemisphere latitudes. The raw data was retrieved from the database of the Advanced Global Atmospheric Gases Experiment (AGAGE).

Natural emissions of $CHCl_3$ are mainly from the surface ocean (~360 Gg year^{-1}) and terrestrial soils (over 200 Gg year^{-1}), such as peatland (Dimmer et al., 2001; Khan et al., 2012), tundra (Johnsen et al., 2016; Macdonald et al., 2020; Rhew et al., 2008b), forest (Albers et al., 2011; Haselmann et al., 2002; Haselmann et al., 2000), rice fields (Khalil et al., 1998; Khan et al., 2011), salt marsh (Wang et al., 2016; Rhew et al., 2008a) and wetland (Jiao et al., 2018). Various $CHCl_3$ flux measurements have been reported from multiple different ecosystems (Rhew et al., 2008a, 2008b; Cox et al., 2004; Hoekstra et al., 1995, 1998, 2001; Khalil et al., 1990, 1998) and the results showed large spatial and temporal variabilities within the same ecosystem. Different $CHCl_3$ production mechanism assumptions have been explored regarding biotic *vs*. abiotic, irradiation induced *vs*. temperature controlled. However, no uniform production mechanism has been proposed to apply to all circumstances.

1.2.2 Methyl chloride (CH_3Cl) and methyl bromide (CH_3Br)

Methyl chloride (CH_3Cl) and methyl bromide (CH_3Br) are the largest natural gaseous carriers of chlorine and bromine, contributing to the reactive chlorine and bromine burden and ozone destruction in the stratosphere (Carpenter et al., 2014; Engel et al., 2018). CH_3Br was once produced anthropogenically and mainly used as to fumigate soil in agriculture, with a minor fraction used for the manufacture of other chemical products. However, anthropogenic application of CH_3Br has been largely curtailed by the Montreal Protocol. Currently, CH_3Br production is exempted only for critical use, namely quarantine and pre-shipment (QPS) fumigation for pest control for the transport of agricultural products (Carpenter et al., 2014; Engel et al., 2018). Since the implementation of the Montreal Protocol, controlled CH_3Br consumption dropped to about 1% of the peak value (0.94 Gg year^{-1} as of 2016), and total reported fumigation emissions have declined by more than 85% since their peak in 1997 (8.4 Gg year^{-1} as of 2016). At present, both CH_3Cl and CH_3Br are mainly from natural sources (Table 1.1).

The latitudinal profile of atmospheric CH_3Cl and CH_3Br molar fractions (Figure 1.4) indicates the different distributions of CH_3Cl and CH_3Br sources. Peak CH_3Cl concentrations are typically observed around the tropical region, suggesting the primary sources are tropical/subtropical ecosystems; while the peak CH_3Br concentrations are around 30-50 °N, indicating large CH_3Br sources exist in mid-latitudes in the northern hemisphere.

Currently, the significant CH_3Cl sources includes tropical and subtropical plants (Bahlmann et al., 2019; Blei et al., 2010; Gebhardt et al., 2008; Lee-Taylor et al., 2001; Saito et al., 2008; Xiao et al., 2010; Yokouchi et al., 2002; Yoshida et al., 2004), biomass

burning (Andreae & Merlet, 2001; Carpenter et al., 2014), the ocean (Hu, 2012; Hu et al., 2013), salt marshes (Deventer et al., 2018; Drewer et al., 2006; Manley et al., 2006; Rhew et al., 2014; 2000), and fungi (Lee-Taylor et al., 2001; Watling & Harper, 1998); significant CH_3Br sources includes ocean (Hu, 2012), biomass burning (Andreae & Merlet, 2001; Carpenter et al., 2014), salt marshes (Deventer et al., 2018; Drewer et al., 2006; Manley et al., 2006; Rhew et al., 2014; 2000), rapeseed (Gan et al., 1998; Jiao et al., 2020; Mead et al., 2008).

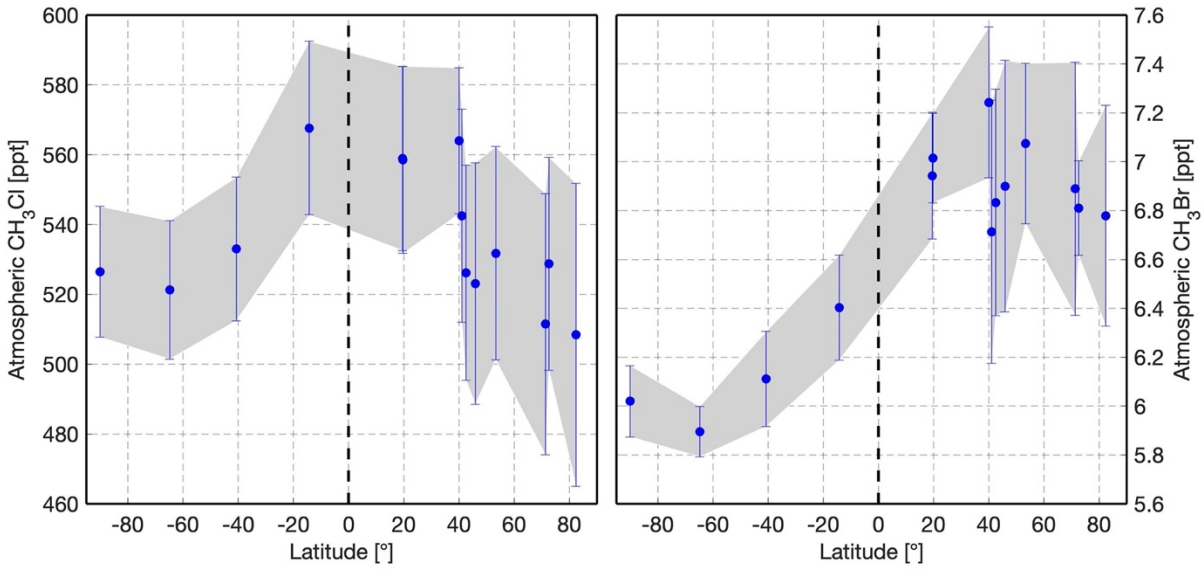

Figure 1.4 Latitudinal profile of atmospheric CH_3Cl and CH_3Br molar fractions in 2019. Each data point represents the annual averaged CH_3Cl or CH_3Br molar fractions and the error bars represent the standard deviation of the annual molar fractions. Positive latitude values represent Northern Hemisphere latitudes, negative latitude values represent Southern Hemisphere latitudes. The raw data was retrieved from the database of the Halocarbons and other Atmospheric Trace Species group, which is under the Global Monitoring Division, Earth System Research Laboratory, National Oceanic and Atmospheric Administration.

1.2.3 Production mechanism of CH_3Cl, CH_3Br and $CHCl_3$

Biogenic formation of CH_3Cl and CH_3Br is from the methylation of halide ions catalyzed by methyltransferases with S-adenosyl-methionine (SAM) serving as a methyl donor (Attieh et al., 1995; Rhew et al., 2003; Saini et al., 1995). CH_3Cl and CH_3Br (and CH_3I) can also be produced in soil or sediment abiotically from the alkalization of halide ions when iron (III) oxidizes the organic matter (Keppler et al., 2000; 2003), in which microbes and sunlight are not required. During the senescence period of plant or biomass burning, pectin can act as a methyl donor to produce large amounts of CH_3Cl, CH_3Br (and

CH_3I) abiotically, a process that is sensitive to temperature (Hamilton et al., 2003; Wishkerman et al., 2008).

Natural $CHCl_3$ can be produced both biotically and abiotically. Biotically, chloroperoxidases (CPOs) excreted from soil microbes can produce hypochlorous acid (HOCl) to chlorinate organic substrates (e.g., humic and fulvic acids), which can then be cleaved to form $CHCl_3$ (Albers et al., 2011; Breider & Hunkeler, 2014b; Ruecker et al., 2014). $CHCl_3$ can also be produced from terrestrial environments when organic matter is oxidized by iron (III) and hydrogen peroxide (H_2O_2) in the presence of chloride ions (Huber et al., 2009).

1.3 Structure of the studies described in the dissertation

I designed and conducted three independent case studies, generally focusing on (1) measurements of $CHCl_3$ fluxes from a degraded wetland in South Carolina, along a salinity gradient, subject to the seawater intrusion induced by sea level rise and storm surges; then quantifying the $CHCl_3$ contributions from degraded wetlands globally to figure out if it is a hotspot of $CHCl_3$ emission; (2) re-quantification of methyl halide emissions with respect to rapeseed (*Brassica napus*), a substantial and ever-growing source due to the expansion of cultivation area, production and yield globally; constructing the relationships of fluxes to the environmental factors driving them and evaluating the global impacts, and (3) laboratory-based incubations to explore the possibility of copper-mediated production mechanisms of methyl halides in human-impacted ecosystems, such as agricultural fields and water bodies.

Chapter two addresses the questions: Are $CHCl_3$ emission rates significantly enhanced when forested wetlands become degraded? How do the $CHCl_3$ emission rates from forested wetlands compare to different terrestrial ecosystems? How big is its overall contribution to atmospheric $CHCl_3$ budgets? What is the mechanism and controlling factors on $CHCl_3$ formation in natural ecosystems?

Chapter three addresses the questions: What is the integrated life-cycle flux of methyl halides from rapeseed *(B. napus)*? Considering the expansion of *B. napus* cultivation area and yield globally, how large is the contribution of *B. napus* to atmospheric methyl halides nowadays and in the future?

Chapter four addresses the questions: Will copper (II) catalyze the production of methyl halides in soils or seawater in a similar manner as iron (III)? Does this production mechanism require oxidizing agents or sunlight? Considering the large application of copper-based pesticides, fungicides and herbicides in global agriculture every year, how big is its contribution to global methyl halide budgets?

Table 1.1 Current identified and quantified budgets of methyl chloride (CH_3Cl), methyl bromide (CH_3Br) and methyl iodide (CH_3I).

	Category	CH_3Cl [Gg year^{-1}]		CH_3Br [Gg year^{-1}]		CH_3I [Gg year^{-1}]	
Source	**Subtotal**	**3977.34**		**80.36**		**456.2**	
	*Leaded gasoline	n.q.		0.3			
	After 2012			0-3	j		
	In 1999			0.6	ag		
	In 1996			4.5 ± 3	ah		
	In 1995			1.5 (<3)	ai		
	*Industrial activity	525		n.q.			
	*coal combustion	162 (29-295)	a				
	*manufacturing industry	363 ± 85	b				
	*Fumigation	n.q.		9.34			
	QPS consumption	n.q.		8.4	aj, ak		
	non-QPS consumption	n.q.		0.94	aj, ak		
	Biomass burning	573		23		6.2	
	natural and *anthropogenic	650	c	29	c	14	c
	South America and Southern Africa	900 (700-1000)	d	(14-24)	d	1.6-4.1	d
	Ivory Coast	515 (226-904)	e				
	Southern Africa savanna fires	1100-1510	f	19-24	f	3.4-8	f
	biomass burning	934 ± 207	g				
	global burning	611 ± 38	h				
	biomass burning	640	i				
	*indoor biofuel	113 (56-169)	j	6 (3-9)	j		
	open field burning	355 (142-569)	j	17 (7-27)	j		
	(Sub-) tropical plants, leaf litter	1906.6		n.q.			
	tropical terrestrial psedobiogenic source	(2330-2430)	k				
	30°N - 30°S biogenic sources	(2430-2900)	h				
	tropical plants	2200 ± 390	g				
	tropical rainforest and leaf litters	1400	l				
	tropical forests	1300	m				
	tropical vegetation	1500 ± 600	n				
	tropical rainforest	670 ± 200	o				
	40°N - 40°S biogenic sources			25.6	al		
	Ocean	700		32		371.4	
	unidirectional gross emission	700 (510-910)	p			177-205	aw
	global ocean	510	h	32 (22-44)	j	127-353	ax

	ocean						1300	ay
	net flux (source - sink)		300-400	q			214	az
	open ocean						270	aag
	global ocean						800	aaf
	southern ocean						247-676	aaj
	global ocean						70-260	aak
	open ocean						298	aal
	global ocean						610	aal
	gross sea-to-air fluxes						176-206	aam
	global ocean						335.6	aan
	global ocean						150	aao
	global waters		4900	aap	300	aap	300-500	aap
	global ocean						303	aaq
	algae: *Prochlorococcus*						592.8	aah
	kelp: *Macrocystis pyrifera*		2	aas	0.1	aas	0.2	aas
	macroalgae						0.6	aat
	microbial degradation of kelp						300	aar
	global phytoplankton						1.2 (1-4)	aau
	Wood-rotting fungi	162.7		r	1.7(0.5-5.2)	am		
	Mid-latitude terrestrial biomes	n.q.			n.q.		33	aac
	Salt marsh	31			3			
	Northern California		31 (10-77)	s	3 (1-8)	s		
	Southern California		(65-440)	t	(7-29)	t		
	Texas		(30-90)	u	(3-9)	u		
	Southern California		49	v	8	v		
	Ria Formosa, Portugal		(2.3-4.5)	w	(0.5-1.0)	w	(0.6-1.2)	w
	salt marsh				7 (0.6-14)	an		
	coastal Scotland				1 (0.5–3)	ao		
	Wetland	48		x	4.6	x	7.3	z
	Mangroves	12		y	1.3	y	11	y
	Rapeseed (*B. napus*)	5.3			2.8		4.0	
	life-cycle measurements		5.3 ± 1.3	†	2.8 ± 0.7	†	4.0 ± 0.8	†
	modeling approximation		n.q.		5.12	ap	n.q.	
	incubation of juveniles		n.q.		6.6 ± 1.8	aq	n.q.	
	Peatland	5.5 (0.9-43.4)		z	0.9 (0.1-3.3)	z	1.4 (0-13)	z
	Rice paddies	3.65			0.7		22.5	
	chamber measurements		5.8	aa	1.3	aa	71	aa
	model approximation		(2.4-4.9)	ab	(0.5-0.9)	ab	(16-29)	ab
							20	av
Sinks	**Subtotal**	**4406**			**123**		**310**	
	Reactions	2832			56		310	
	with OH, Cl	3614 (3000-3564)		o				
	with OH	2832 (2470-3420)		j	56 (48-63)	j	< 2 %	aae
	with OH		3994 ± 42	h				
	photolysis						304	az
	photolysis						1650	aai
	Soil	1058			30			

	Soil	1058 (664-1482)	j	30 (19-41)	j		
	Soil	>1000	ac	32 (19-44)	an		
	Soil	250(200-1000)	o	42 ± 32	ar		
	forest/savanna	69	h				
	temperate forest/grassland	137	h	2.2 ± 0.9	as		
	temperate forest/grassland			69.6 ± 39.9	at		
	boreal forest	16	h				
	cultivated land	34	h	65.8 ± 29.2	at		
	shrubland	15 ± 6	ad	0.7 ± 0.2	ad		
	Arctic tundra	<11.2	ae, af	0.3	ae		
Ocean		370		33		0.01	
	ocean	370 (296-445)	j	33 (20-44)	j	0.01	aw
	unidirectional gross uptake	370 (300-430)	p	29-32	au	0.011-0.014	aam
	Stratosphere	146	j	4	j		
Imbalance		**-428.66**		**-42.64**		**146.2**	

***** denotes the anthropogenic sources. "n.q." means not quantified. "**✝**" refers to the study described in chapter 3 of this dissertation.

a - (Archie McCulloch et al., 1999), CH_3Cl source size estimation based on chlorine contents in coals, as well as national statistics of coal quantity and quality in power and heat generation, including industrial conversion, residential and commercial heating.

b - (Li et al., 2017), estimation on CH_3Cl budget with respect to manufacturing industries (including coal combustion, feedstocks, chemical production) by inter-species correlation method with high-frequency and high-precision *in situ* atmospheric CH_3Cl concentrations monitoring data.

c - (Andreae & Merlet, 2001), global extrapolation on methyl halide emissions with respect to both natural and anthropogenic biomass burning, including forest, biofuel, charcoal and agricultural residues, by emission ratios reported in literatures, which is obtained by simultaneous measurements of trace gases and reference gases (CO_2 or CO) in a fire plume.

d - (Blake et al., 1996), total biomass burning emission rates for savannas and worldwide were calculated for methyl halides by extrapolating with the ratios of methyl halides and CO_2 or CO in aircraft canister-sampling during the dry season (1992 September - October) biomass burnings in South America (eastern Brazil, 5°S and 15°S) and southern Africa (eastern side, 5°S and 25°S).

e - (Rudolph et al., 1995), CH_3Cl emission with respect to biomass burning was extrapolated by the measured ratio of CH_3Cl/CO_2 and/or CH_3Cl/CO in savanna fire plumes in Ivory Coast (6°13'N , 5°02'W) in February 1991.

f - (Andreae et al., 1996), methyl halides budgets with respect to biomass burning estimated by determining the ratio of methyl halides and CO_2 or CO from experimental savanna fires in South Africa (Kruger National Park) and Zambia during the 1992 fire seasons (August to October).

g - (Xiao et al., 2010), inverse-modeling of CH_3Cl sources/sinks with atmospheric CH_3Cl concentrations from high frequency in-situ observation networks (AGAGE, SOGE, NIES, and NOAA/ESRL HATS) and low frequency flask network (NOAA/ESRL HATS).

h - (Yoshida et al., 2004), modeling (GEOS-CHEM) approximation of CH_3Cl budgets with 7 surface sites observations and 9 aircraft field experiments with assimilated meteorology fields for 7 years.

i - (Lobert et al., 1999), biomass burning CH_3Cl budget was estimated by incorporating emission ratios relative to CO, CO_2 and the chlorine content of biomass burning fuel into carbon emission inventory.

j - (Carpenter et al., 2014)

k - (Lee-Taylor et al., 2001), modeling global CH_3Cl budget by incorporating know terrestrial and oceanic source/sink terms into a three-dimensional chemical transport model of the lower atmosphere (5° × 5° horizontal resolution plus 25 vertical σ-coordinate levels).

l - (Blei et al., 2010), extrapolation based on static-chamber measurements on branches (mainly *Dipterocarpaceae* family) and ground litters at the Danum Valley Field Station (4°58'N, 117°48'E, 400 m a.s.l.).

m - (Saito et al., 2008), extrapolation based on (i) vial enclosure of detached leaves (mainly *Dipterocarpaceae* family); (ii) canopy-scale flux estimated by vertical concentration gradient; at the Pasoh Forest Reserve (2°58'N, 102°18'E, 75-150 m a.s.l.).

n - (Gebhardt et al., 2008), CH_3Cl budget determined by large-scale approach with airborne measurements over the Atlantic Ocean and the pristine tropical rainforest in Suriname and French Guyana (3-6° N, 51-59° W, 1000 km scale).

o - (Bahlmann et al., 2019), modeling on tropical rainforest CH_3Cl budget by applying kinetic carbon isotope effects of various sources/sinks processes.

p - (Hu et al., 2013), approximation of CH_3Cl unidirectional gross emission and uptake rate from the sea globally by a CH_3Cl temperature and salinity dependent solubility function developed by lab experiments.

q - (Moore, 2000), estimation on global oceanic net flux of CH_3Cl by measuring the Henry's law constant for CH_3Cl.

r - (Watling & Harper, 1998), estimation on CH_3Cl budget with respect to wood-rotting fungi by taking into account woody tissue chlorine content, global abundance of CH_3Cl-releasing fungal species (mainly *Phellinus* and *Inonotus*) and the annual decomposed woody tissue mass. The estimation can be sub-grouped into temperate (38.7 Gg $year^{-1}$), tropical (115.2 Gg $year^{-1}$) and Australia (8.8 Gg $year^{-1}$).

s - (Deventer et al., 2018), extrapolation based on ecosystem-scale annual measurements by relaxed eddy accumulation and static-chamber measurements at a salt marsh (69% *Salicornia pacifica*, 12% *Lepidium latifolium*, 3% *Frankenia salina*) in northern California (38.02°N, 122.03°W).

t - (Rhew et al., 2000), extrapolation based on static-chamber measurements at salt marshes (peak emissions from *Salicornia* family, *Batis maritima*, and *Frankenia grandifolia*) at the Mission Bay marsh (32°47'N, 117°13'W) and the San Dieguito lagoon (32°58'N, 117°15'W).

u - (Rhew et al., 2014), extrapolation based on static-chamber measurements at salt marshes (species includes *Avicennia germinans*, *Batis maritima*, *Borrichia frutescens* and *Monanthochloe littoralis*) at coastal Texas (27°38'-27°52'N, 97°03'-97°12'), USA.

v - (Manley et al., 2006), estimation by biweekly incubation enclosure of a single plant species (including *Spartina foliosa*, *Salicornia virginica*, *Batis maritime* and *Frankenia grandifolia*) from the Upper Newport Bay, California (33°38.75N, 117°52.94W) over a 1-2 years period.

w - (Weinberg et al., 2015), methyl halide budgets estimation by conducting dynamic-chamber measurements at a coastal marsh (species dominated by *Zostera noltii* with some *Zostera Marina L.* and *Cymodocea nodosa*) in the vicinity of Faro, Portugal (37.0°N, 7.6°W) during summer and spring period.

x - (Varner et al., 1999), extrapolation by transparent chamber measurements at Sallie's fen (43°12.5'N, 71°03.5'W, species dominated by *Sphagnum* spp. and *Carex* spp.) and Angie's bog (43°26.2'N,71°10.4'W, species dominated by *Sphagnum* spp.) in NH, USA during the growing season.

y - (Manley et al., 2007), methyl halide budgets extrapolated from land area normalized fluxes which were derived from leaf area normalized fluxes measured by enclosing mangroves (*Avicennia germinans* and *Rhizophora mangle*) in greenhouse bin containers.

z - (Dimmer et al., 2001), extrapolation based on static-chamber measurements at seven peatlands (predominate species includes *Molinia caerulea*, *Carex panicea*, *Calluna vulgaris*, *Ulex europaeus*, *Erica cinerea*, *Myrica gale*, *Eriophorum angustifolium*, *Bryophytes* and *Phragmites australis*) in Ireland (53°19'N, 9°54'W).

aa - (Redeker et al., 2000), extrapolating by life-cycles static-chamber measurements at rice paddies in Maxwell, California (39°17'N; 122°07'W), and in Houston, Texas (29°46'N, 96°01'W).

ab - (Lee-Taylor & Redeker, 2005), modeling budget with raw data from Redeker et al (2000) by taking into account rice crop growing conditions, distribution and seasonality and conditions-dependent methyl halide fluxes from rice crops.

ac - (Keppler et al., 2005), budget calculation by conserving the mass balance of carbon isotopes in CH_3Cl with process-based isotopic fingerprint values and sources/sinks inventory data in the literature.

ad - (Rhew et al., 2001), extrapolation based on static-chamber measurements of coastal shrublands (predominated by *Artemisia californic*, *Carpobrotus eduli*, *Bromus diandrus*, *Avena fatua* and *Adenostoma fasciculatu*) and desert shrublands (predominated by *Larrea tridentat* and *Franseria dumosa*) at southern California, USA (32°52'-33°39'N, 116°22'-117°15'W).

ae - (Rhew et al., 2007), CH_3Cl and CH_3Br estimation based on static-chamber measurements of Arctic sedge tundra (predominate species includes *Carex aquatilis*, *Eriophorum russeolum*, *Eriophorum angustifolium*, *Dupontia fisheri*, and *Arctophila fulva*) at Alaska, USA (71°N, 157°W) during the growing season.

af - (Hardacre et al., 2009), extrapolation from static-chamber measurements at subarctic wetland (main plant species includes *Carex rostrata*, bryophytes, *Equisetum palustre*, sphagnum mosses, *Vaccinium* spp., *Betula nana*, *Empetrum nigrum*, *Andromeda polifolia*, *Eriophorum* spp., *Rubus chamaemorus*, lichens, bryophyte) in northern Sweden (68°28'N, 18°49'E) throughout the growing season.

ag - (Bertram & Kolowich, 2000), estimation by analyzing exhaust CH_3Br and fuel bromine concentrations in non-catalyst automobile experiments.

ah - (Chen et al., 1999), estimation based upon "air volume × CH_3Br enhancements in the whole air samples" collected in Santiago, Chile (33°21.6'-33°32.7'S , 70°31.8'-70°47.4'W).

ai - (Baker et al., 1998), estimation with CH_3Br/CO ratio from the roadside vehicle exhaust collected in UK and global CO emission budgets.

aj - (UNEP, 2017), data for quarantine and pre-shipment uses (QPS) methyl bromide and non-QPS consumption come from https://ozone.unep.org/countries/data.

ak - (Engel et al., 2018), emission factor for OPS methyl bromide is 84% and for non-QPS methyl bromide is 65%.

al - (Warwick et al., 2006), CH_3Br budgets estimated by a global three-dimensional chemical transport model testing with a base-line emission scenario and five further plausible scenarios.

am - (Lee-Taylor & Holland, 2000), estimation on CH_3Br budget from wood-rotting fungi by taking into account the information of global distribution and quantity of litter decay, litter bromine content, and the halide methylation rate by fungal species in the literature.

an - (Montzka et al., 2011)

ao - (Drewer et al., 2006), budget extrapolated by static-chamber measurements at a salt marsh (dominate species include *Aster tripolium*, *Festucarubra*, *Spergularia salina*, *Plantago maritime*, *Armeria maritima*) in coastal Scotland (56°00'N, 2°35'W) over a year.

ap - (Mead et al., 2008), extrapolation with raw data from Gan et al with 1960-2003 FAOSTAT data.

aq - (Gan et al., 1998), extrapolation with Manson jar incubations of juvenile rapeseed plants with 1998 FAOSTAT data.

ar - (Shorter et al., 1995), CH_3Br-dosed field enclosures at a mixed deciduous and conifer forest at Durham, NH, USA (43°08'N, 71°57'W).

as - (Varner et al., 2003), extrapolation with static chamber measurements at a temperate forest soil at College Woods, NH, USA (43°08'N, 71°57'W).

at - (Serça et al., 1998), extrapolation with static-chamber measurements at a bared agricultural site (Longmont, CO), a temperate forest site (Denver, CO), a grassland site (Boulder, CO) and a bog site.

au - (Lee-Taylor et al., 1998), global oceanic CH_3Br budget modeled by incorporating know source/sink terms into a three-dimensional chemical transport model of the lower atmosphere (5° × 5° horizontal resolution plus 25 vertical σ-coordinate levels).

av - (Muramatsu & Yoshida, 1995), extrapolated CH_3I budget with respect to rice was by enclosed bag measurements of CH_3I fluxes from the cultivated rice plants (*Oryza sativa cv. Nihonbare*) in the flooded soils over it life cycle.

aw - (Ziska et al., 2013), sea-to-air CH_3I budget was calculated from the global maps (1° × 1° resolution) of marine and atmospheric surface CH_3I concentrations with either raw data from the database or extrapolated with latitudinal and longitudinal dependent regression techniques.

ax - (Moore & Groszko, 1999), sea-to-air flux calculated based on the CH_3I concentrations in air samples, surface, and subsurface water samples collected at the cruise campaigns at the northwestern Atlantic (1995.07), northeastern Atlantic (1996.06), and Pacific Oceans (1995.10-11).

ay - (Rasmussen et al., 1982), oceanic CH_3I flux estimation based on sea-to-air two film model with more than 450 measurements of CH_3I concentrations in the air and in the seawater ranging from the arctic circle to the south pole.

az - (Bell et al., 2002), net oceanic CH_3I flux computed by the coupled ocean-atmosphere GEOG-CHEM model with parameters of mixed layer temperature, solar radiation flux at the surface, dissolved organic carbon and wind speed.

aac - (Sive et al., 2007), terrestrial CH_3I flux extrapolated from diurnal CH_3I profile at a field forest at North Carolina (35.58°N, 79.05°W).

aae - (Brown et al., 1990), atmospheric CH_3I partial lifetime with respect to OH was determined by measuring the reaction rates of CH_3I and OH within an apparatus over a wide temperature range of 271-423K.

aaf - (Reifenhäuser & Heumann, 1992), extrapolation by the two-film model of a gas-liquid interface with sea water and air samples collected at Antarctica Peninsula (60-67°S).

aag - (Liss & Slater, 1974), sea-to-air flux extrapolated by plugging both atmospheric and surface oceanic CH_3I concentrations (measured by the RRS Shackleton Royal research ship along the Atlantic Ocean from UK to Antarctica in 1971-1972) into the two-film model of a gas-liquid interface.

aah - (Smythe-Wright et al., 2006), global CH_3I flux with respect to *Prochlorococcus* was extrapolated on the equation Flux = $k(C_{water}-C_{air})$ with raw data collected by cruises from Spain to Greenland and around the Mascarene Plateau in the Indian Ocean and confirmed by laboratory culture experiments.

aai - (Cox et al., 2005), estimation of photolysis sink for CH_3I after Roehl et al (1997).

aaj - (Cohan et al., 2003), extrapolated based on the seasonally averaged fluxes from the Southern Ocean (40-50°S) estimated by a 3-layer ocean-air model with data from Cape Grim measurements.

aak - (Stemmler et al., 2014), air-sea fluxes (production rates, net emission/outgassing rates, and degradation rates) were approximated by running a ocean general circulation model coupled with a marine carbon cycle model in the scenarios of biological production only, photochemical production only and mixed productions.

aal - (Butler et al., 2007), global air-sea fluxes of CH_3I extrapolated by the measurements of CH_3I mixing ratios in both the surface seawater and the marine boundary layer collected by seven cruises in the Pacific and the Atlantic from 1994-2004.

aam - (Ziska et al., 2013), global sea-to-air fluxes calculated based on data-based high resolution estimated fluxes from surface observations within the HalOcAt database, which were interpolated into classified oceanic regions model.

aan - (Jones et al., 2010), total global CH_3I fluxes from the ocean extrapolated by simultaneous air and seawater measurements of CH_3I during two cruises in the Atlantic Ocean (16-36°N, 25-13°W; 53-58°N, 7-13°W) in 2006 and 2007.

aao - (Campos et al., 1996), global ocean CH_3I flux extrapolated based on CH_3I emission rates measured by cruise at the southern North Sea (~55°N, ~0-8°E, 1989.01-09), assuming it is globally homogeneous.

aap - (Singh et al., 1983), global oceanic methyl halide fluxes extrapolated by following the same air-sea two-layer model as Liss & Slater, 1974, (see aag.) with raw data from the samples collected at Point Arena, California (38°57'N, 123°44'W, 1979-1981), and the vessel (USCGC Polar Sea) from California to Chile (1981.12).

aaq - (Ordóñez et al., 2012), the emission rate came from the global chemistry-climate model CAM-Chem with raw inventory data mainly from Bell et al., 2002 (see *az*).

aar - (Manley & Dastoor, 1988), global CH_3I fluxes from microbial degradation of kelp extrapolated based on laboratory incubations of five axenic kelp-tissues and their microbial degradation.

aas - (Manley & Dastoor, 1987), estimated global methyl halide fluxes with respect to giant kelp assuming all kelps has the same methyl halide fluxes as those of *Macrocystis pyrifera*, which were measured by dark and light incubations of kelp blades.

aat - (Manley et al., 1992), global CH_3I production rates from marine macroalgae extrapolated from laboratory incubations of 11 species of marine macroalgae, such as *Pterocladia capillacea*, *Macrocystis pyrifera*, *Ulva sp*.

aau - (Manley & Cuesta, 1997), global phytoplankton CH_3I flux was extrapolated from measured CH_3I fluxes (normalized to phytoplankton and bacterial cell numbers) from unialgal incubations of 15 species (significant emitters includes *Phaeocystis sp.*, *Porosira glacialis*, *Navicula sp.*, *Nitzschia sp.*, *Nitzschia punctate*, *Thalassiosira pseudonana*.

Chapter 2. Halocarbon emissions from a degraded forested wetland in coastal South Carolina impacted by sea level rise

The material for this chapter was previously published as: Jiao, Y., Rücker, A., Deventer, M. J., Chow, A. T., & Rhew, R. C. (2018). Halocarbon emissions from a degraded forested wetland in coastal South Carolina impacted by sea level rise. *ACS Earth & Space Chemistry*, 2 (10), 955-967. DOI: 10.1021/acsearthspacechem.8b00044; and is adapted with permission from the American Chemical Society.

2.1 Abstract

Tropical and subtropical-storm surges combined with sea level rise cause saltwater intrusions into low-lying coastal ecosystems along the southeastern coast of the USA, gradually converting freshwater forested wetland into salt marsh. The transition zone between freshwater and saltwater ecosystems becomes a degraded forested wetland, where the combination of high levels of soil organic matter and elevated concentrations of halide ions creates a dynamic biogeochemical environment that may be a potential hotspot for halocarbon formation such as chloroform, methyl chloride and methyl bromide. This study conducted field measurements at a transition zone in coastal South Carolina to quantify halocarbon exchange rates, and laboratory soil incubations to determine the contributions of biotic versus abiotic processes. The degraded forested wetland showed significant chloroform emission rates (146 ± 129 nmol m^{-2} d^{-1}). The degraded forested wetland remained a net sink for methyl chloride and a negligible source/sink for methyl bromide, unlike the salt marsh which was a significant source for both. The laboratory incubations strongly suggest that methyl halide consumption in soils at the field site was biotic and that production of methyl halides and chloroform was largely abiotic and temperature-dependent, although additional experiments are required to rule out possible biotic production involving heat-resistant microbes. The results suggest that sea level rise and more frequent storm surges derived from global climate change, in the long term, may increase emissions of chloroform from coastal degraded forested wetlands and of methyl halides if salt marshes expand, with potential impacts for stratospheric ozone depletion.

2.2 Introduction

In the lower stratosphere, the photolysis of halocarbons from both anthropogenic and natural sources releases free chlorine and bromine radicals, catalyzing stratospheric ozone depletion. Following the Montreal Protocol in the 1980s, anthropogenic production and use of long-lived ozone depleting substances (ODSs) have been regulated, and hence

since 1997, atmospheric concentrations of these halocarbons have been declining (Carpenter et al., 2014; Elkins et al., 1993; Velders et al., 2007). However, non-controlled halocarbon emissions and emission variations associated with land use change (Mead et al., 2008), biomass burning (Ferek et al., 1998; Rudolph et al., 1995), seawater warming (Smythe-Wright et al., 2006; Yokouchi et al., 2001), and sea level rise (Wang et al., 2016) could offset some of the reductions achieved by regulatory efforts, highlighting the importance of further exploration of natural sources of ODSs.

Among the natural emitted halocarbons, methyl chloride (CH_3Cl), chloroform ($CHCl_3$) and methyl bromide (CH_3Br) are believed to be the first and second largest natural carrier of reactive chlorine (Clerbaux et al., 2007; Rhew et al., 2008a) and the largest natural carrier of reactive bromine (Butler, 2000) respectively. However, the known sources presently cannot balance the reported sinks for methyl halides (Carpenter et al., 2014), which suggests that either currently identified sources are underestimated or significant sources are missing. There is also a discrepency between identified sources and sinks for $CHCl_3$, with sources exceeding sinks 150-170 Gg each year (Cox et al., 2003; Keene et al., 1999). In order to close the gap in the global budgets of methyl halides and $CHCl_3$, a better mechanistic understanding of natural halogenation reactions and their contribution to the global budgets is needed. In particular, the contribution of abiotic and biotic reaction pathways to the overall halocarbon formations is still a matter of debate (Hamilton et al., 2003; Huber et al., 2009; Keppler et al., 2000; Leri et al., 2015; Rhew & Østergaard et al., 2003).

Soils are the second largest natural source for $CHCl_3$ after the ocean (Cox et al., 2003; Keene et al., 1999), and the second largest sink for methyl halides after the reaction with hydroxyl radical (·OH) (Carpenter et al., 2014). Most studies suggest that $CHCl_3$ formation in soils is mediated by haloperoxidases (HPOs) that oxidize halide ions with H_2O_2, but there is also evidence of abiotic $CHCl_3$ formation in soils (Hoekstra et al., 1998) which involves Fenton-like reaction conditions (Fe^{3+} and hydrogen peroxide), elevated halide content and soil organic matter with resorcin-like dihydroxylated compounds (Huber et al., 2009). The biotic pathway of methyl halide formation involves SAM (S-adenosyl-methionine) - dependent methyl transferases that are found widely in plants (Attieh et al., 1995; Ni & Hager, 1998, 1999; Rhew & Østergaard et al., 2003; Saini et al., 1995; Wuosmaa & Hager, 1990), especially those in the Subclass *Dilleniidae* (Gan et al., 1998; Rhew et al., 2002; Yokouchi et al., 2000). The abiotic formation of methyl halides within soils is believed to be related to Fenton-like reactions with organic matter and halide ions, although different from the mechanisms outlined for chloroform above (Keppler et al., 2000). The abiotic Fenton-like halogenation reactions are also believed to be responsible for sediment organohalogen formation (Leri et al., 2015). Thus, elevated halide content and soil organic matter content can stimulate both the biotic and abiotic pathways of halocarbon production.

Coastal wetlands in southeastern United States that undergo storm-induced seawater intrusion (storm surges) and sea level rise may potentially be hotspots of both $CHCl_3$ and methyl halide production due to their soil biogeochemical properties. Large areas (over

2000 km^2) of low-lying coastal tidal wetlands in southeastern United States, from Texas to North Carolina, have been slowly inundated with saltwater and will be converted from freshwater forested wetland to degraded forested wetland and ultimately to salt marsh (Cormier et al., 2013; Doyle et al., 2007). These degraded forested wetlands, with large amounts of organic matter from fallen branches and leaves and additional halogen input from seawater intrusion, have a significantly different biogeochemical environment in comparison to the adjacent ecosystems. The interaction of halogens with organic-rich sediments can result in the formation of organohalogens (Montelius et al., 2016; Zlamal et al., 2017), thus making the degraded forested wetland potentially a hotspot for halocarbon emissions. However, only one set (n = 4) of chloroform fluxes from this degraded ecosystem have been reported thus far, and the fluxes were on average higher than the bracketing freshwater wetland and salt marsh ecosystems, an observation that was also consistent with soil core incubations from these same ecosystems (Wang et al., 2016). However, the fluxes were also highly variable, leading to questions about the magnitude of annual emissions and the environmental factors controlling these emissions. CH_3Cl and CH_3Br fluxes were also measured but not yet reported (Wang et al., 2016), in the degraded forested wetland, the freshwater wetland and the salt marsh ecosystems, providing a basis of comparison for the present study.

In order to evaluate the ozone-depleting impact of the gradual turnover from freshwater forest to salt marsh over the long term, and to assess the regional or global implications of the observed biogeochemical transition in coastal ecosystem soils, this study conducted both field and laboratory incubations to quantify spatially and temporally resolved fluxes of $CHCl_3$, CH_3Cl and CH_3Br. Certain environmental (e.g., temperature, insolation) and biological (e.g., growth cycle of plants, litterfall) controls on fluxes show distinct seasonal cycles, while other potential controls (e.g., flooding, soil salinity, buried soil organic matter) may not. Hence, the seasonality of field-based flux measurements can reveal the relative importance of different biochemical factors and abiotic controls. Furthermore, the production and consumption mechanisms of halocarbons were tested in laboratory soil incubations by manipulating temperature regimes and conducting heat-sterilization on sampled soil cores.

2.3 Methods

2.3.1 Site description

Winyah Bay (33°32'N, 79°25'W), a National Estuarine Research Reserve, is located in South Carolina on the southeastern coast of the United States and next to the Atlantic Ocean (Figure 2.1). The upland freshwater forested wetland is dominated by bald cypress (*Taxodium distictum*) and swamp tupelo (*Nyssa sylvatica* var. *biflora*) (Busbee et al., 2003; Chow et al., 2013). The coastal wetlands are subject to seawater intrusion due to tropical storm-derived tidal surges in the short term and sea level rise in the long term. The increasing soil salinity has converted coastal freshwater forests to degraded forested

wetlands and will eventually convert them to salt marshes (Chow et al., 2013; Cormier et al., 2013; Krauss et al., 2009). Forest dieback due to the increasing soil salinity has partially opened the canopy, leaving more ground area exposed to sunlight. The fallen leaves and branches have led to relatively high organic matter content and surged seawater has increased soil salinity.

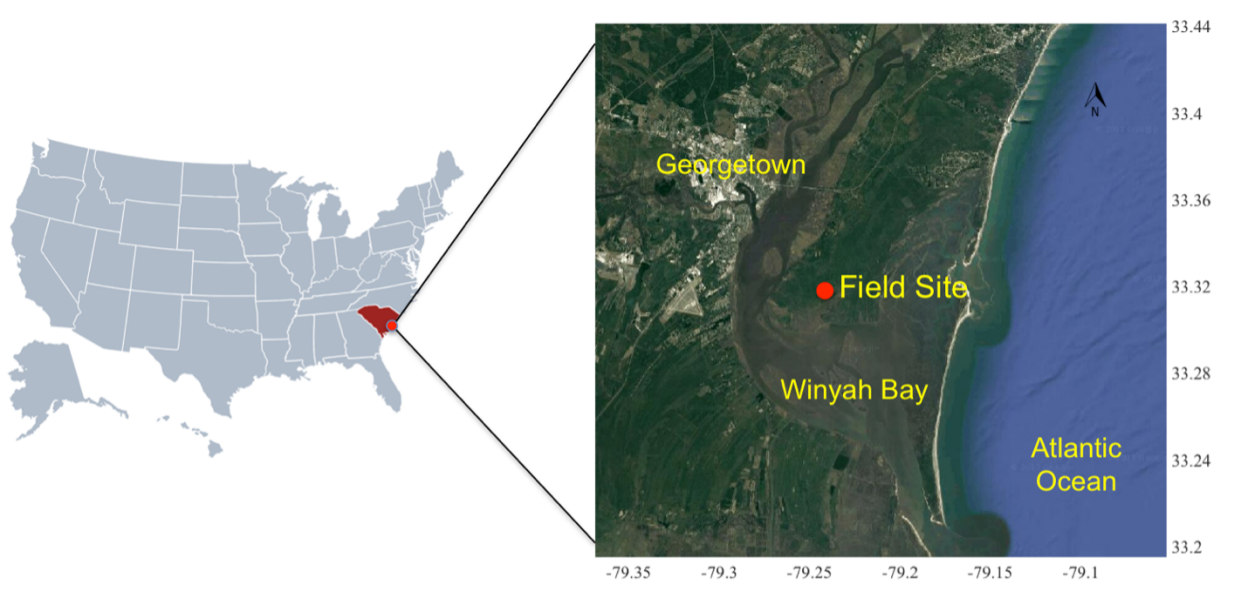

Figure 2.1 Location of the field site in Northern Inlet-Winyah Bay National Estuarine Research Reserve, South Carolina, USA. The expanded image (Google) shows Winyah Bay and the adjacent Atlantic Ocean with bathymetry. Longitude and latitude coordinates (°) are labelled.

The Winyah Bay region has a humid subtropical climate, with hot summers (average temperature 32°C) and mild winters (average temperature 15°C). Thunderstorms due to hot and humid conditions, together with tropical cyclones or hurricanes, contribute to the annual precipitation of 1427 mm in 2016 (National Weather Service, 2017). In October 2016, Hurricane Matthew traversed the field site and dropped precipitation of up to about 800 mm over a three-day period, submerging the wetland thoroughly for about 2 weeks. Following this flooding period, water levels dropped to sub-surface levels in November, exposing the soil to ambient air again.

2.3.2 In-situ gas collections and measurements

Static chamber description: *In-situ* static chamber measurements were conducted at a freshwater forested wetland (n = 4), degraded forested wetland (n = 4) and salt marsh (n

= 4) along a salinity gradient (0.1, 2 and 7 ‰, respectively) on 14-17 May 2012; the freshwater forested wetland and salt marsh were inundated, and the degraded forested wetland had saturated soil (Wang et al., 2016). Subsequently, bi-monthly field flux measurements were conducted from January to December 2016 within the degraded forested wetlands (Figure 2.2). Three replicate sampling sites (within 10 meters of each other) were chosen for static chamber measurements in the degraded transition zone undisturbed by human activities. To reduce the potential disturbance to the soils and the micro-environment, open-ended aluminum bases (L × W × H: 52 cm × 52 cm × 15 cm) were inserted into the soil at a depth of about 10 cm in December 2015, one month prior to the first sampling. Fallen and decomposing leaves and branches were enclosed in the chamber footprint.

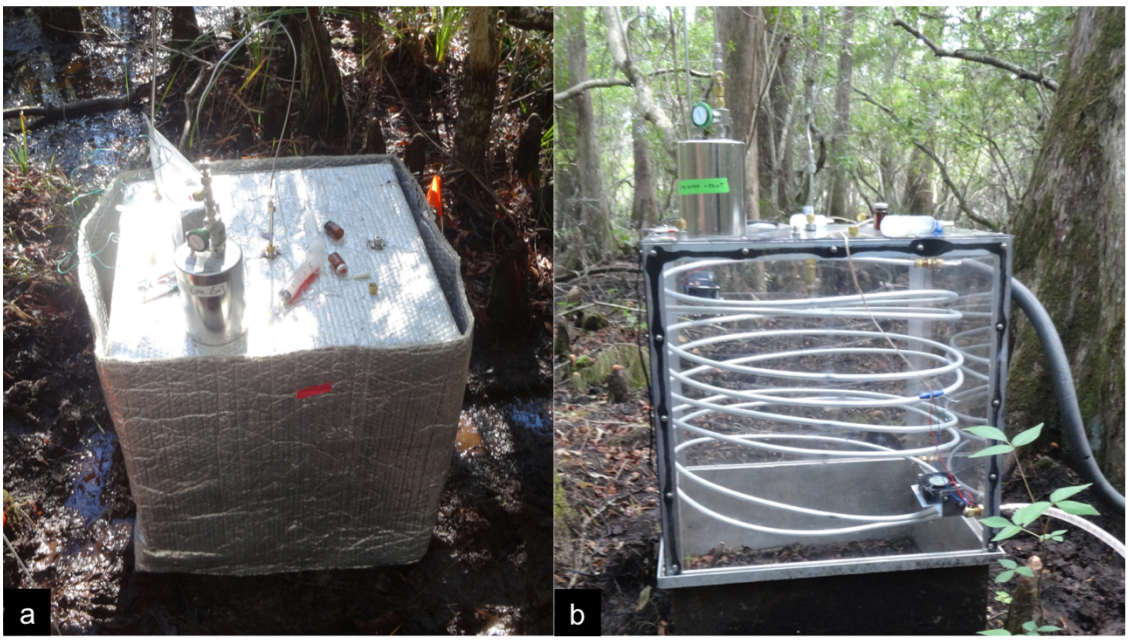

Figure 2.2 (a) Dark Aluminum chamber with thermal-reflective cover and (b) plastic transparent chamber with coiled water circulation tubes.

To conduct the static chamber measurement, an opaque aluminum chamber lid (L × W × H: 53 cm × 53 cm × 45 cm) was placed on top of the previously situated base, which had a 2 cm deep channel filled with deionized water surrounding its lip, to create an airtight seal between base and lid. Two electric fans were mounted inside the chamber to mix the air during the enclosure time period. In four out of the six outings, a transparent chamber lid (same dimensions as the aluminum lid) made of polycarbonate was used to explore the influence of irradiation. To keep temperatures within the chambers stable, the opaque chamber was covered by thermal reflective insulation during sampling while the transparent chamber was actively cooled by pumping water through an aluminum tube

(length 13 m, diameter 1 cm) inside the chamber. Chamber air temperatures were recorded every minute with iButton temperature data loggers (Embedded Data Systems, Lawrenceburg, Kentucky, USA); internal temperatures were stable within two degrees Celsius. Blank static chamber measurements using a mirror-polished aluminum sheet with Viton gasket as the base were carried out previously to ensure that the chamber material had no potential contamination in terms of halocarbons (Rhew et al., 2010).

Sample collection: Starting from the 5th minute after chamber enclosure, air samples were taken three times at intervals of 15 minutes into pre-evacuated canisters (1 L, electro-polished stainless steel, LabCommerce, Inc., San Jose, California) for halocarbon analysis and GC headspace vials (10 mL, glass) for the greenhouse gases (CO_2, CH_4) analysis respectively. When taking the air samples, a stainless-steel vent tube was opened to ambient air to maintain pressure equilibrium and avoid negative drawing air from the soil pore space.

Sample measurements: Each gas sample was measured at least twice for halocarbons and greenhouse gas concentrations. For halocarbon ($CHCl_3$, CH_3Cl and CH_3Br) analysis, samples were pre-concentrated with cryo-trap and then analyzed by gas chromatography coupled with a mass spectrometer (GC/MS; Agilent 6890N/5973, Agilent Technologies, Santa Clara, California) (Rhew et al., 2007b). Calibration curves were constructed before and after each batch of samples with a natural air standard collected at Trinidad Head, California, which was calibrated at the Scripps Institution of Oceanography, University of California at San Diego. For CO_2 and CH_4 analyses, samples were analyzed as duplicates using a Shimadzu GC2014 greenhouse gas analyzer coupled with three detectors: ECD/FID/TCD. Certified greenhouse gas standard mixtures (Air Liquide LLC., Houston, Texas) were used for calibration of CO_2 and CH_4. The concentrations were reported in parts per million (ppm) for greenhouse gases and parts per trillion (ppt) for halocarbons.

Flux calculation: Positive fluxes (emissions) were calculated based on the slope derived from the best linear fit between the corresponding gas concentrations and enclosure time. When negative fluxes (uptakes) were observed, a first order consumption rate (k) was calculated and then normalized to Northern Hemisphere background air concentrations (Carpenter et al., 2014). Fluxes were reported as the change of the number of moles of gas per unit area and per unit time (moles m^{-2} d^{-1}). Flux errors were derived from the propagation of the 90% confidence interval of the slope and in the number of moles of air within the chambers. The paired-*t*-test (type I error rate at 5% level) was applied to detect statistically significant differences between fluxes measured with opaque and transparent chambers.

Soil property measurements: Surface soil (0-5cm) samples were collected using a small spade and transported to the laboratory for further analysis. Dissolved organic carbon (DOC) and total dissolved nitrogen (TDN) of soil extracts were analyzed with at least two replicate extracts from each site. The soil extract was prepared and analyzed according to Emmerich et al (2012) and Ruecker et al (2014). Gravimetric soil moisture (g_{H2O}/g_{soil} wet

wt.) was measured by water loss after oven-drying subsamples (50g, fresh weight) at 105°C overnight (except for January and December). Soil temperatures (at ~3cm depth) were recorded with iButton temperature data loggers (Embedded Data Systems, Lawrenceburg, KY). Soil pH measured previously in this ecosystem was 7.0 (Wang et al., 2016).

2.3.3 Laboratory soil core incubations

Soil collection and incubation: Intact soil cores (n = 10, depth: 5.0 cm, diameter: 4.5 cm) from the degraded forested wetland were collected on July 28 and 29, 2016 using a slide hammer (AMS, Inc., American Falls, Idaho) and stored at 5°C until the start of experiments. Soil cores inside a sheath and base (stainless steel or aluminum) were placed in 1.9 L Mason jars for incubations. The jar was initially sealed, and 50-100 mL of headspace was withdrawn to remove accumulated gas within the soil pores. Then the jars were opened and flushed with ambient air for approximately 30 seconds prior to sealing again with a Viton O-ring and a stainless-steel lid to start the actual incubation. A short length of stainless-steel tubing was used both as a sampling volume and as the conduit between the jar and the pre-concentration system of the GC/MS. Approximately 15 ml of air sample was drawn from the jar headspace every 40 minutes for three times, starting at 1 minute after sealing. The gas fluxes were calculated based on the change of the number of moles of gas species per unit time and per unit exposed soil core surface area (15.9 cm^2), reported in units of moles m^{-2} d^{-1}. After the first incubation, a standard was measured. Meanwhile, the jar was opened and flushed with ambient air. The soil cores were then measured a second time within an hour of the first incubation.

Temperature controlled incubation: The same batch of soil cores were incubated at different temperatures, ranging from 5°C to 40°C, at steps of 5°C. To simulate different temperatures, Mason jars were situated in a temperature-controlled water/ethylene glycol bath (Model 1180S, VWR International, West Chester, Pennsylvania). At each temperature, the jars were sealed first and then placed in the bath for at least 12 hours in order to reach an equilibrium temperature with the surrounding liquid bath. Water loss in between runs was assumed to be negligible. Prior to each incubation, the jar was flushed with ambient air for 30 seconds and gas fluxes were quantified as described above.

Thermal sterilization: To distinguish between abiotic and biotic contributions to halocarbon emissions, aluminum foil covered-soil cores were thermally sterilized at 150 °C under atmospheric pressure for two hours to destroy the enzymes and stop microbial activity in the soil (Keppler et al., 2000; Rhew et al., 2003). The soils were not heated to complete dryness and deionized water was added to the soil to account for water loss during the thermal sterilization process. Approximately 12 hours later, the sterilized soil cores were incubated for flux measurements as described above, along the same temperature gradient (range: 5°C to 40°C with steps of 5°C). Paired-*t*-test (type I error rate at 5% level) was applied on flux comparisons between soil cores before and after thermal treatments.

Arrhenius formula: The effect of temperature on halocarbon production was explored by fitting measured fluxes from the temperature-controlled incubations with the Arrhenius equation. The Arrhenius formula proposed by Svante Arrhenius in 1889, is usually used for the temperature dependence of reaction rates:

$$k = Ae^{-\frac{E_a}{RT}} \quad \ldots\ldots \text{(Eq 2.1)}$$

where A is the frequency factor or pre-exponential factor, T is the soil temperature in Kelvin, k is the reaction rate constant (here k represents trace gas fluxes in nmol m^{-2} d^{-1}), E_a is the activation energy for the reaction (J mol^{-1}) and R is the universal gas constant (8.314 J mol^{-1} K^{-1}). The linear relationship between temperature and reaction rate constant is shown by rearranging the Arrhenius equation as follows:

$$\ln(k) = -\frac{E_a}{R} \cdot \frac{1}{T} + \ln(A) \quad \ldots\ldots \text{(Eq 2.2)}$$

With the temperature gradient incubations of the soil cores (range: 5°C to 40°C with steps of 5°C), the logarithmic value of chloroform fluxes was plotted against the inverse of temperature (in Kelvin).

2.4 Results

2.4.1 Seasonal variabilities of halocarbons fluxes from degraded forested wetland

2.4.1.1 Chloroform ($CHCl_3$)

The degraded forested wetland was consistently a net source for $CHCl_3$ over the period of measurement, with an overall annual mean net flux of 146 ± 129 nmol m^{-2} d^{-1} and a full range of 12-511 nmol m^{-2} d^{-1} (Figure 2.3a). These fluxes showed large temporal variability, with the highest fluxes observed in December 2016 (427 ± 95 nmol m^{-2} d^{-1}) and the lowest fluxes observed in January 2016 (44 ± 7 nmol m^{-2} d^{-1}). The three study sites also showed large spatial variability, illustrated by the standard deviations. However, spatial variability was significantly smaller than variability over time (two-way analysis of variance at $p = 0.05$). Variations in the seasonal $CHCl_3$ pattern did not resemble the seasonal variations of air or soil temperature, suggesting that temperature was not the major controlling factor for $CHCl_3$ emissions between the sites. Differences between the opaque and the transparent chamber were found to be statistically not significant (paired-*t*-test). Environmental parameters other than temperature, solar radiation and soil moisture were not concurrently monitored and are excluded from the discussion. Average $CHCl_3$ fluxes from 2016 accounted for 69.9% of these measured in May 2012, but the range of fluxes from both studies were comparable (Wang et al., 2016).

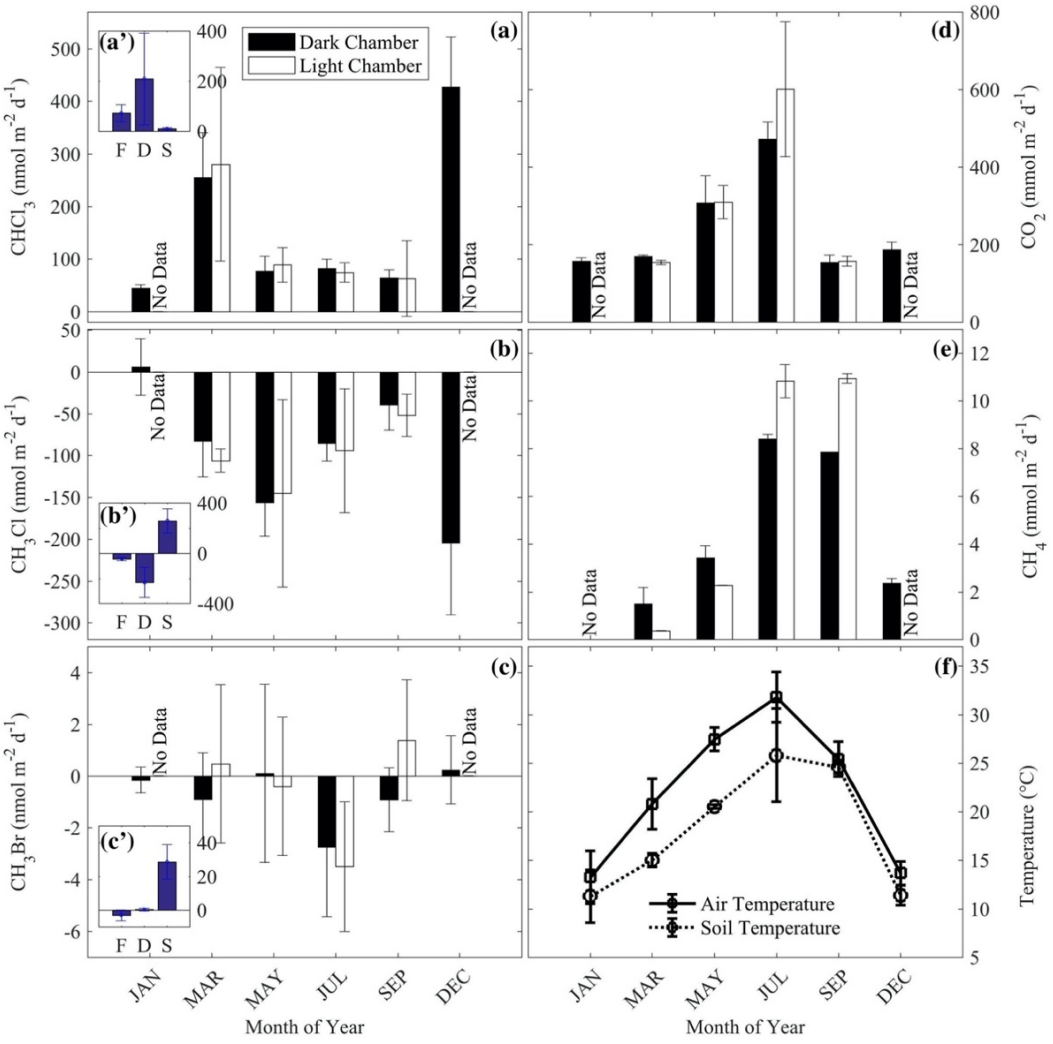

Figure 2.3 Bi-monthly fluxes in 2016 from the degraded forested wetland (a) chloroform ($CHCl_3$), (b) methyl chloride (CH_3Cl), (c) methyl bromide (CH_3Br), (d) carbon dioxide (CO_2), (e) methane (CH_4), and (f) annual air/soil temperatures. Inset bar plot of fluxes in May 2012, of (a') chloroform ($CHCl_3$)(Wang et al., 2016) (b') methyl chloride (CH_3Cl), (c') methyl bromide (CH_3Br) from freshwater forested wetland (F), degraded forested wetland (D) and salt marsh (S) along a salinity gradient. "No Data" indicates the corresponding measurement was not taken. Height of the bars represent the averaged values of measured fluxes among replicates (n = 3 for a, b, c, d and e; n = 2 for f; n = 4 for a', b', c'), and error bars represent the standard deviations of measured fluxes among replicates.

2.4.1.2 Methyl chloride (CH_3Cl)

The degraded forested wetland was a net sink for CH_3Cl (Figure 2.3b). Negative fluxes were observed at nearly all sampling spots in 2016, with an annual mean net flux of

-90 ± 61 nmol m^{-2} d^{-1} and a range of -293-41 nmol m^{-2} d^{-1}. Large temporal variability was observed, with the largest uptake rate of CH_3Cl in December with -204 ± 86 nmol m^{-2} d^{-1}. In January, the soil showed negligible average CH_3Cl fluxes (6 ± 34 nmol m^{-2} d^{-1}). The bi-monthly fluxes of CH_3Cl were also highly variable over time and did not follow the annual temperature pattern. No statistically significant difference (paired-*t*-test) was observed between CH_3Cl fluxes measured with the opaque chamber and the transparent chamber. In May 2012, the degraded forested wetland was a large net CH_3Cl sink (-232 ± 120 nmol m^{-2} d^{-1}), in contrast to the small net uptake rates observed at the freshwater forested wetland (-44 ± 15 nmol m^{-2} d^{-1}) and the relatively large net emissions observed at the salt marsh (258 ± 95 nmol m^{-2} d^{-1}) (Figure 2.3b').

2.4.1.3 Methyl bromide (CH_3Br)

In contrast to $CHCl_3$ which showed only emissions and to CH_3Cl which primarily showed uptake, no significant exchange rate was observed for CH_3Br from the degraded forested wetland (Figure 2.3c). Bi-monthly measured net fluxes fluctuated between slightly positive and slightly negative values in the range of -6 nmol m^{-2} d^{-1} to 4 nmol m^{-2} d^{-1} with an annual mean flux of -3.1 ± 2.6 nmol m^{-2} d^{-1}. The temporal variability also did not follow soil or air temperature trends. In the 2012 study (Figure 2.3c'), the degraded forested wetland also showed negligible fluxes (0.3 ± 0.8 nmol m^{-2} d^{-1}), whereas the salt marsh was a source (28.6 ± 10.2 nmol m^{-2} d^{-1}) and freshwater forested wetland a modest sink (-3.1 ± 3.2 nmol m^{-2} d^{-1}).

1.3.1.1 Methane (CH_4) and carbon dioxide (CO_2)

The degraded forested wetland soil was a net source for both CO_2 and CH_4. The annual CO_2 emission rates were 267 ± 157 mmol m^{-2} d^{-1} and the annual CH_4 emission rates were 5.3 ± 4.2 mmol m^{-2} d^{-1} (Figure 2.3d, e). The annual emission patterns of both CO_2 and CH_4 followed the seasonal pattern in ambient/soil temperatures, which suggested that the production of CO_2 and CH_4 were primarily mediated by temperature-dependent microbial activity.

Table 2.1 Temperatures and soil chemical properties at the field sampling sites (n = 3). Symbol (*) indicates that the corresponding measurement was not taken.

Date	Air temp. (°C)	Soil temp. (°C)	Soil moist (H_2O wt/wet wt, %)	DOC (mg/L)	TDN (mg/L)
01/27/2016	13.2 ± 2.7	11.3 ± 2.7	*	*	*
03/24/2016	20.8 ± 2.6	15.0 ± 0.7	25.7 ± 5.2	*	*
05/26/2016	27.5 ± 1.2	20.5 ± 0.2	14.0 ± 1.1	11.8	0.5
07/28/2016	31.8 ± 2.6	25.8 ± 4.8	7.5 ± 2.8	11.6	1.1
09/26/2016	25.4 ± 1.8	24.6 ± 0.7	50.5 ± 3.2	14.4	0.8
12/05/2016	13.7 ± 1.2	11.4 ± 1.0	*	16.6	1.8

Table 2.2 Chloroform ($CHCl_3$) fluxes from coastal ecosystems (freshwater forested wetland, degraded forested wetland and salt marsh) along a salinity gradient in South Carolina.

Study	Note	$CHCl_3$ flux [nmol m^{-2} d^{-1}]		
		Freshwater forested wetland	**Degraded forested wetland**	**Salt marsh**
Wang *et al.* (2016)	One-time measurement	71.9 ± 33.4	209 ± 183	9.7 ± 3.9
This study	Annual mean	--	146 ± 129	--
	Maximum	--	511 ± 19	--

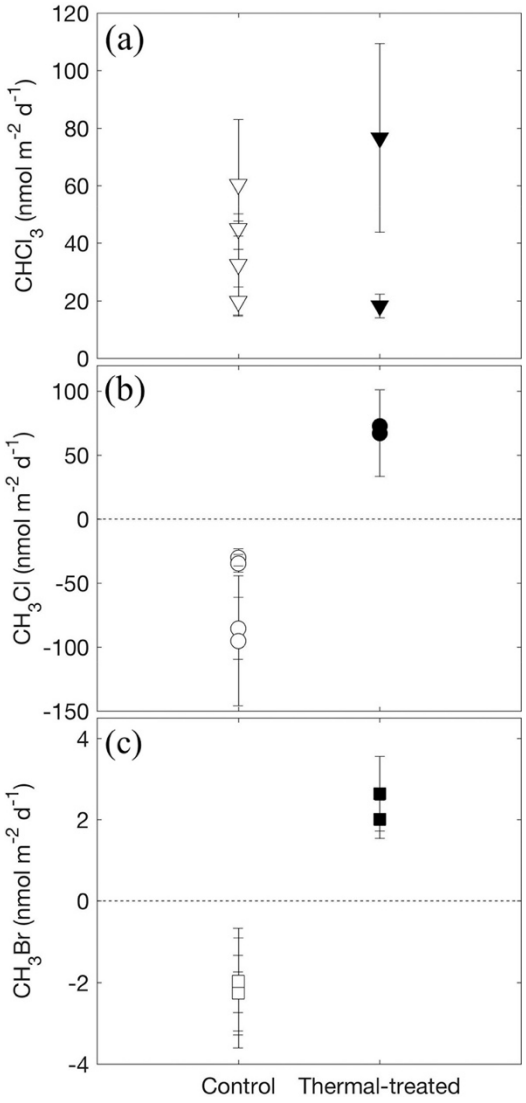

Figure 2.4 Plot of (a) chloroform ($CHCl_3$), (b) methyl chloride (CH_3Cl) and (c) methyl bromide (CH_3Br) fluxes from soil cores pre- (n = 4) and post-thermal treatment (n = 2). The incubations were conducted at room temperature (22°C). Values above the dashed line at zero indicate a net source whereas values below the dashed line indicate a net sink. Error bars represent the standard deviation of the replicates.

2.4.2 Lab soil incubations for halocarbons fluxes

2.4.2.1 Soil laboratory incubation fluxes in comparison to field measurements

The laboratory soil core incubation results yielded similar results to the field measurements from July, when the soil cores were collected. Both soil incubations and

field measurements demonstrated that the degraded forested wetland soils emitted a significant amount of $CHCl_3$. The soil cores incubated at room temperature (T = 21.5°C, n = 8) revealed a mean flux of 39 ± 17 nmol m^{-2} d^{-1}, which was lower than but of the same magnitude as the field measurements in July (opaque and transparent chambers averaged, 78 ± 18 nmol m^{-2} d^{-1}). Soil core incubations also showed the same magnitude and direction of CH_3Cl exchange rate (-61 ± 34 nmol m^{-2} d^{-1}) and CH_3Br fluxes (-2.2 ± 0.8 nmol m^{-2} d^{-1}) as in the field in July (CH_3Cl flux: -90 ± 48 nmol m^{-2} d^{-1}, CH_3Br flux: -2.2 ± 0.1 nmol m^{-2} d^{-1}, opaque and transparent chambers averaged).

2.4.2.2 Soil core fluxes after thermal treatments

The fluxes observed from the untreated room temperature soil cores, described above, were compared with room temperature (T = 21.5°C) flux measurements of the same soil cores following thermal sterilization and restoration of soil moisture levels. The thermal treatment was designed to stop enzymatic and microbial activity during a short heating period that limited the physical disturbance to the soil structure. Mean $CHCl_3$ fluxes slightly increased from pre-treament values of 39 ± 17 nmol m^{-2} d^{-1} (n = 4, see above) to 47 ± 41 nmol m^{-2} d^{-1} (n = 2) post-treatment (Figure 2.4a). However, differences were statistically not significant (paired-*t*-test). In contrast, after thermal treatment soils acted as sources of CH_3Cl and CH_3Br uniformly whereas they acted as net sinks before heat treatment. The methyl halide fluxes switched from pre-treatment net sinks (see above) to post-treatment sources of CH_3Cl (70 ± 4 nmol m^{-2} d^{-1}) and CH_3Br (2.3 ± 0.4 nmol m^{-2} d^{-1}) (Figure 2.4).

2.4.2.3 Temperature gradient incubations

$CHCl_3$ fluxes from both pre- and post-thermal treated soil cores increased with incubation temperatures (Figure 2.5a). Arrhenius plots of the natural log of $CHCl_3$ emission fluxes versus 1/T showed similar slopes and correlations for the pretreated (R^2 = 0.96) and post-thermal treated soil incubations (R^2 = 0.93, Figure 2.5d).

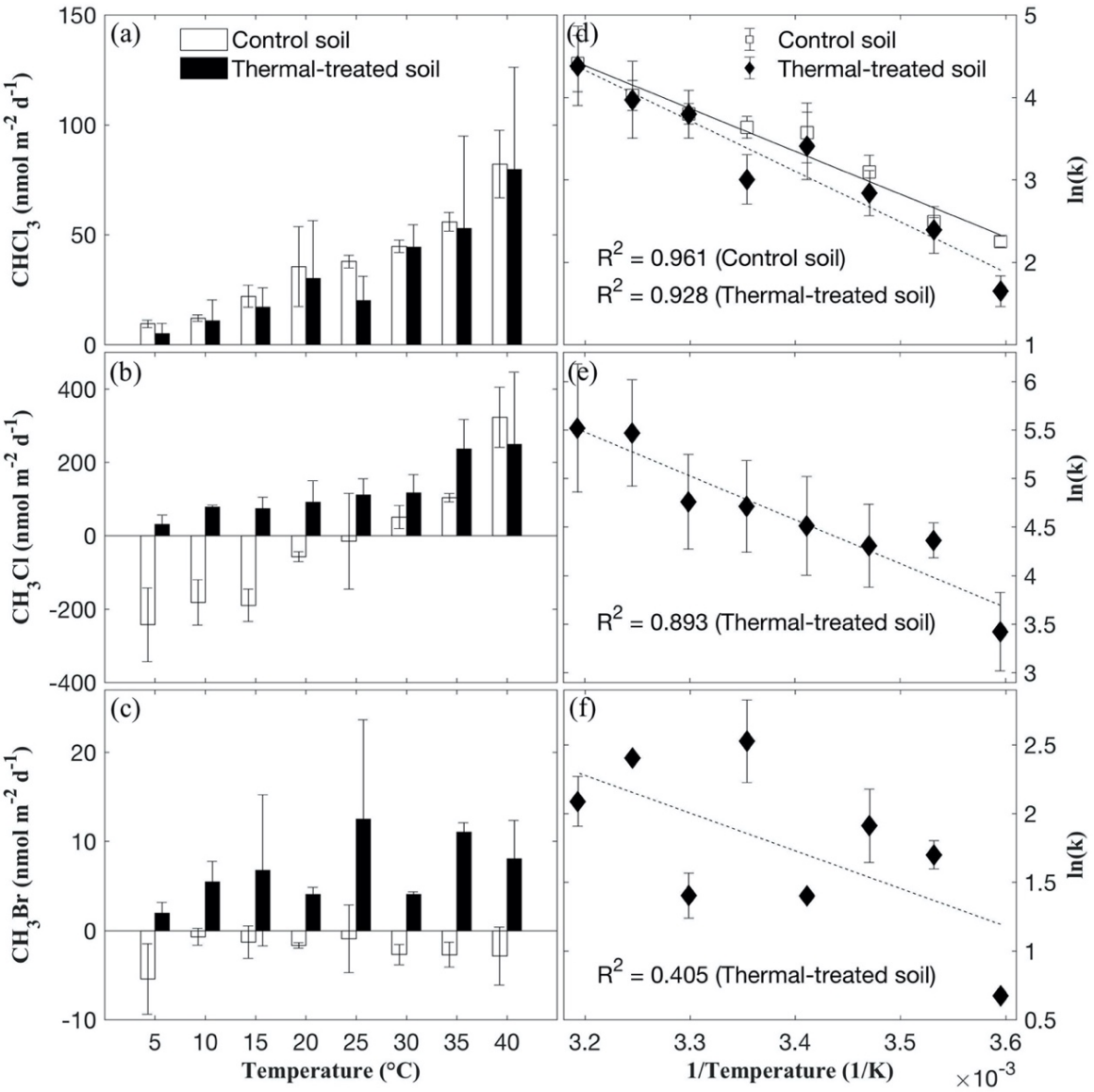

Figure 2.5 Bar plot of (a) chloroform ($CHCl_3$), (b) methyl chloride (CH_3Cl) and (c) methyl bromide (CH_3Br) fluxes in laboratory soil incubations (n = 4) at different temperatures. Arrhenius plots for production rates of (d) chloroform ($CHCl_3$), (e) methyl chloride (CH_3Cl) and (f) methyl bromide (CH_3Br) from incubated soil cores (n = 4) at different temperatures. k represents the emission rate of the corresponding halocarbons (unit: nmol m^{-2} d^{-1}). Error bars represent the standard deviation of measured fluxes among replicates.

Pre-thermal treated soil cores gradually switched from CH_3Cl sinks to sources as temperature increased: -180 to -240 nmol m^{-2} d^{-1} at 5-15°C, -15 to -60 nmol m^{-2} d^{-1} at 20-25°C, 50-130 nmol m^{-2} d^{-1} at 30-35°C and 320 nmol m^{-2} d^{-1} at 40°C (Figure 2.5b). For

individual flux measurements, the largest uptake of CH_3Cl was observed at the lowest temperature (-314 ± 73 nmol m^{-2} d^{-1} at 5°C), and the largest emission was observed at the highest temperature (381 ± 110 nmol m^{-2} d^{-1} at 40°C). However, post-thermal treated soil cores became CH_3Cl sources uniformly under all temperatures. CH_3Cl fluxes from post-thermal treated soil cores also increased with incubation temperature and can be represented by the Arrhenius equation (R^2 = 0.89, Figure 2.5e, Eq 2.2). Plotting the Arrhenius relation for methyl halides from pre-thermal treated soil cores is not possible due to negative methyl halide fluxes.

Soil core incubations revealed negligible CH_3Br absorption rates and emission rates before and after the thermal treatments respectively (Figure 2.5c), which is consistent with the field results. Control soil cores were CH_3Br sinks at any temperature uniformly but switched to CH_3Br sources after the thermal treatment. The Arrhenius fit showed a linear trend with a moderate R^2 value (R^2 = 0.405, Figure 2.5f).

2.5 Discussion

2.5.1 Chloroform ($CHCl_3$)

2.5.1.1 Comparison to fluxes from other ecosystems

Results suggest that the transitional zone (degraded forested wetland) of coastal South Carolina can be a significant source of $CHCl_3$ to the atmosphere. The mean ± 1σ annual $CHCl_3$ flux calculated from the bi-monthly measurements is 146 ± 129 nmol m^{-2} d^{-1} from the field chambers and 39 ± 17 nmol m^{-2} d^{-1} from laboratory incubations. These emission rates are slightly lower than but comparable to the 209 ± 183 nmol m^{-2} d^{-1} emissions observed at this site on May 12-14, 2012 (Wang et al., 2016). Nevertheless, the mean (146 nmol m^{-2} d^{-1}) and the highest (511 nmol m^{-2} d^{-1}) of observed net $CHCl_3$ emission rates in 2016 are larger than or comparable to reported fluxes from other natural significant $CHCl_3$ sources (Table 2.3), including tropical rainforest (Khalil & Rasmussen, 2000), subtropical shrubland and salt marsh (Rhew et al., 2008a; Wang et al., 2016), temperate peatland (Dimmer et al., 2001), temperate coniferous forest (Albers et al., 2011), temperate pasture (Cox et al., 2004), temperate salt marsh (Cox et al., 2004), rice field (Khalil et al., 1998; Khalil & Rasmussen, 2000), boreal pine forest (Hellén et al., 2006), subarctic shrubland, wetland, bog, birch forest and coniferous forest (Johnsen et al., 2016), arctic tundra (Rhew et al., 2008b). Similar to most of these ecosystems, $CHCl_3$ fluxes observed here show relatively high spatial variability, despite the proximity of sampling sites and visible homogeneity of enclosed soils. Given the experience at other ecosystems (Albers et al., 2011; Pickering et al., 2013), it is unlikely that these measurements captured the full spatial variability of fluxes.

It is possible that increased availability of Cl^- associated with storm surges contributes to the high $CHCl_3$ fluxes in the degraded forested wetland, the spatial extent of

which are expected to increase with projected sea level rise. The May 2012 study also showed that $CHCl_3$ emissions in the degraded forested wetland was greater than those in the adjacent salt marsh and freshwater forested wetland (Figure 2.3a and a', Table 2.2), although the freshwater wetland was flooded at that time (Wang et al., 2016). Demonstrating the enhancement of $CHCl_3$ emissions from the salt-induced degradation of freshwater forested wetlands will require a corresponding study in unaltered freshwater forested wetlands. The consistently smaller $CHCl_3$ emissions from salt marsh sites both here as well as elsewhere suggests that salt marshes are indeed smaller sources of $CHCl_3$ (Cox et al., 2004; Rhew et al., 2008a).

2.5.1.2 Abiotic versus biotic mechanisms of $CHCl_3$ production

Both biotic and abiotic mechanisms that produce $CHCl_3$ are known and assessing which mode of production dominates in the degraded forested wetland is necessary to predict changes in future emissions. Regarding biotic mechanisms, haloperoxidases (HPOs) are known to catalyze the halogenation reaction between hydrogen peroxide, organic matter and halide ion (X: Cl^-, Br^-, I^-) resulting in the production of relevant intermediate compounds including HOX or enzyme-bound intermediates, which then contribute to the formation of haloform (Brown & Hager, 1967; Neumann et al., 2008; Wagner et al., 2009; Walter & Ballschmiter, 1992; Weigold et al., 2016). Hoekstra et al (2001) conducted laboratory-based simulating reactions with humic acid, chloride and chloroperoxidase and also suggested that chloroperoxidase-mediated chlorination of humic materials is an environmentally significant process accounting for $CHCl_3$ emissions from natural soils. Field measurements also showed that wood-degrading areas and soils with a humic layer could emit more $CHCl_3$ (maximum 201.0 nmol m^{-2} d^{-1}) than areas without humic layers (Hoekstra et al., 2001).

However, the activity of chloroperoxidases (CPOs), like most enzymes, is inhibited at high temperatures. For example, the activity of chloroperoxidase from the fungus *Caldariomyces fumago* reaches 100% at 35°C and drops to almost 0% after incubation at 60°C for 15 minutes (Pickard & Hashimoto, 1988). Another study showed that chloroperoxidase from the same fungus retained only about 10% peroxidase activity after exposure at 50°C for 6 hours (Liu & Wang, 2007). Much higher thermostability (activity midpoint temperature of 90°C) was observed from a different fungus chloroperoxidase (*Curvularia inaequalis*), but its activity reduced to 0% at 100°C (Van Schijndel et al., 1994). The loss of activity presumably represents the denaturing of the enzyme. In the controlled incubations with soil cores pre- and post-thermal treatment, no significant difference was observed in terms of $CHCl_3$ fluxes (paired-*t*-test, n = 4). Assuming that chloroperoxidase was destroyed during the thermal treatment process (2 hours at 150°C), these results suggest that abiotic production dominates the $CHCl_3$ emissions at the field site. The linear Arrhenius relation with high R^2 values over the whole temperature range is consistent with a non-enzymatic process (Figure 2.5d), unless the dominant chloroperoxidase has high thermostability. One caveat is that the thermal treatment may

decrease organic matter content in soils and increase dissolved organic matter content in pore water which may change concentrations of available reactants involved in the abiotic production of halocarbons (Berns et al., 2008).

Table 2.3 Literature summary of chloroform ($CHCl_3$) emission rates at different ecosystems.

Geographic zone	Ecosystem	$CHCl_3$ flux 'ange (mean) [b] (nmol m^{-2} d^{-1})	n	Location	Time of measurement	Ref.
Tropical	ainforest soil	(25)	6	2°S 50°W	1987 (May)	1
Tropical	Rice paddies	(201)	--	23°09'N 113°21'E	1995 (Aug-Oct)	2
Subtropical	Rice paddies	20-101	21	30°N 104°E	1985-1987	1
Subtropical	Agricultural soil (canola, crops)	34-50	3	29°30'N 106°42'E	1988 (Apr)	1
Subtropical	Shrubland	-3-31 (6.6)	41	32-33°N 116-117°W	1997-2000	3
Subtropical	Salt marsh	-1-83 (15)	32	32°N 117°W	1997-2000	3
Subtropical	Degraded forested wetland	12-511 (146 ± 129)	36	33°32'N 79°25'W	2016 (bi-monthly)	c
Subtropical	Degraded forested wetland [a]	20-60 (39 ± 17)	8	33°32'N 79°25'W	2016 (Jul)	c
Subtropical	Degraded forested wetland	(209 ± 183)	4	33°16'N 79°14'W	2012 (May)	4
Subtropical	Salt marsh	(10 ± 4)	4	33°16'N 79°14'W	2012 (May)	4
Subtropical	Freshwater forested wetland	(72 ± 33)	4	33°16'N 79°14'W	2012 (May)	4
Temperate	Rice paddies	0-300	12	38°06'N 121°39'W	2009 (life cycle)	5
Temperate	Rice paddies	121-885	--	40°30'N 116°24'E	1992-1993 (Jul-early Oct)	2
Temperate	Forest soil	25-435	56	38°S 146°W	1985 (Apr-Nov)	1
Temperate	Tussock grassland	9-965 (362 ± 322)	10	40°41'S 144°41'E	1999-2001 (quasi-annual)	6
Temperate	Pasture	14-422 (241 ± 221)	10	40°41'S 144°41'E	1999-2001 (quasi-annual)	6
Temperate	Eucalypt forest soil/litter	322-1005 (603 ± 583)	8	40°41'S 144°41'E	2000-2001 (quasi-annual)	6
Temperate	Melaleuca forest soil/litter	32-191 (64 ± 60)	10	40°41'S 144°41'E	2000-2001 (quasi-annual)	6
Temperate	Wetland (salt marsh)	3-54 (15 ± 9)	10	40°41'S 144°41'E	2000-2001 (quasi-annual)	6
Temperate	Rain forest (fir, hemlock)	-26-125	12	49°52'N 125°20'W	2012 (May)	7
Temperate	Peatland (coniferous forest)	25-4574 (3352)	14	53°20'N 9°49'W	1998 (Sep)	8
Temperate	Peatland (bog)	2-652	22	53°20'N 9°49'W	1998 (Sep)	8
Temperate	Peatland soil (drained) [a]	3-3004 (258 ± 288)	36	38°06'N 121°39'W	2009-2010 (monthly)	9
Temperate	Coastal marsh	34-101 (78)	26	53°19'N 9°54'W	1998 (Sep)	8
Temperate	Inland marsh	117-262	10	53°20'N 9°49'W	1998 (Sep)	8
Temperate	Coniferous forest soil	3-402	20	56°23'N 8°57'E	2009 (Mar, Jun)	10
Temperate	Coniferous forest soil	8-538	30	56°02'N 12°04'E	2009 (Mar, Jun, Sep)	10
Subarctic	Coniferous forest soil	8-573	20	68°13'N 19°42'E	2012-2014 (spr, sum, aut)	11
Subarctic	Birch forest soil	2-116	20	68°13'N 18°49'E	2012-2014 (spr, sum, aut)	11
Subarctic	Boreal pine forest	0-241 (20-160)	16	61°51'N 24°17'W	2005 (Apr, May, Jun)	12
Subarctic	Lichen-graminoid heath	3-27	10	61°11'N 45°22'W	2012-2014 (spr, sum, aut)	11
Subarctic	Bog	2-26	20	68°26'N 18°34'E	2012-2014 (spr, sum, aut)	11
Subarctic	Shrubland (birch/willow)	1-8	18	61°09'N 45°21'W	2012-2014 (spr, sum, aut)	11

Arctic	Sedge wetland	10-105	10	66°59'N 50°54'W	2012-2014 (spr, sum, aut)	11
Arctic	Mossy tundra	(293)	2	68°N 50°W	1986 (Jul)	1
Arctic	Tundra (dwarf-shrub)	3-35	50	67°N 50°W 69°N 53°W	2012-2014 (spr, sum, aut)	11
Arctic	Tundra	0-118 (36.1)	16	68°N 149°W	2006 (Aug)	3
Arctic	Tundra	1.3-258 (47.5)	60	71°N 157°W	2005 (Jun., Aug.), 2006 (Jul.)	3

a denotes soil core incubations, all the others are static chamber measurements; b when available, the standard deviation is reported. c denotes this study. References cited in the table: 1. Khalil & Rasmussen, 2000; 2. Khalil et al., 1998; 3. Rhew et al., 2008b; 4. Wang et al., 2016; 5. Khan et al., 2011; 6. Cox et al., 2004; 7. Pickering et al., 2013; 8. Dimmer et al., 2011; 9. Khan et al., 2012; 10. Albers et al., 2011; 11. Johnson et al., 2016; 12. Hellen et al., 2006.

The behavior of production in the degraded forested wetland may differ from other forest soils. For example, Danish spruce forest soil has peak $CHCl_3$ emissions in warm and humid spring and autumn, thus suggesting that soil microorganisms were responsible for the $CHCl_3$ production (Haselmann et al., 2002). However, at this field sites, the peak $CHCl_3$ emissions were observed in December, during the coldest period of the year with relatively low CO_2 emission rates (Figure 2.3d). The different phase of CO_2 and $CHCl_3$ fluxes suggests that $CHCl_3$ emissions do not correspond with the general activity of microorganisms or fungi, assuming that CO_2 is largely a function of their respiration. Albers et al (2011) studied coniferous forests soil and reached a similar conclusion that the general microbial activity could not explain the $CHCl_3$ production within soils.

Several abiotic $CHCl_3$ production mechanisms in soil have been proposed. One abiotic mechanism is the decarboxylation of trichloroacetic acid (CCl_3COOH) (Albers et al., 2017; De Leer et al., 1985; Frank et al., 1989; Matucha et al., 2007). Trichloroacetic acid in the soil could arise from multiple pathways, including the oxidative biotransformation of trichloroethene (C_2HCl_3) and tetrachloroethene (C_2Cl_4) (Müller et al., 1972) and mainly anthropogenic use of herbicide (Frank 1991). The addition of trichloroacetic acid into spruce forest soil leads to an increased release of $CHCl_3$, suggesting that trichloroacetic acid does contribute to the $CHCl_3$ formation (Haselmann, Laturnus, et al., 2000). However, the field site is located at remote coastal forested area, far away from industrial pollution sources, and the $CHCl_3$ fluxes showed large temporal variations, suggesting that decarboxylation alone is not likely to explain the high $CHCl_3$ fluxes from soil.

Another possible abiotic mechanism for $CHCl_3$ production involves the transformation of carbon tetrachloride (CCl_4) in iron (III)-reducing environments through mineral mediated or sulfate-reducing reactions (Devlin & Müller, 1999; Laturnus et al., 2005; McCormick et al., 2002). The measured CCl_4 fluxes were uniformly negligible (0.4 ± 2.1 nmol m^{-2} d^{-1}) and showed no correlations to $CHCl_3$ fluxes in this study, suggesting that the pathway of CCl_4 transformation could not account for the $CHCl_3$ production at the field sites. Huber et al (Huber et al., 2009) conducted laboratory incubations and concluded that Fenton-like reaction conditions (iron (III) and hydrogen peroxide), elevated halide content, and an extended reaction time could produce $CHCl_3$ through the degradation pathway starting from resorcin-like dihydroxylated compounds. Breider et al (2014a) also simulated $CHCl_3$ formation with pure chemicals (phenol and propanone) in laboratory incubations. This abiotic pathway could happen in soil with typical pH range of 4.5 - 7.5 (Breider & Albers, 2015) and could potentially explain the high $CHCl_3$ emission features because the field site meets two of the essential factors: high organic matter content and elevated soil salinity.

In this study, the highest $CHCl_3$ flux was observed in December, after the water level retreated back to sub-surface levels after Hurricane Matthew. Page et al (Page et al., 2012) found that reactive oxygen species, including hydroxyl radical (·OH), intermediacy of hydrogen peroxide (H_2O_2), were produced during the oxidation of reduces humic acid in soils by exogenous O_2. Thus, one hypothesis is that the Hurricane Matthew-induced

water level rise could have produced an environment conducive to iron reduction to Fe (II), which could then participate in Fenton reactions once H_2O_2 becomes available when water levels drop. In this case, the soil redox potential may relate to $CHCl_3$ formation. Using CH_4 flux as an indicator for soil redox potential, the fact that relatively low CH_4 fluxes were measured in spring and winter when high $CHCl_3$ fluxes were observed (Figure 2.3a and e) suggests that $CHCl_3$ production favorably occurs when the system is not anaerobic.

Although the $CHCl_3$ production mechanism in the degraded forested wetland soil cannot fully be identified in the scope of this study, results suggest that abiotic processes dominate the $CHCl_3$ formation at the field sites.

2.5.1.3 Environmental controls on $CHCl_3$ emissions

Temperature is well known to control $CHCl_3$ formation rates in soils and water. In a seasonal measurement of $CHCl_3$ from arctic and subarctic ecosystems, highest fluxes were observed in summer (Johnsen et al., 2016). Indeed, fluxes from laboratory soil core incubations showed a positive correlation with incubation temperatures and could be satisfactory described by linear Arrhenius equations (R^2 = 0.96, Figure 2.5b, Eq 2.2). Nevertheless, as shown in Figure 2a, f and Table 1, the $CHCl_3$ emission rates in South Carolina are not correlated with annual temperature fluctuations, suggesting that temperature is not the sole controlling factor of soil $CHCl_3$ emissions at the field site. Based on these seemingly contradictory results, we hypothesize, that over the time scale of a year, environmental factors other than temperature (e. g. soil redox potential, chemical precursors advection by high/low tide cycles) dominate the soil $CHCl_3$ production in natural systems. When other geochemical factors are held constant, temperature appears to control the $CHCl_3$ production rate, following the Arrhenius equation.

Hydrological extremes also affect fluxes. For example, the lowest flux (44 ± 7 nmol m^{-2} d^{-1}) was recorded in January when the site was flooded, suggesting that standing water can inhibit $CHCl_3$ emissions by limiting the mass transfer between soil pore air and the ambient air. The highest $CHCl_3$ fluxes were observed from the moist soils in March and December during the transition periods between the flooding and drained conditions. The finding is consistent with the results of fieldwork and laboratory incubations conducted with Alaska Arctic tundra soils (Rhew et al., 2008b; Teh et al., 2009), which demonstrated that either flooded or drier conditions reduces $CHCl_3$ emissions while saturated (moderate moist) soil without standing water is a common feature for large $CHCl_3$ emissions. This may be related to the fluctuating soil redox potentials as discussed above.

The potential impact of sunlight on halocarbon fluxes is supported by halocarbon emissions following the diurnal cycle of irradiation during measurements in Irish peatlands (Dimmer et al., 2001). However, in the opaque versus transparent chamber measurements, there was no statistically significant difference in $CHCl_3$ fluxes (paired-*t*-test). This suggests that $CHCl_3$ formation in this ecosystem is independent of solar radiation. Results from laboratory incubations of soil cores from Alaska arctic tundra also suggested that

formation processes are not necessarily dependent on sunlight (Rhew et al., 2008b). Thus, it is possible that temperature increases in chambers (varies +15°C on days with bright sunshine) may account for the previously observed diurnal cycles (Dimmer et al., 2001) instead of sunlight. However, it is noted that the photosynthetic active radiation intensity (10-87 μmol m^{-2} s^{-1}) under the canopy of the degraded forested wetland was low, which may hinder the conclusion above that sunlight was not involved in the $CHCl_3$ production.

2.5.2 Methyl halides (CH_3Cl and CH_3Br)

2.5.2.1 Comparison to fluxes from other terrestrial ecosystems

In contrast to salt marshes which are significant sources of methyl halides (Drewer et al., 2006; Manley et al., 2006; Rhew et al., 2000), results from this study indicate that the adjacent transitional zone (degraded forested wetland) acts as a net sink for CH_3Cl with an annual mean ± 1σ of -90 ± 61 nmol m^{-2} d^{-1}. As shown in Table 2.4, the observed net uptake rate of CH_3Cl is on the same order of magnitude but smaller than reported fluxes from tropical rain forest soils (Khalil & Rasmussen, 2000), subtropical coastal/chaparral shrublands (Rhew et al., 2001), temperature pasture and grassland (Cox et al., 2004), boreal forest soils (Rhew et al., 2003), and Arctic non-flooded tundra (Rhew et al., 2007), but larger than fluxes from Arctic Greenland mossy soil (Khalil & Rasmussen, 2000), temperate wetland (Cox et al., 2004), and Arctic flooded tundra (Rhew et al., 2007).

As for CH_3Br fluxes in our field measurements, they fluctuated between slightly positive and slightly negative values in the range of -6 nmol m^{-2} d^{-1} to 4 nmol m^{-2} d^{-1}, which were negligible.

2.5.2.2 CH_3Cl and CH_3Br consumption and production mechanisms

The thermal treatment (150°C for 2 hrs) switched the soil cores from net sinks to sources for CH_3Cl and CH_3Br. This high temperature should deactivate the microbial and enzymatic activities (Hines et al., 1998) therefore the switch from sink to source suggests that the consumption of methyl halides within the soil was biotic and the production was abiotic predominately. The finding is further supported by other studies (Rhew et al., 2003; 2007; 2010; Teh et al., 2008). Biotic consumption exceeded abiotic production, thus yielding net sinks, similar to other soils where gross fluxes were measured (Rhew et al., 2003; 2007; Teh et al., 2008). An abiotic production mechanism (Keppler et al., 2000; 2003) for methyl halides entails the alkylation of halide ions during the oxidation of organic matter by an electron acceptor such as Fe(III) even in the absence of sunlight or microbial activity. This mechanism may be linked to the $CHCl_3$ production described above. Indeed, the correlation between net $CHCl_3$ emissions and the abiotic production of CH_3Cl from the thermally treated soil cores is strong (R^2 = 0.928, Figure 2.5d).

Table 2.4 Literature summary of methyl chloride (CH_3Cl) consumption rates at different ecosystems.

Geographic zone	Ecosystem	CH_3Cl consumption rate (nmol m^{-2} d^{-1}) [b]	n	Location	Time of measurement	Ref.
Tropical	.ainforest soil	(129.5)	8	2°S 50°W	1985 (Jul)	1
Tropical	.ainforest soil	(176.6)	6	2°S 50°W	1987 (May)	1
Subtropical	Degraded forested wetland	-41-292 (90 ± 61)	36	33°16'N 70°14'W	2016 (bi-monthly)	c
Subtropical	Degraded forested wetland [a]	25-131 (61 ± 34)	8	33°16'N 70°14'W	2016 (Jul)	c
Subtropical	Shrubland (coastal)	6-250	10	32°52'N 117°15'W	1997 (Dec), 1998 (Mar, Jul), 2000 (May)	2
Subtropical	Shrubland (chaparral)	46-430	10	32°52'N 117°14'W	1998 (Apr), 2000 (May)	2
Subtropical	Shrubland (desert)	4.4-133	6	33°38'N 116°22'W	1998 (Jan), 2000 (Apr)	2
Temperate	Tussock grassland	-87-480 (144 ± 161)	10	40°41'S 144°41'E	1999-2001 (quasi-annual)	3
Temperate	Pasture	4-310 (144 ± 119)	10	40°41'S 144°41'E	1999-2001 (quasi-annual)	3
Temperate	Eucalypt forest soil/litter	-367-310 (51 ± 184)	8	40°41'S 144°41'E	2000-2001 (quasi-annual)	3
Temperate	Melaleuca forest soil/litter	37-480 (283 ± 311)	10	40°41'S 144°41'E	2000-2001 (quasi-annual)	3
Temperate	Wetland (salt marsh)	-215-10 (-85 ± 90)	10	40°41'S 144°41'E	2000-2001 (quasi-annual)	3
Subarctic	Boreal forest soil	(400 ± 150)[b]	6	60-64°N 147-150°W	2002 (Sep, Oct)	4
Arctic	Greenland mossy/gras	47-94	12	68°N 50°W	1986 (Jul)	1
Arctic	Coastal tundra (drained)	(617 ± 43)	9	71°N 157°W	2005 (Jun, Aug)	5
Arctic	Coastal tundra (moist)	(483 ± 77)	8	71°N 157°W	2005 (Jun, Aug)	5
Arctic	Coastal tundra (wet)	(195 ± 57)	10	71°N 157°W	2005 (Jun, Aug)	5
Arctic	Coastal tundra (flooded)	(14 ± 4)	12	71°N 157°W	2005 (Jun, Aug)	5

a denotes soil core incubations, all the others are static chamber measurements; b The flux format is range (mean or mean ± standard deviation) and it is the consumption rate (positive values represent absorption from the air, negative values represent emission from the soil); c denotes this study. References cited in the table: 1. Khalil & Rasmussen, 2000; 2. Rhew et al., 2001; 3. Cox et al., 2004; 4. Rhew et al., 2003; 5. Rhew et al., 2007.

However, the high CH_3Cl and CH_3Br productions within the salt marsh are likely created by enzymatic processes in salt marsh plants, which involves SAM (S-adenosyl-methionine) - dependent methyl transferases that are found widely in plants (Attieh et al., 1995; Ni & Hager, 1998, 1999; Rhew & Østergaard, et al., 2003; Saini et al., 1995; Wuosmaa & Hager, 1990).

2.5.2.3 Environmental controls on CH_3Cl emissions

A dependence of methyl halide formation on solar irradiation was proposed previously (Amiro & Johnston, 1989; Muramatsu & Yoshida, 1995). However, there is no statistically significant difference between the CH_3Cl fluxes measured with opaque and transparent chambers (paired-*t*-test), suggesting that sunlight was not required for either degradation or abiotic production of CH_3Cl. The abiotic production of methyl halides through the oxidation of organic matter by iron (III) is not dependent on sunlight (Keppler et al., 2000). On the other hand, the photosynthetic active radiation intensity (10-87 μmol m^{-2} s^{-1}) on the ground of the degraded forested wetland where chambers were placed is low, which may mitigate the conclusion above that sunlight was not involved in the production or degradation of CH_3Cl. Therefore, further experiments in more light-exposed environments (e.g., advanced degraded forests with more open canopies) should be conducted to test the light effect.

The post-thermal treated soil incubations demonstrated that the abiotic production of CH_3Cl was temperature controlled and could be described by Arrhenius equations (Figure 2.5d, Eq 2.2).

Over the course of the year, neither the highest nor the lowest CH_3Cl fluxes were observed during flooding season in January and the dry period in July. However, large CH_3Cl uptake rates were observed in May and December during the middle of flooding-drainage cycles when comparably moderate soil moisture was recorded, suggesting that the consumption of CH_3Cl is maximum at intermediate soil moisture and reduced at both low and high ends of the range (Rhew & Mazéas, 2010).

2.5.3 Regional and global implications

Due to the large variability of observed $CHCl_3$ and CH_3Cl fluxes, the heterogeneity of soils and the limited scale of the flux chamber coverage area, any extrapolations to the global scale will introduce large uncertainties. However, a simple quantitative extrapolation can help us to assess the significance of degraded forested tidal wetland in terms of regional halocarbon budgets.

Assuming the annually averaged fluxes of $CHCl_3$ (146 ± 129 nmol m^{-2} d^{-1}) and CH_3Cl (-90 ± 61 nmol m^{-2} d^{-1}) are representative of coastal degraded forested wetland, and using the degraded forested wetland area of 1.7×10^{11} m^2 (including the coastal freshwater

wetland subject to seawater inundation) for the continental United States (Dahl et al, 2011), we estimate a total annual flux of 1.06 ± 0.15 Gg $CHCl_3$ and -0.46 ± 0.05 Gg CH_3Cl. Considering sea level rise and increasing frequency of extreme weather events due to global climate change (Tebaldi et al., 2012), the investigated environments thus may become a more important source of ozone-depleting $CHCl_3$. If an annual flux of 270 Gg is needed to balance the OH sink for $CHCl_3$ (O'Doherty et al., 2001), the coastal forested wetland within the continental United States accounts for 0.4% of the global annual $CHCl_3$ flux, which is not that significant. The uptake of CH_3Cl within the continental United States is also minor compared to the global scale sources and sinks. However, the contributions of global coastal freshwater wetland to halocarbon budgets are expected to be much higher. Unfortunately, the global coastal forested wetland subject to seawater intrusion area data are not currently available (Herbert et al., 2015). Over longer time scales with sea level rise, the transitional zone is likely to shift further inland and the original degraded forested wetland would convert to salt marsh. Hence, it is conceivable that the current CH_3Cl sink will become a CH_3Cl source (258 nmol m^{-2} d^{-1} as in May 2012), and instead of an annual uptake of 0.46 Gg CH_3Cl, the area that is currently degraded forested wetland could produce 1.79 Gg of CH_3Cl per year. A longer-term network of measurements across the southeastern US will provide a more accurate assessment of the impact of degraded forested wetlands on ozone-depleting compound budgets at the regional or global scale.

2.6 Conclusion

Results from this study suggest that when freshwater forest becomes degraded through seawater intrusion due to storm surges and sea level rise, it emits significant amounts of $CHCl_3$ through abiotic pathways and absorbs CH_3Cl through biotic pathways predominately, and if these lands are overtaken by salt marshes, methyl halide emissions, instead of consumptions, will likely increase. Thus, global warming induced sea level rise could lead to a potential impact on stratospheric ozone depletion by altering the atmospheric halocarbon budgets. However, it is not yet proven that emissions will dramatically differ from freshwater wetlands, owing to the large spatial and temporal variability of observed fluxes and the limited number of freshwater wetland measurements. Variations could be even larger under different climate conditions (i.e., hurricane, wet year with more precipitation.).

Chapter 3. Global methyl halide emissions from rapeseed (*Brassica napus*) using life cycle measurements

The material for this chapter was previously published as: Jiao, Y., Acdan, J., Xu, R., Deventer, M. J., Zhang, W., & Rhew, R. C. (2020). Global methyl halide emissions from rapeseed (*Brassica napus*) using life cycle measurements, *Geophysical Research Letters*, 47, e2020GL089373. DOI: 10.1029/2020GL089373; and is adapted with permission from the American Geophysical Union.

3.1 Abstract

Stratospheric ozone absorbs incoming solar UV radiation, attenuating the harmful radiation exposure for life on Earth's surface. Halogen atoms transported via halocarbons, including methyl halides, can catalyze ozone destruction efficiently in the stratosphere. Anthropogenic sources of halocarbons have been decreasing consistently since the implementation of the 1987 Montreal Protocol and its amendments. However, some natural sources, especially those influenced by anthropogenic activities, may offset some of the achievement of reduced halocarbon emissions. This study quantifies methyl halide emissions from cultivated rapeseed (*Brassica napus*, cultivar: Empire), based on life cycle measurements and normalized to seed production. This yields a global crop contribution of 2.8 ± 0.7 Gg of methyl bromide (CH_3Br) annually, which is smaller than previous estimates (5.1-6.6 Gg), even after accounting for the doubling of global annual rapeseed production since then. It supports the conventional view that there must be other unidentified or underestimated sources for CH_3Br. This study also quantifies for the first time that rapeseed emits 5.3 ± 1.3 Gg of methyl chloride (CH_3Cl) and 4.0 ± 0.8 Gg of methyl iodide (CH_3I) each year. Due to the increasing demand on rapeseed products such as canola oil, its global methyl halide emissions are expected to grow in the future.

3.2 Introduction

As a result of the Montreal Protocol, atmospheric levels of most anthropogenic ozone-depleting halocarbons (e.g., CFCs, HCFCs, carbon tetrachloride and methyl chloroform) have decreased (Montzka et al., 2003; Montzka et al., 1996), leaving halocarbons from natural sources relatively more pronounced, especially those influenced by human activities and climate change (Liang et al., 2017). Among the halocarbons with natural sources, methyl chloride (CH_3Cl) and methyl bromide (CH_3Br) are presently the largest carriers of chlorine and bromine, respectively, to the stratosphere. Methyl iodide

(CH_3I) also contributes to ozone destruction, though mostly in the lower troposphere due to its relatively shorter lifetime of 12-15 days (J. Zhang et al., 2020).

Known methyl halides sources include biomass burning (Andreae et al., 1996), tropical forests (Bahlmann et al., 2019; Xiao et al., 2010; Yokouchi et al., 2007), salt marshes (Drewer et al., 2006; Manley et al., 2006; Rhew et al., 2000), wetlands (Lee-Taylor et al., 2001; Varner et al., 1999), oceans (Carpenter et al., 2014; Hu et al., 2013), fungus (Lee-Taylor et al., 2001; Lee-Taylor & Holland, 2000), agricultural fields (such as rapeseed (Gan et al., 1998; Mead et al., 2008), rice paddies (Lee-Taylor & Redeker, 2005; Redeker et al., 2000)) and anthropogenic sources (such as coal combustion (McCulloch et al., 1999) and the use of CH_3Br as a fumigant for quarantine and pre-shipment uses (Carpenter et al., 2014)). Estimated magnitudes of these sources do not balance the known sinks (Carpenter et al., 2014), including loss to the stratosphere, reaction with OH radicals, degradation in oceans and soils (bi-directional interfaces), which suggests that either missing or underestimated sources exist. The magnitude of the "missing" sources for CH_3Cl and CH_3Br are 748 Gg $year^{-1}$ and 39 Gg $year^{-1}$, equivalent to 20% and 46% of all known sources, respectively; global CH_3I emissions are also not well constrained (Table 1-4 and 1-8 in Carpenter et al., 2014).

The second largest estimated biological terrestrial source of CH_3Br is the global crop of rapeseed (*Brassica napus*), with an estimated global emission of 5.2 Gg $year^{-1}$ (Carpenter et al., 2014). Plants of the *Brassicaceae* family were first reported to have large emission potentials for methyl iodide (CH_3I) based on a survey of floating leaf discs of 118 herbaceous species in KI solutions (Saini et al., 1995). Among several species of *Brassica* plants, *B. napus* emitted the largest amount of CH_3Br per unit biomass, and that the global crop flux scaled to 6.6 Gg $year^{-1}$ (Gan et al., 1998). However, these studies were limited to juvenile plants in laboratory-based incubations or snapshot measurements in the field. Rapeseed has a usual lifetime of 130-160 days (Buntin et al., 2007; Diepenbrock, 2000) with physiological factors at different life stages varying significantly, such as leaf area index, flower number, pocket number, biomass, plant height. (Bouttier & Morgan, 1992; Morrison et al., 1992). It is expected that rapeseed, similar to other biological emitters, would reveal varied methyl halide emission levels over the life cycle (Deventer et al., 2018; Khan et al., 2013; Manley et al., 2006; Redeker et al., 2000). Extrapolating a global CH_3Br budget after incorporating the life cycle variations in emissions may improve estimates.

Using the laboratory-based measurements of juvenile plants and field measurements from Gan et al. (1998), Mead et al. (2008) applied the global crop harvest index and life length to extrapolate the rapeseed flux to yield 5.1 Gg $year^{-1}$. Rapeseed is the third largest source for vegetable oil (Liu et al., 2016), and its production (20-fold increase), and growing area (6-fold increase) have been consistently increasing over the last six decades (FAOSTAT Database). Therefore, methyl halide emissions from rapeseed have likely increased with time and since the most recent quantification was conducted (Mead et al., 2008).

Biological methyl halide production can occur when S-Adenosyl-L-methionine (SAM) donates methyl groups to bond with halogen ions to form methyl halides and with bisulfide to produce methane thiol, reactions catalyzed by SAM-halide/thiol methyltransferases (Attieh et al., 2000; Bayer et al., 2009; Rhew et al., 2003). Thus, rapeseed should have the potential to produce the other ozone destroying compounds, CH_3Cl and CH_3I. Improved estimates of all of these methyl halide emissions from rapeseed will help predict the impact of this crop expansion on the future of stratospheric ozone.

In this study, methyl halide emissions were measured from the whole plants of *B. napus* "Empire" over their entire life cycle, as well as from soil samples collected from the field. These results are used to provide an updated global CH_3Br budget and the first estimates of CH_3Cl and CH_3I emissions with respect to rapeseed.

3.3 Methods

3.3.1 Site description and rapeseed cultivation

The cultivation of rapeseed (*Brassica napus*, "Empire") was conducted both in the greenhouse and in the field at Oxford Tract (37°52'31"N, 122°16'01"W), a University of California, Berkeley facility located approximately 5 km east of San Francisco Bay. The greenhouse was vented and was not temperature controlled during the experiment. The field plot (6 m×30 m) was located at the southeastern corner of the tract, adjacent to cultivated corn crops. The tract was ploughed regularly each year and was irrigated roughly twice a week with treated tap water from the East Bay Municipal Utility District during the dry season (July to September). Air temperature was recorded for every 10 minutes via sensors (HOBO® U23 Pro v2 Data Logger, Onset Computer Corporation, Bourne, MA).

On July 3rd, 2015, uncoated seeds (i.e., no neonicotinoids) of *B. napus* (Empire, non-GMO), from the Brassica Breeding and Research group, University of Idaho, were sowed into six different trays (L×W×D: 56 cm×56 cm×30 cm) of soil. On August 5th, 2016, *B. napus* seeds were sowed in the field garden (Figure 3.1).

Prior to both experiments, the soil above 20 cm depth was removed and autoclaved at 145°C for 6 hours to destroy the viability of weed seeds and pests and returned either to the field or translocated to the trays. Open-ended aluminum chamber bases (L×W×H: 52 cm×52 cm×22.5cm) were inserted 10 cm into the soil and remained there for the duration of the growing season for static-chamber enclosure measurements. For the field measurements only, leaf area, plant height, flower numbers and fruit pocket numbers, if available, were recorded each week over the life cycle (Figure 3.2) and the above-ground biomass was harvested and dried after the seeds were collected at the end of the experimental cultivation. The harvest data for the greenhouse measurements were lost; thus, only the diurnal studies (see below) were used for the derivation of normalized flux responses to temperature (Figure 3.3), while the weekly fluxes were used to plan for the field study.

Figure 3.1 Life cycle of rapeseed (*Brassica napus*) from one of the enclosed chamber bases in the field. The date and the week number after germination are labeled accordingly. Subfigures (a) - (d) represent leafing period; (e) - (j) represent flowering period; (k) represents fruiting period and (l) represents senescence period.

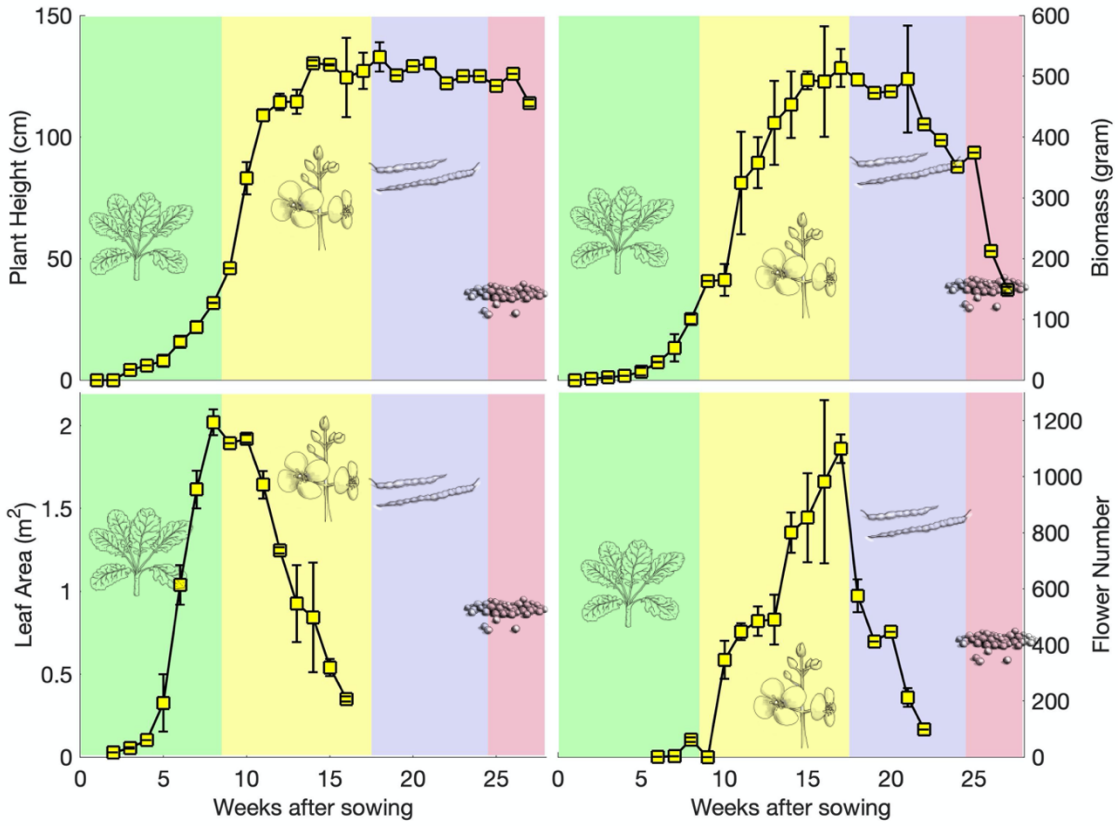

Figure 3.2 Averaged plant height, dry biomass, leaf area and flower number of the enclosed chambers over the life cycle of rapeseed (n = 2). The four different background colors represent the four life stages: leafing, flowering, fruiting and senescence.

3.3.2 Gas collection and analysis

Starting from the 5th day after sowing, static flux chamber measurements were conducted over two rapeseed plots/trays (n = 2) each week until the end of the life cycle. For headspace air sampling, an aluminum chamber lid (L × W × H: 53.5 cm × 53.5 cm × 44.5 cm) was placed on top of an aluminum base, which was rimmed with aluminum channels (width: 3 cm) filled with deionized water, making an airtight seal. Gas samples were collected into previously evacuated canisters (1-L electro-polished stainless steel (Lab Commerce, San Jose, California) or 1-L or 3-L silica-lined stainless steel (Restek Corporation, Bellefonte, Pennsylvania)) through stainless-steel tubing at 2 min, 17 min and 32 min after the chamber closure. The entire chamber was covered by reflective insulation to maintain a stable internal temperature. Air inside the chamber was well mixed with two electric fans (0.012 m^3 min^{-1} each) on opposite ends, angled in different directions to enhance circulation. The temperature within the chamber was recorded with the stainless-

steel thermocouple dataloggers (iButtons, Maxim Inc., Sunnyvale, California). When the rapeseed plants grew higher than the chamber lid, an intermediate connection piece (L × W × H: 54.5 cm × 54.5 cm × 45 cm) was placed in between the base and the lid to increase the overall height to 1.2 meters; at the maximum plant heights (1.3 m), stems were bent gently to avoid breakage.

Methyl halide concentrations were analyzed by gas chromatography coupled with mass spectrometry (GC/MS; Agilent 6890N/5973, Agilent Technologies, Santa Clara, California) with a custom pre-concentration system (Jiao et al., 2018). Each gas sample was analyzed at least twice consecutively, and the concentration was reported as the average ± standard deviation in units of ppt (parts per trillion). Before and after the measurements of each batch of gas samples, calibration curves and daily instrumental drift corrections were constructed using a whole-air standard collected at Niwot, Colorado, and calibrated at the Global Monitoring Division Laboratory of the National Oceanographic and Atmospheric Administration. The averaged instrumental precisions for CH_3Cl, CH_3Br, and CH_3I after applying drift corrections were 1.0%, 1.9%, and 8.7%, respectively.

3.3.3 Flux calculation and approximation

Fluxes were calculated (Eq 3.1) by linear regression between methyl halide concentrations and the enclosure time (dc/dt), converted to a net rate of change of moles of trace gas in the chamber (Na) and then normalized to the basal area of the chamber (A) and expressed in the units of micromoles per square meter per day (μmol m^{-2} day^{-1}).

$$F = \frac{N_a}{A}\frac{dc}{dt} \qquad \ldots\ldots \quad (Eq\ 3.1)$$

Methyl halide emissions have been shown to vary dramatically with stage of plant growth (Deventer et al., 2018; Khan et al., 2013; Redeker & Cicerone, 2004). Therefore, the life cycle of rapeseed was segmented into four growing stages in this study: leafing period (from sowing to the maximum leaf area), flowering period (to the maximum flower number), fruit-bearing period (to when the seed pods started to dry out) and the senescence period (to harvest).

For the flux chamber measurements in the greenhouse, a 24-hour study was conducted at three- or four-hour intervals starting at 0:00 on a randomly selected day within each of the four growing stages to capture the diurnal relationships between fluxes and air temperature. Assuming the biogenic methyl halide fluxes have an exponential relationship with the air temperature (Deventer et al., 2018; Guenther et al., 2012), an equation can be proposed as,

$$F_i = \mathrm{f(Temp)} = \mathrm{p} * \mathrm{e}^{\mathrm{q*Temp}} \qquad \ldots\ldots \quad \text{(Eq 3.2)}$$

Where F_i represents the flux of the gas species i; Temp is the air temperature within the chamber when the flux measurement was carried out and p, q are unknown coefficients, which can be derived from fitting with exponential regression ($R^2 > 0.90$, Table 3.1).

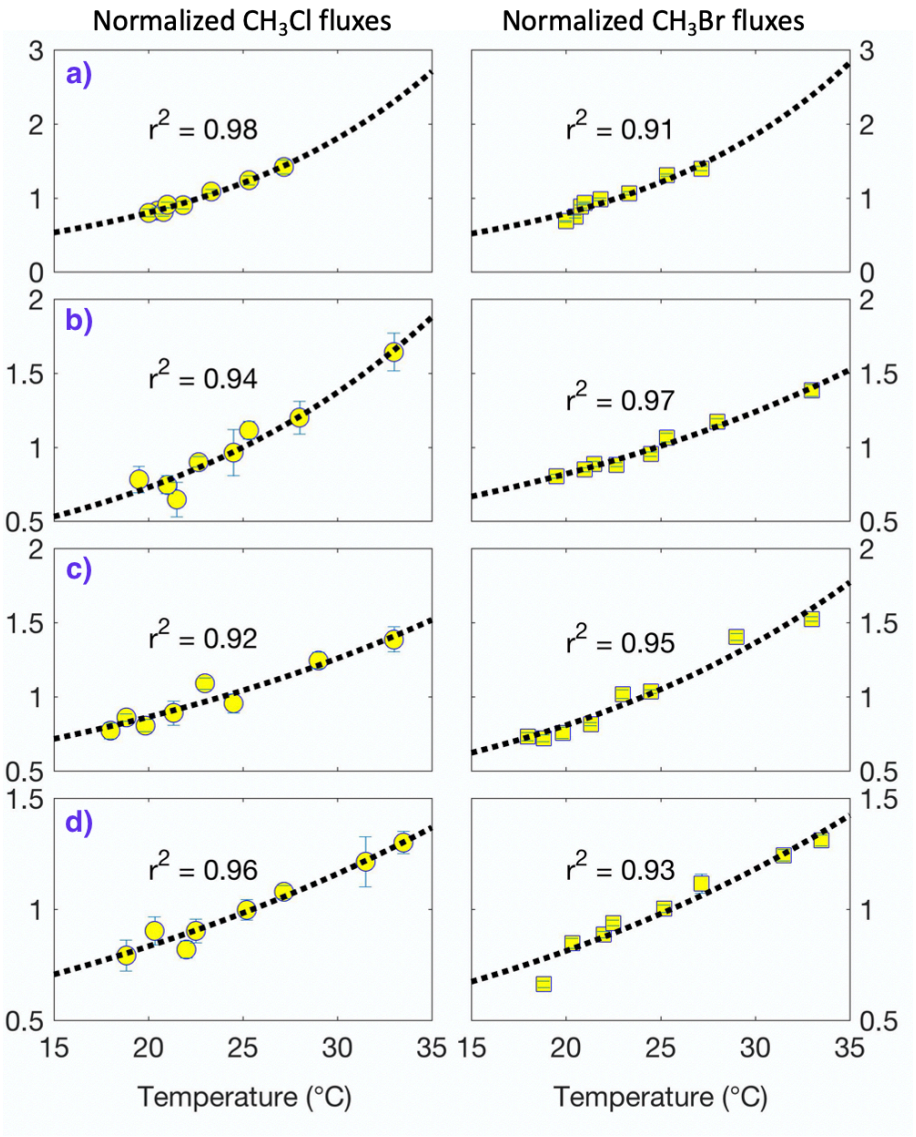

Figure 3.3 CH_3Cl and CH_3Br fluxes (normalized to the daily average) response to daily temperature change at different life stages of rapeseed (*B. napus*), including (a) leafing period, (b) flowering period, (c) fruiting period, and (d) senescence period (n = 2). The error bars represent the standard deviations.; the dashed lines represent least squares exponential-fitting between the normalized fluxes and temperature.

Table 3.1 The p, q coefficients of Eq 3.2 and the calculated Q10 values for CH_3Cl and CH_3Br fluxes at the four different life stages of rapeseed (*B. napus*). The values within the square brackets denote the 95% confidence bounds. Daily (24-hr)

measurements for CH_3I fluxes were missing, therefore, p, q coefficients for CH_3I were estimated as the means of CH_3Cl and CH_3Br coefficients.

Coefficients		Leafing period	Flowering period	Fruiting period	Senescence period
CH_3Cl	p	0.157 [0.121, 0.194]	0.206 [0.124, 0.289]	0.406 [0.296, 0.517]	0.430 [0.352, 0.507]
	q	0.081 [0.072, 0.091]	0.063 [0.048, 0.078]	0.038 [0.027, 0.048]	0.033 [0.026, 0.040]
	Q_{10}	2.25 [2.04, 2.48]	1.88 [1.62, 2.18]	1.46 [1.31, 1.62]	1.39 [1.30, 1.49]
CH_3Br	p	0.145 [0.062, 0.229]	0.360 [0.306, 0.414]	0.283 [0.202, 0.364]	0.384 [0.280. 0.487]
	q	0.085 [0.060, 0.109]	0.041 [0.036, 0.047]	0.052 [0.042, 0.063]	0.037 [0.028, 0.047]
	Q_{10}	2.34 [1.83, 2.98]	1.51 [1.43, 1.60]	1.69 [1.52, 1.88]	1.45 [1.32, 1.60]

Furthermore, assuming a similar methyl halide flux response to the temperature both in the greenhouse and in the field, the daily averaged methyl halide fluxes can be calculated by the exponential model with the following equation:

$$F_{day} = \frac{1}{24}\sum_{i=1}^{24}\left(\frac{f(T_i)}{f(T_{Meas.})} \times F_{Meas.}\right) \quad \ldots\ldots \quad \text{(Eq 3.3)}$$

Where F_{day} represents the average flux over the course of a day, T_i represents air temperature measured at the i^{th} hour of the day, $T_{Meas.}$ and $F_{Meas.}$ represent the temperature within the chamber when measurement was carried and the corresponding trace gas flux, respectively.

After the autoclaved soil was returned back to the field, intact soil cores (diameter: 4.5 cm; depth: 10 cm) from adjacent sites undergoing similar treatment were collected with a slide hammer (AMS, Inc., American Falls, Idaho) during each growing stage. The cores were subsequently incubated in the laboratory in glass jars (V = 1.9L) to derive the background methyl halide fluxes from the soil by analyzing the changing methyl halide concentrations in the headspace over enclosure time.

3.3.4 Emission extrapolation

Studies have shown that the leafing area, floral initiation, floral bud number, and yield of rapeseed are proportional to each other and to the accumulated air temperatures (Luo et al., 2018; Wright et al., 1988). Therefore, to correct for the local temperature bias, the weekly methyl halide fluxes were integrated over the plant life span and then normalized to the weight of the seeds harvested for enclosed plants at the end of the experiment to derive a total "flux per gram of seed". This is multiplied by the global seed

harvest, assuming that the harvest-normalized methyl halide production rates in this study are representative of crops globally. An unquantified uncertainty is the variation of methyl halide emissions between different plant cultivars, as only one cultivar was analyzed in this study. Cultivar has been shown to be a significant variable in rice plants (Redeker & Cicerone, 2004). The annual data of global/regional rapeseed production, yield, and cultivation area since 1961 is accessible to the public from the online Food and Agriculture Organization Corporate Statistical Database.

3.4 Results and discussion

3.4.1 Methyl halide fluxes from plant-soil system

The average soil fluxes of CH_3Cl, CH_3Br, and CH_3I were 66 ± 33, 2.1 ± 0.3, 17 ± 24 nmol m^{-2} d^{-1} during the leafing period, 98 ± 163, 2.8 ± 3.9, 20 ± 4 nmol m^{-2} day^{-1} within the flowering period, -172 ± 37, 1.6 ± 4.3, 5.6 ± 0.9 nmol m^{-2} day^{-1} over the fruiting period, and -211 ± 97, 2.8 ± 0.8, 12.0 ± 0.1 nmol m^{-2} day^{-1} at the senescence period, respectively (Table 3.2). CH_3Br and CH_3I fluxes from soil were relatively consistent while CH_3Cl gradually switched from net emissions to net absorption over the experiment. Soil is usually a bi-directional interface for methyl halide with abiotic production and biotic degradation happen concurrently (Keppler et al., 2020). The switch from CH_3Cl soil sink to source may be a result of the initial autoclave process killing methyl halide consuming microbes, which slowly recolonized the soils over the season.

Table 3.2 Soil fluxes across the life cycle of rapeseed during the experiment.

Life Stages	CH_3Cl [nmol m^{-2} d^{-1}]	CH_3Br [nmol m^{-2} d^{-1}]	CH_3I [nmol m^{-2} d^{-1}]
Leafing	66.4 ± 33.0	2.1 ± 0.3	17.1 ± 23.9
Flowering	97.6 ± 163.2	2.8 ± 3.9	20.4 ± 3.7
Fruiting	-172.2 ± 37.2	1.6 ± 4.3	5.6 ± 0.9
Senescence	-211.2 ± 97.2	2.8 ± 0.8	12.0 ± 0.1

Flux measurements from cultivated rapeseed (*B. napu*s) plots were much larger than incubated soil fluxes, roughly 10, 100 and 20 times larger in magnitude for CH_3Cl, CH_3Br and CH_3I, respectively. CH_3Cl, CH_3Br and CH_3I emissions all had similar seasonal patterns over the life cycle of the crop, with the peak emissions observed during the flowering period (Figure 3.4). The average fluxes (note different units) of CH_3Cl, CH_3Br, and CH_3I during the leafing period were 0.29 ± 0.33 μmol m^{-2} day^{-1}, 0.06 ± 0.09 μmol m^{-2} day^{-1}, 0.13 ± 0.18 μmol m^{-2} day^{-1}; then climbed up to 2.04 ± 0.46 μmol m^{-2} day^{-1}, 0.65 ± 0.19 μmol m^{-2} day^{-1}, 0.57 ± 0.18 μmol m^{-2} day^{-1} within the flowering period; decreased to 0.77 ± 0.40

μmol m^{-2} day^{-1}, 0.19 ± 0.06 μmol m^{-2} day^{-1}, 0.17 ± 0.07 μmol m^{-2} day^{-1} over the fruiting period; and dropped further to 0.12 ± 0.03 μmol m^{-2} day^{-1}, 0.02 ± 0.01 μmol m^{-2} day^{-1}, 0.03 ± 0.03 μmol m^{-2} day^{-1} at the senescence period, respectively.

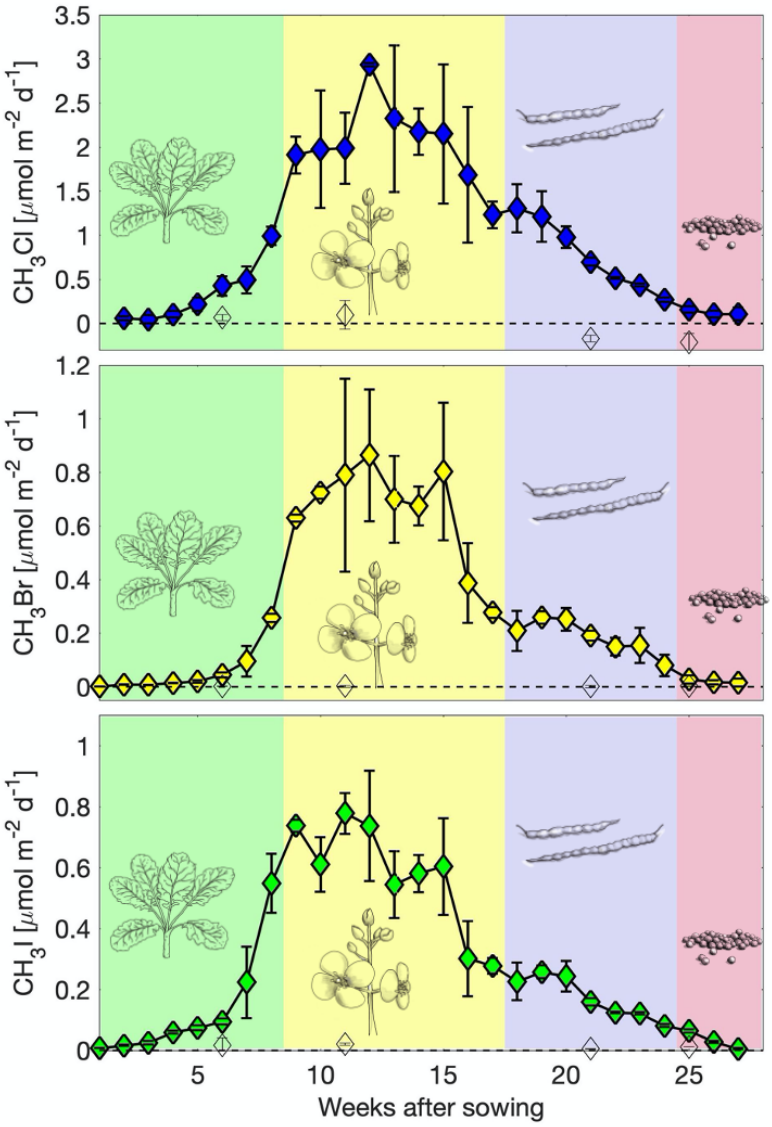

Figure 3.4 Life cycle emissions of methyl chloride (CH_3Cl), methyl bromide (CH_3Br) and methyl iodide (CH_3I) from rapeseed (*B. napus*) normalized to per unit area. Error bars represent the standard deviations of the replicates (n = 2). The four different background colors represent the four life stages as indicated by the drawings: leafing, flowering, fruiting and senescence. The open diamond symbols represent the background soil fluxes based on the controlled laboratory incubations.

Fluxes of methyl chloride (CH_3Cl) and methyl bromide (CH_3Br) both showed strong correlations with air temperature (Figure 3.3, Table 3.2) within each plant life stages ($R^2 > 0.90$). Similar results were found for perennial pepperweed (*Lepidium latifolium*), a related species within the Brassicaceae family, which increased with temperature towards an optimum temperature at 33°C, consistent with enzymatically mediated production by the plants (Deventer et al., 2018). This is also consistent with measurements from rice plants where biogenic production of methyl halides correlated with temperature over a large range, with an optimum temperature around 36°C (Redeker & Cicerone, 2004). It is proposed that SAM acts as a methyl donor to halogen ions to form the respective methyl halides catalyzed by methyltransferase enzyme (Rhew et al., 2003; Saini et al., 1995). Studies reported some methyltransferases, such as nicotinic acid-N-methyltransferase from soybeans (*Glycine max*) and (S)-tetrahydroprotoberberinecis-N-methyltransferase from *Eschscholtzia* and *Corydalis*, have an optimum temperature at 40°C and remain stable up to 45°C (Chen & Wood, 2004; Rueffer et al., 1990). However, the temperature during the experimental period of this study was almost entirely under 33°C. Therefore, impacts of high temperature could either enhance or reduce enzymatic activity, but these are not accounted for in this study. In addition, the temperature sensitivity of CH_3Cl and CH_3Br emissions varies across the life stages: leafing, flowering, fruiting and senescence (Table 3.1), which suggest life cycle scale methyl halide emissions from rapeseed were predominantly influenced by physiological factors.

3.4.2 Global methyl halide emissions from rapeseed

CH_3Br emissions from several *Brassica* plants were found to be linearly correlated to soil halide content (Gan et al., 1998). In the present study, soil bromide content was 1.1 ± 0.3 mg kg^{-1}, similar to the typical bromide content (1.0 mg kg^{-1}) in natural soils globally (Flury & Papritz, 1993). Allometric factors of rapeseed may be influenced by several factors, including local climate, agrarian techniques and chemical inputs, such as fertilizer, pesticide. As a consequence, the yield and density of rapeseed may vary significantly across the producing regions (e. g. Canada, China, Europe, India) with different local climates. The single cultivar (*Empire*, non-GMO) used in this experiment may show different methyl halide emission patterns compared to other genotypes. However, studies have shown that leafing area, floral bud numbers, and yield of rapeseed are proportional to each other and to the accumulated air temperatures (Luo et al., 2018; Wright et al., 1988). Rapeseed in this experiment showed a harvest index of 24.4 ± 2.2, which was close to those (21.3 ± 1.5) of hundreds of other genotypes of rapeseed (Lu et al., 2016). Therefore, methyl halide emissions per gram of seed harvested (corrected for soil fluxes) were calculated as a means to partially offset the locality bias in plant vitality. Daily fluxes were calculated based on the weekly flux measurements and temperature relationships (Eq 3.3) and summed over the plant life span. The integrated life cycle emissions were then divided by the fresh weight of the seeds to determine total emissions

per gram of seed produced. This method provides both a means for inter-site comparison as well as for global extrapolation using agricultural commodity data.

In this experiment, methyl halide production rates by seed biomass were 71.0 ± 17.1 ug g^{-1}, 37.8 ± 9.8 ug g^{-1}, and 53.2 ± 11.4 ug g^{-1} for CH_3Cl, CH_3Br and CH_3I, respectively. Assuming these parameters are representative globally, 2.8 ± 0.7 Gg CH_3Br were emitted from global cultivated rapeseed in 2018. This is smaller than the prior estimations, which concluded rapeseed emitted 5.1-6.6 Gg of CH_3Br each year (Gan et al., 1998; Mead et al., 2008). The lower value is determined despite the fact that the global production of rapeseed has more than doubled as well as the growing area has increased over 1.5-fold from 1998-2003 to 2018.

The major reason for the discrepancy involves the method of extrapolation. Prior extrapolations (Gan et al., 1998; Mead et al., 2008) were based on CH_3Br fluxes in low bromide soils (25 ng g^{-1} dry wt above ground biomass day^{-1}), which scaled up 20-fold to 515 ng g^{-1} day^{-1} assuming a global average soil bromide content of 1 mg kg^{-1}. The end result was roughly 9 times the life cycle average flux reported here despite similar soil bromide contents (Table 3.3). On the other hand, numerous other factors remain to be accounted for, including variations in cultivar, agricultural practices, climate, and soils. The low number of replicates (n = 2) also poses substantial uncertainties in representing the true mean flux for the field site. Based on studies of chamber variance in rice paddies, we estimate that these measurements are within 30% of the field means (Redeker et al., 2002).

Interestingly, this study yielded a much larger average emission rate for CH_3Br per unit above-ground biomass than the prior study, which was based on the leafing phase only. The life cycle average was twice that of the prior study. Considering the leafing phase only, the emission rate in this study (82 ng g^{-1} dry wt day^{-1}) was over 3-fold the prior study. Thus, while this study supports the assumption of higher emissions with higher soil bromide content, it does not concur with the magnitude of scaling up.

Table 3.3 The comparison of measured or extrapolated methyl bromide (CH_3Br) fluxes per unit above-ground biomass from rapeseed at different life stages.

Comparison	**Prior studies** [1]	**This study** [2]				
Measurement period	**Leafing**	**Leafing**	**Flowering**	**Fruiting**	**Senescence**	**Life cycle average**
unit [ng g^{-1} d^{-1} (dry weight)]	25					
	515	82.0 ± 32.4	89.2 ± 50.5	16.8 ± 6.0	2.8 ± 1.8	55.9 ± 48.6

1. The previous studies include Gan et al. (1998) and Mead et al. (2003).
2. The averaged soil bromide content of this study was 1.1 ± 0.3 mg kg^{-1}. CH_3Br fluxes of this study listed in the table were normalized to per unit above-ground biomass in order to provide comparison to prior studies. However, the global extrapolation of this study was calculated from fluxes per unit of seeds harvested.

Even with smaller CH_3Br annual fluxes than previously estimated, rapeseed remains one of the largest non-industrial terrestrial sources of CH_3Br, next to biomass burning, 23 Gg $year^{-1}$ (Andreae et al., 1996; Blake et al., 1996), salt marshes, 8-29 Gg $year^{-1}$ (Deventer et al., 2018; Manley et al., 2006; Rhew et al., 2014; Rhew et al., 2000), and wetlands, 4.6 Gg $year^{-1}$ (Varner et al., 1999). However, CH_3Br budgets with respect to rapeseed still cannot balance the current identified and quantified sources and sinks, with the missing sources estimated to be about half the magnitude of all the known sources put together.

The average chloride content in soils globally is about 100 mg kg^{-1} (Geilfus, 2019), which is slightly lower than that of the soil (148 ± 71 mg kg^{-1}) in this experiment. Using the same extrapolation method and assumptions yields a global CH_3Cl source from rapeseed of 5.3 ± 1.3 Gg in 2018, which is comparable to that of rice paddies, 2.4-5.8 Gg $year^{-1}$ (Lee-Taylor & Redeker, 2005; Redeker et al., 2000), mangroves, 12 Gg $year^{-1}$ (Manley et al., 2007), and at the lower limit of that of salt marshes, 10 Gg $year^{-1}$ (Deventer et al., 2018). However, rapeseed itself cannot bridge the considerably large CH_3Cl gap between currently identified sources and sinks.

As for CH_3I, rapeseed is estimated to account for an annual flux of 4.0 ± 0.8 Gg $year^{-1}$, which is a minor source. The ocean is believed to be the largest CH_3I source, with an average flux of 371.4 Gg $year^{-1}$, predominantly through abiotic photochemical production (Butler et al., 2007; Stemmler et al., 2014) and/or biogenic emissions from phytoplankton and algae (Manley & Cuesta, 1997; Smythe-Wright et al., 2006), depending on the region or season. The largest identified terrestrial source for CH_3I is rice paddies, with a quantified flux of 16 to 71 Gg $year^{-1}$ (Lee-Taylor & Redeker, 2005; Redeker et al., 2000). However, a CH_3I profile measurement study at North Carolina (Sive et al., 2007) suggested the existence of mid-latitude terrestrial sources of 33 Gg $year^{-1}$, in which rapeseed (*B. napus*) would be considered as one of them. Other ubiquitous species among the *Brassicaceae* family, such as *Brassica oleracea* (e.g., broccoli, brussels sprout, cabbage, cauliflower, collards, kale), *Brassica rapa* (e.g., bok choy, Chinese cabbage, turnip), *Brassica juncea* (mustard), *Lepidium latifolium* (e.g. perennial pepperweed), have been reported as significant emitters for CH_3Cl and CH_3Br (Gan et al., 1998; Khan et al., 2013; Deventer et al., 2018). Thus, it is rational to speculate that they may account for part of the terrestrial sources of CH_3I as well. However, measurements of CH_3I from these widespread species have not been reported, and their global budget extrapolations have not been established as a consequence. In contrast to CH_3Cl and CH_3Br, currently identified and quantified sources of CH_3I exceed the sum of the sinks, with a positive imbalance of ~146 Gg $year^{-1}$, suggesting that either the oceanic CH_3I production may be overestimated and/or the photolysis sinks of CH_3I may be underestimated.

Atmospheric CH_3Br concentrations have an inter-hemispheric ratio of 1.130 (NH/SH, 2017) (NOAA HATS Data Archive), suggesting the unevenly distributed regional sources with the major sources located in the Northern Hemisphere, especially in the mid northern latitudes. This is in agreement with a hypothesis of the existence of

significant terrestrial sources or biogenic sources. Given the geographical distribution of rapeseed, methyl halides from this crop are mainly emitted in the Northern Hemisphere (93.6%, 2018), which will contribute to this inter-hemispheric gradient. However, the updated CH_3Br budget of rapeseed itself cannot account for the inter-hemispheric difference due to its size. The dominant emission of CH_3Cl from rapeseed from the Northern Hemisphere also has a negligible impact on the inter-hemispheric gradient of CH_3Cl. Atmospheric CH_3Cl displayed a relatively even distribution across the hemispheres with the peak concentrations observed at the intertropical zone (NOAA HATS Data Archive), suggesting the predominant sources are located near the equator.

Global estimates of rapeseed emissions will be improved after additional measurements are conducted at different agricultural sites and with different cultivars. This study demonstrates the importance of life cycle measurements to determine overall emissions per seed crop biomass, a key metric to extrapolate results over time. Emission rates by biomass are highest during the leafing and flowering stage and are highest by surface area at the flowering stage. This study also demonstrates the relative importance of rapeseed on the global CH_3Cl and CH_3I budgets.

The increase of rapeseed harvest area and production over the past 60 years have resulted in increased emissions of CH_3Cl, CH_3Br and CH_3I by 21-fold between 1961 and 2018 (Figure 3.5). The demand for rapeseed oil in the world is projected to grow even larger in the future (Jat et al., 2019). Using the extrapolations developed here and assuming the future global rapeseed production follows the same rate of increase as the past 60 years, the atmospheric sources of CH_3Cl, CH_3Br and CH_3I may increase to 13.1 Gg $year^{-1}$, 7.0 Gg $year^{-1}$, and 9.8 Gg $year^{-1}$, respectively by 2050, highlighting the increasing contribution from natural sources of ozone depleting substances influenced by human activities. Non-controlled anthropogenic halocarbon emissions (Dhomse et al., 2019; Li et al., 2017; Montzka et al., 2018), together with the projected increasing of natural sources associated with global warming (Smythe-Wright et al., 2006; Yokouchi et al., 2001), land use change (Deventer et al., 2018; Mead et al., 2008), biomass burning (Blake et al., 1996; Westerling et al., 2006), and sea level rise (Jiao et al., 2018; Wang et al., 2016) may offset some of the halocarbon emission reductions achieved by the Montreal Protocol (Liang et al., 2017).

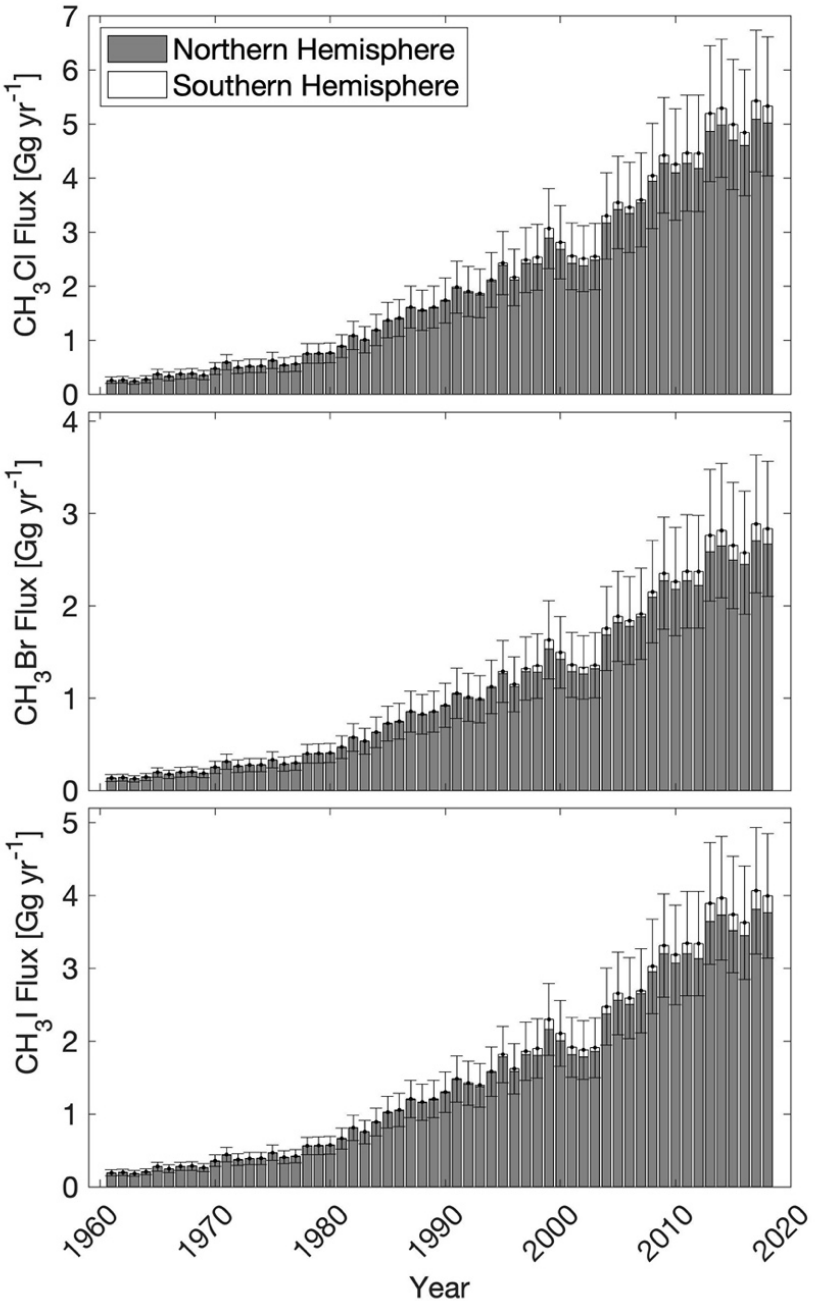

Figure 3.5 Extrapolated global methyl chloride (CH_3Cl), methyl bromide (CH_3Br) and methyl iodide (CH_3I) budgets with respect to rapeseed (*B. napus*) from 1961 to 2018. Estimated emissions from the Northern Hemisphere (shaded bars) greatly exceed those from the Southern Hemisphere (white bars).

3.5 Data availability statement

Rapeseed global annual production data can be accessed through the Food and Agriculture Organization Database at http://www.fao.org/faostat/en/#data/QC. The dataset of weekly methyl halide fluxes, rapeseed physiological variables, soil halide contents, and temperature is available at doi:10.6078/D1WD8H.

Chapter 4. Abiotic methyl chloride and methyl bromide formation catalyzed by copper amendment and solar radiation

4.1 Abstract

Methyl chloride (CH_3Cl) and methyl bromide (CH_3Br) are major carriers of atmospheric bromine and chlorine, respectively, which can catalyze ozone depletion in the stratosphere. However, in our current understanding, there are missing sources associated with these two species. Here we investigate the effect of Cu(II) on CH_3Cl and CH_3Br production from soil, seawater and model organic compounds: catechol (benzene-1,2-diol) and guaiacol (2-methoxyphenol). We show that copper sulfate ($CuSO_4$), in conjunction with either hydrogen peroxide (H_2O_2) or solar radiation, significantly enhances CH_3Cl and CH_3Br production rates from the soil and seawater. This represents a novel abiotic production pathway of CH_3Cl and CH_3Br perturbed by anthropogenic application of Cu(II). Hence, we suggest that the widespread application of copper-based pesticides, herbicides and fungicides in agricultural fields or water bodies and the discharge of anthropogenic Cu to the oceans may increase the regional atmospheric concentrations of CH_3Cl and CH_3Br and account for part of their missing global sources.

4.2 Introduction

Methyl chloride (CH_3Cl) and methyl bromide (CH_3Br) are the most abundant brominated and chlorinated hydrocarbons in the atmosphere (Carpenter et al., 2014). They have average tropospheric lifetimes of 0.9 and 0.8 years (Carpenter et al., 2014), respectively, which are longer than the typical time scale of transport across tropical tropopause to the stratosphere (Levine et al., 2007). Thus, atmospheric CH_3Cl and CH_3Br can reach up to the lower stratosphere and disassociate chlorine and bromine radicals to catalyze stratospheric ozone depletion. At present, the sizes of identified sources of CH_3Cl and CH_3Br are smaller than those of the quantified sinks with a -748 Gg $year^{-1}$ imbalance for CH_3Cl and a -39 Gg $year^{-1}$ imbalance for CH_3Br, respectively (Carpenter et al., 2014). These significant discrepancies and uncertainties need to be resolved to better understand their roles in stratospheric chemistry and to predict ozone recovery in the future. Since the implementation of the Montreal Protocol, anthropogenic sources of listed ozone-depleting substances (ODSs), including CH_3Br, have been largely restricted (Carpenter et al., 2014). It is believed that present atmospheric CH_3Cl and CH_3Br originate from predominantly natural sources. Human influences on terrestrial sources, such as biomass burning (Andreae, 2019; Mead et al., 2008), global warming (Smythe-Wright et al., 2006; W. Zhang et al., 2020), sea level rise (Jiao et al., 2018; Wang et al., 2016), agricultural cultivation (Jiao et al., 2020; Mead et al., 2008), land use change (Deventer et al., 2018),

are becoming ever larger challenges for the recovery of stratospheric ozone (Fang et al., 2019; Liang et al., 2017), together with the non-compliant anthropogenic sources (Montzka et al., 2018; Rigby et al., 2019).

Among the known sources and sinks of CH_3Cl and CH_3Br, soil is believed to be an important bi-directional interface with simultaneous abiotic production (Keppler et al., 2000; Wishkerman et al., 2008) and biotic degradation (Hines et al., 1998; Shorter et al., 1995). Within the soil, abiotic Fenton-like reactions that involve Fe(III) oxidizing organic matter in the presence of halide ions are responsible for the production of methyl halides (Keppler et al., 2000; Wishkerman et al., 2008). This pathway is believed to be ubiquitous and make a significant contribution to the global methyl halide budgets. It is reasonable to postulate that the Fenton-like mechanism may be catalyzed by other transition metal ions, such as copper(II). A setting where copper might be present in abundance is in agriculture, where copper-based fungicides, such as copper(II) sulfate, are widely used globally, especially in the fields of rice, oranges, walnuts, and grapes (Epstein & Bassein, 2001; California Department of Pesticide Regulation, 2019). In 2008, copper compounds accounted for 17% (the second most) of total fungicides applied in the U.S. agriculture (Fernandez-Cornejo et al., 2014). In California in 2017, approximately 3.7×10^6 kg of copper-based pesticides were applied to over 1.0×10^4 cumulative km^2 of agricultural land (California Department of Pesticide Regulation, 2019), while roughly 1.15×10^{11} kg of copper (II) sulfate were used as fungicide, herbicide, or pesticide each year worldwide, in addition to smaller quantities of other copper compounds.

In this study, soil, seawater and model compounds of organic carbon were incubated with different copper treatments and methyl halide production rates were measured, aiming to (1) determine the effect of copper compounds on methyl halide formation; (2) elucidate the copper-catalyzed halocarbon production mechanism, and (3) determine if the application of copper pesticides and fungicides in agriculture could impact the atmospheric methyl halide budgets.

4.3 Materials & Methods

4.3.1 Experimental procedure

Three sets of experiments were conducted. The first set involved incubation of soil samples either unamended conditions or with chemical reagent supplements, such as copper(II) sulfate ($CuSO_4$) or hydrogen peroxide (H_2O_2) or both, to investigate the impact of Cu(II) amendments on the production of methyl halides in soils. The second set of measurements involved incubations of solutions with catechol (benzene-1,2-diol) and guaiacol (2-methoxyphenol), compounds with (methoxy-) phenolic structures. These organic compounds are used as chemical models for natural organic matter in soil (Keppler et al., 2000; Krause et al., 2014), and the stepwise addition of reagents to these solutions elucidate the conditions required for methyl halide formation. The third set involved

incubation of seawater samples under different conditions: Cu(II) *vs.* no Cu(II) amendment, and light *vs.* dark. All three sets of incubations followed the same experimental set-up, as described in 4.3.5.

4.3.2 Soil sample reactions

4.3.2.1 Soil sample preparation

Surface soil was collected from the Oxford Tract (37°52'34"N 122°16'02"W), an agricultural research facility of the University of California, Berkeley. The soil type was a Tierra (Fine, montmorillonitic, thermic Molloc Palexerafls) - Urban land complex with a clay loam texture. Before incubation, rocks and visible litter were removed, and the soil was sieved through a 2 mm standard test sieve (Fisher Scientific Company, New Hampshire, U.S.) to homogenize its texture. The soil was sealed and stored at about 5 °C and incubated within six months of collection. Part of the soil samples were oven-dried at 60°C until constant weight to calculate soil water content based on the weight loss.

4.3.2.2 Incubation of soil with chemicals.

Live soil study. For each live soil experiment, 50 g (dry weight) of soil sample ("live") and 20 ml of deionized water were mixed and incubated following the method as described in section 2.5, from which the background production rate was inferred.

Sterilized soil experiments. To differentiate between microbial and abiotic geochemical processes on methyl halide production and degradation (Keppler et al., 2000), a parallel set of soil samples was autoclaved at 105º C overnight and then incubated in the same way as the live experiment.

Mineral soil experiments. To prepare mineral soil, organic matter content was depleted using the "loss on ignition" method: oven-dried soil samples were sieved through a 2 mm mesh and then heated in a furnace at 375 °C for 24 hours to combust the soil organic matter. The resulting mineral soil samples (5g of each) were then incubated to determine the essential role of natural organic matter in methyl halide formation (Figure 4.1).

Cu(II) addition experiments. To examine the effect of Cu(II) on methyl halide production, 50 g (dry weight) of soil sample was mixed with 10 mL of solution containing $CuSO_4$ at 0 mM (water only) or 50 mM, within 30 minutes prior to incubation.

Hydrogen peroxide (H_2O_2) addition experiments. In conjunction with the Cu(II) addition experiments, an additional 10 mL of solution containing H_2O_2 at 0 mM (water only) or 50 mM was injected into the mixture within 30 minutes prior to the incubation to examine the influence of H_2O_2 on methyl halide production.

Time series experiments. To examine the response rate, persistence and renewal ability of Cu(II) on soil methyl halide production, a time series experiment was conducted

as follows: autoclaved soil samples were first incubated under control conditions, and then 10 ml of copper sulfate ($CuSO_4$) solution at 1.25 mM was added followed by daily measurements over an 8-day period. On the 9th day after the initial $CuSO_4$ supplement, another dose of $CuSO_4$ (10 ml at 1.25 mM) was added.

Figure 4.1 Picture of an exemplary set of mineral soil (left) and autoclaved soil (right) samples used in this study. The reddish-brown color of the mineral soil indicated the majority organic matters were depleted after the "Loss on Ignition" combustion process.

4.3.3 Model substance reactions

4.3.3.1 Chemicals

The following chemicals were used in the experiments of model substance of organic matter reactions: catechol, $C_6H_4(OH)_2$ (≥ 99%, Sigma-Aldrich); guaiacol, $C_6H_4(OH)(OCH_3)$ (≥ 99%, Sigma-Aldrich); potassium chloride, KCl (≥ 99.0%, Sigma-Aldrich), potassium bromide, KBr (≥ 99.0%, Sigma-Aldrich); hydrogen peroxide, H_2O_2 (35%, Acros Organics - Thermo Fisher Scientific); copper(II) sulfate, $CuSO_4$ (≥ 99.99%, Sigma-Aldrich), iron(III) sulfate, $Fe_2(SO_4)_3$ (97%, Sigma-Aldrich).

All the chemicals above were prepared as solutions with deionized water (Ultra-pure type I, ChemWorld) and stored in volumetric flasks. Catechol and guaiacol were configured at 10 mM (millimole per liter; same hereafter); KCl and KBr were configured

at 20 mM; $CuSO_4$ and H_2O_2 were configured at 50 mM. Because each $Fe_2(SO_4)_3$ molecule can dissociate into two Fe^{3+} ions, $Fe_2(SO_4)_3$ was configured at 25 mM to get the same ion concentration as the Cu(II) solution.

4.3.3.2 Incubation of model substances

Control experiments. control experiments were conducted with a mixture of 10 ml of 10 mM catechol, 20 ml water and 10 ml of 20 mM KCl for CH_3Cl studies or 20 mM KBr for CH_3Br studies.

Concentration of hydrogen peroxide (H_2O_2). 10ml of 50 mM $CuSO_4$ solution was added to the control mixture. In order to investigate the response of methyl halide formation to varied oxidizing environments, 10 ml of H_2O_2 solution at 0 mM, 10 mM, 20 mM, 30 mM, 40 mM and 50 mM were added into the mixture for incubation.

Concentration of copper sulfate ($CuSO_4$). 10ml of 50 mM H_2O_2 was added to the control mixture. To examine the response of methyl halide formation to varied Cu(II) concentrations, 10 ml of $CuSO_4$ at 0 mM, 10 mM, 20 mM, 30 mM, 40 mM and 50 mM were added into the mixture for incubation.

Effect of solar radiation. UV radiation may facilitate the formation of volatile halogenated compounds (Liu et al., 2020; Moore, 2008; Yang et al., 2020) as well as naturally originated H_2O_2 in seawater (Clark et al., 2009). Accordingly, the potential role that solar radiation may play was also tested as follows: a sealed transparent glass jar containing the control mixture was exposed under sunlight for three hours (12:00 – 15:00, 10/23/2019, PDT, sunny day, 37°52'26"N 122°15'34"W) and then brought back to the lab. Subsequently, 10 ml each of either 50 mM H_2O_2 or 50 mM $CuSO_4$ was added into the incubations.

Reactions with another carbon model substance. Guaiacol can be halogenated to produce CH_3Cl catalyzed by Fe(III), without needing sunlight or microbial mediation (Keppler et al., 2000); however, sunlight may replace the role of Fe(III) during this process (Yang et al., 2020). In the proposed mechanism, the aromatic ring remains intact while the methoxy group provides methyl radicals to produce methyl halides. To determine if Cu(II) behaved similarly to Fe(III) in this well-known pathway, two additional sets of experiments were conducted with 10 ml each of 10 mM guaiacol, 20 mM KCl, and either 50 mM $CuSO_4$ or 25 mM $Fe_2(SO_4)_3$.

4.3.4 Seawater sample reactions

4.3.4.1 Seawater sample preparation

Unfiltered seawater samples (n = 20) were collected from the San Francisco Bay (37°51'45"N 122°18'50"W) using glass jars (V ≈ 1.9 L, Ball Corporation, California,

USA). The jars were previously acid washed and then rinsed with deionized water, ethanol, and acetone to ensure purity of the jars. Samples were stored at about 5 °C after collection, prior to the testing.

4.3.4.2 Incubation of seawater with chemicals.

Seawater incubations consisted of 500 mL samples in glass jars, subjected to the following 4 treatments: dark control (n = 2), daylight control (n = 5), dark Cu(II) addition (n = 7), and daylight Cu(II) addition. The dark control experiment entailed storing the sample unsealed for 1.5 hours in a dark environment. The daylight control experiment entailed storing the sample unsealed for 1.5 hours under ambient light (noontime, sunny day). The Cu(II) incubations entailed the addition of 0.3 mg $CuSO_4$ to the seawater, which were mixed and dissolved in the solution, before situating under dark or light conditions. Immediately following the above treatments, the seawater samples were incubated following the method described in Section 4.3.5.

4.3.5 Incubations & halocarbon analysis

For all incubations, the soils, seawater, or chemical mixtures were mixed well in glass jars, which were then situated in a thermostatted bath of circulating water and ethylene glycol mixture (VWR Model 1180S, Pennsylvania, USA) at 20 °C. The jars were connected to a coiled pre-evacuated stainless-steel tube (14.5 mL), which served as a sampling volume. Headspace air samples from the jars were drawn at 30 min intervals into a cryotrap, followed by desorption, cryofocusing, and injection into a gas chromatograph-mass spectrometer (Agilent 6890N/5973, Agilent Technologies, California, USA) for analysis of methyl halide concentrations. Emission rates from the samples were calculated based on the change in headspace concentration over time. At least two ($n \geq 2$) incubations were conducted for each treatment of the chemical mixtures or soils.

Weekly calibration curves were constructed using whole ambient air standards collected at Niwot Ridge, Colorado, and calibrated at the Global Monitoring Division Laboratory of the National Oceanographic and Atmospheric Administration. Each calibration curve was made up of 10-18 data points by trapping various volumes of standard gas to capture the full range of chromatogram peak areas observed in the samples. The daily drift of instrumental signals was also corrected using multiple daily runs of the same standard.

4.4 Results & Discussion

4.4.1 Methyl halide production in soil

The incubations of live, autoclaved and mineral soil samples showed methyl chloride (CH_3Cl) fluxes of -1.8 ± 0.8, 3.3 ± 2.8 and 0.3 ± 1.4 nmol kg^{-1} d^{-1}, respectively; and methyl bromide (CH_3Br) fluxes of -0.01 ± 0.03; 0.11 ± 0.10; 0.01 ± 0.00 nmol kg^{-1} d^{-1}, respectively, switching from methyl halide net sinks to net sources after sterilization and then declining to near zero after depletion of organic matter (Figure 4.2). These results are consistent with the conventional idea that soils act as a bi-directional interface for methyl halides with simultaneous microbial degradation and abiotic production (Jiao et al., 2018; Keppler et al., 2005; W. Zhang et al., 2020), and that soil organic matter is an essential substrate for the formation of methyl halides.

Addition of copper(II) sulfate ($CuSO_4$) at different dosages yielded enhancements in CH_3Cl and CH_3Br production rates from both live and autoclaved soil samples, and the increments were positively correlated to the amount of $CuSO_4$ added (Figure 1, Spearman's rank correlation, $r > 0.91$, $p < 0.05$). No such trend was observed from the organic matter-depleted mineral soil. Notably, the production of CH_3Br was roughly 10 times that of CH_3Cl, despite Cl^- being 100 times more abundant than Br^- in the soils.

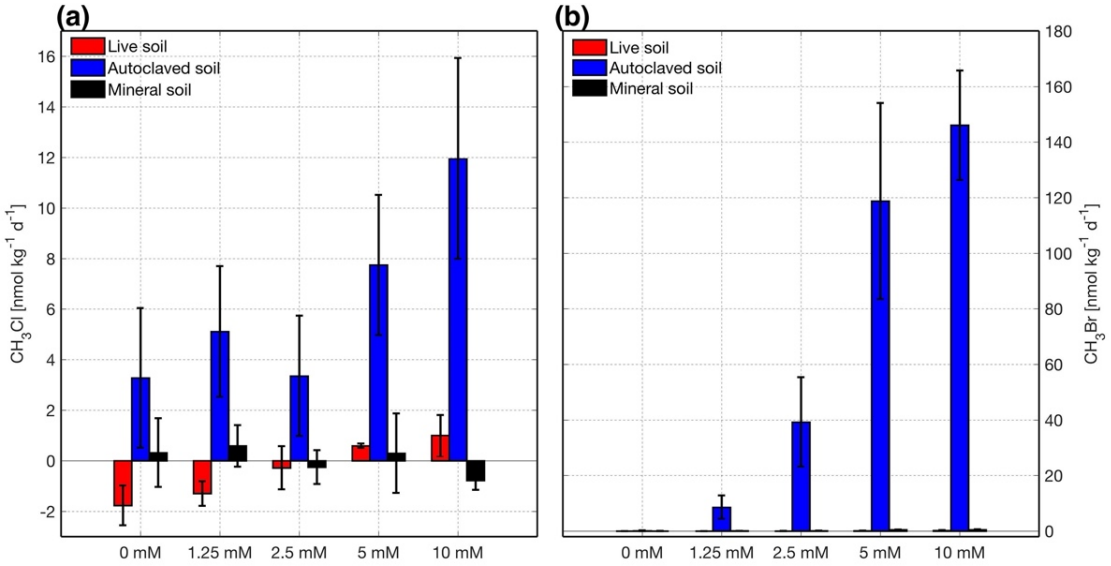

Figure 4.2 (a) Methyl chloride (CH_3Cl) and (b) methyl bromide (CH_3Br) production rates from live, autoclaved and mineral soil samples mixed with 10 ml of different concentrations of $CuSO_4$ solution. Each incubation had two replicates (n = 2).

It has been previously demonstrated that halide ions can be alkylated to produce volatile halogenated carbons when soil or sediment organic matter is oxidized by Fe(III) (Keppler et al., 2000) without the mediation by sunlight or microbial activities. Therefore, it is postulated here that Cu(II), as an electron acceptor, may also oxidize organic matter during the halogenation process to produce volatile methyl halides in a similar manner as Fe(III). The lack of production in mineral soils demonstrates the need for organic matter in the formation of methyl halides and that atmospheric CO_2 is not used as the carbon source.

The increases in methyl halide production rates from the copper-supplemented autoclaved soil samples were much larger than those in live soil samples. For example, CH_3Cl fluxes from live soil samples gradually switched from -1.8 ± 0.8 to 1.0 ± 0.8 nmol kg^{-1} d^{-1}, while emissions from autoclaved soils increased from 3.3 ± 2.8 to 12.0 ± 4.0 nmol kg^{-1} d^{-1} as the Cu(II) addition increased from 0 mM to 10 mM. For CH_3Br fluxes, they shifted from -0.01 ± 0.03 to 0.17 ± 0.14 nmol kg^{-1} d^{-1}, and from 0.11 ± 0.10 to 146.07 ± 19.69 nmol kg^{-1} d^{-1}, respectively. These results are consistent with the deactivation of methyl halide-consuming microorganisms following heat treatment (Rhew et al., 2003), such that the autoclaved soil creates a one-way interface of CH_3Cl and CH_3Br emissions. Alternatively, it is possible that thermal treatment promoted the fracture of humic substances in soil (Fang et al., 2005; Furutani et al., 2017; Lomnicki et al., 2008; Ormond et al., 2018), making the organic carbon more readily available for the formation of volatile halogenated compounds.

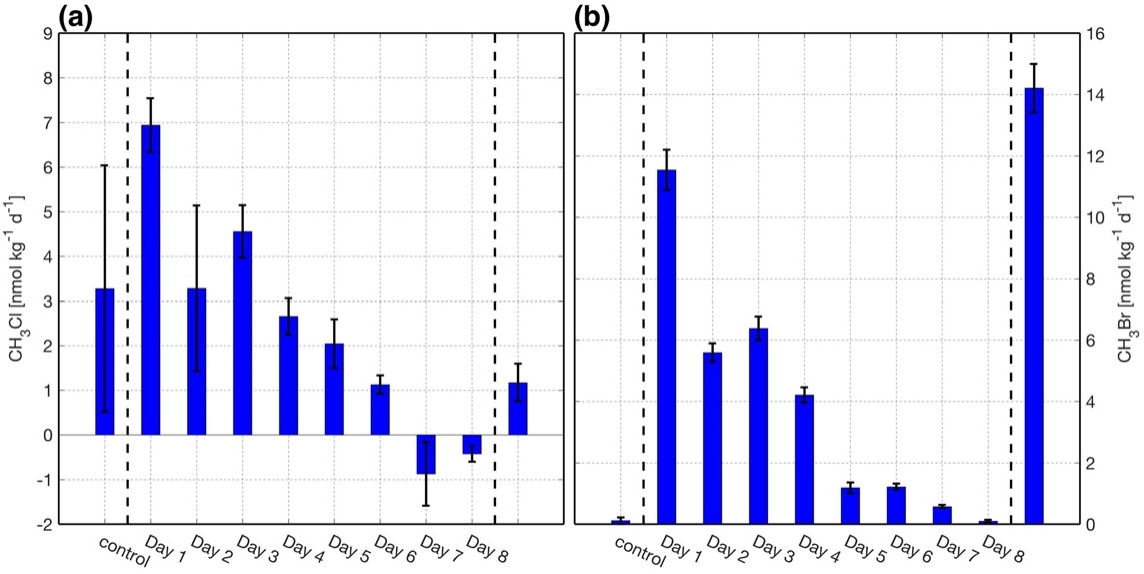

Figure 4.3 (a) Methyl chloride (CH_3Cl) and (b) methyl bromide (CH_3Br) production rates over time from autoclaved soil samples. On day 0, soils are incubated under control conditions and then 10 ml of $CuSO_4$ solution at 1.25 mM are added on day 1. Daily incubations are conducted for 8 days, and on the 9th day after the initial $CuSO_4$ supplement, another 10 ml of $CuSO_4$ at 1.25 mM was added.

The time series experiments showed that the production rates of CH_3Cl and CH_3Br were highest immediately following the addition of $CuSO_4$, and then declined to negligible levels over the following week (Figure 4.3). Net CH_3Cl fluxes turned negative by day 7, indicating net consumption. Studies have shown some soil microorganisms can form dormant spores to survive thermal sterilization and begin to germinate for proliferation as fast as within ten days after the initial thermal perturbation (Bárcenas-Moreno et al., 2011; Jurburg et al., 2017). Therefore, the phenomenon that the soil samples switched from CH_3Cl sources to sinks on the 7th day after Cu(II) application might be attributable to the re-habitation of methyl halide-consuming microbial communities which consume CH_3Cl more readily than CH_3Br given ambient concentrations (Zhang et al., 2012). On the other hand, the depletion of Cu(II) may also contribute to the decline of CH_3Cl and CH_3Br production. Hence, CH_3Cl and CH_3Br were produced again when another 10 ml of $CuSO_4$ was added on the 9th day, although the CH_3Cl production rate increased by only about 17 ± 6% of the day 1 emission rate.

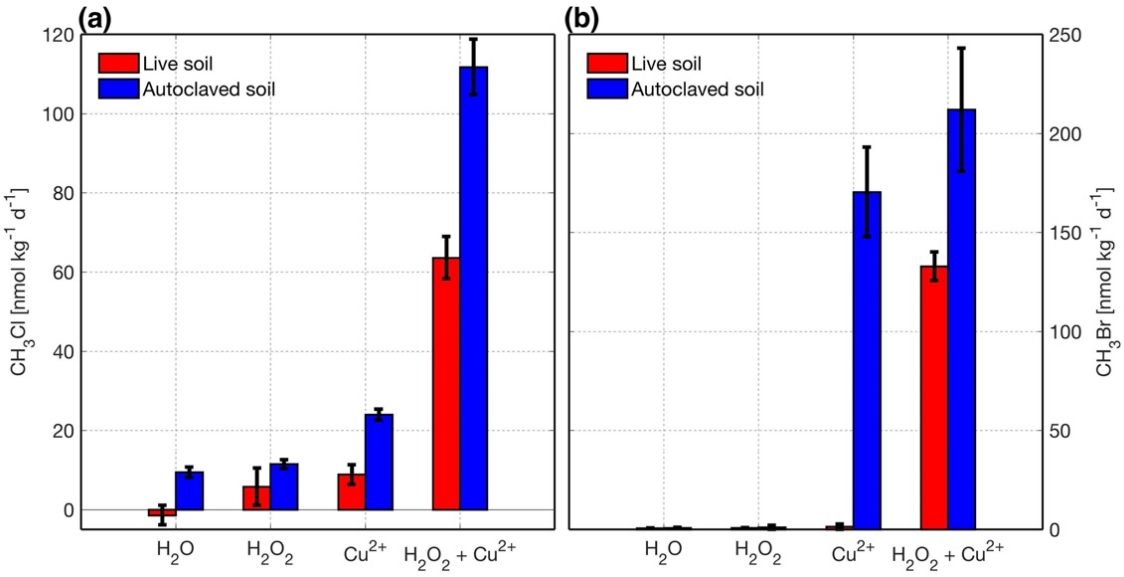

Figure 4.4 (a) Methyl chloride (CH_3Cl) and (b) methyl bromide (CH_3Br) production rates from live and autoclaved soil samples under different amendments: (a) 10 ml of deionized water was added; (ii) 10 ml of 50 mM H_2O_2 was added; (iii) 10 ml of 50 mM $CuSO_4$ was added; (iv) 5 ml each of 50 mM H_2O_2 and 50 mM $CuSO_4$ at were added. Each incubation had two replicates (n = 2).

The addition of H_2O_2 to soils also enhanced methyl halide production in both live and autoclaved soils (Figure 4.4). However, the observed enhancements in emissions were not as large as those caused by the addition of Cu(II) to soils. The addition of H_2O_2

amplified the effect of Cu(II) on CH_3Cl and CH_3Br production in both live and autoclaved soil samples (Figure 4.4). Compared to experiments with Cu(II) addition only, the amendment of both H_2O_2 and Cu(II) increased the production rates of CH_3Cl and CH_3Br (despite only half of the copper addition) by 8.1 folds and 94.9 folds, respectively, in live soils; and by 4.9 folds and 1.2 folds, respectively, in autoclaved soils. The effect on methyl halide production enhancements from the combination of H_2O_2 and Cu(II) was also much larger than H_2O_2 only despite having only half of the H_2O_2 addition. It is postulated that the combination of Cu(II) and H_2O_2 produced hydroxyl radicals (•OH) (Perez-Benito, 2001), which is a powerful, nonspecific oxidant agent. Subsequently, the •OH radicals react with both organic compounds and/or halide ions to enhance the copper-mediated reaction to form volatile organochlorine compounds, such as CH_3Cl and CH_3Br.

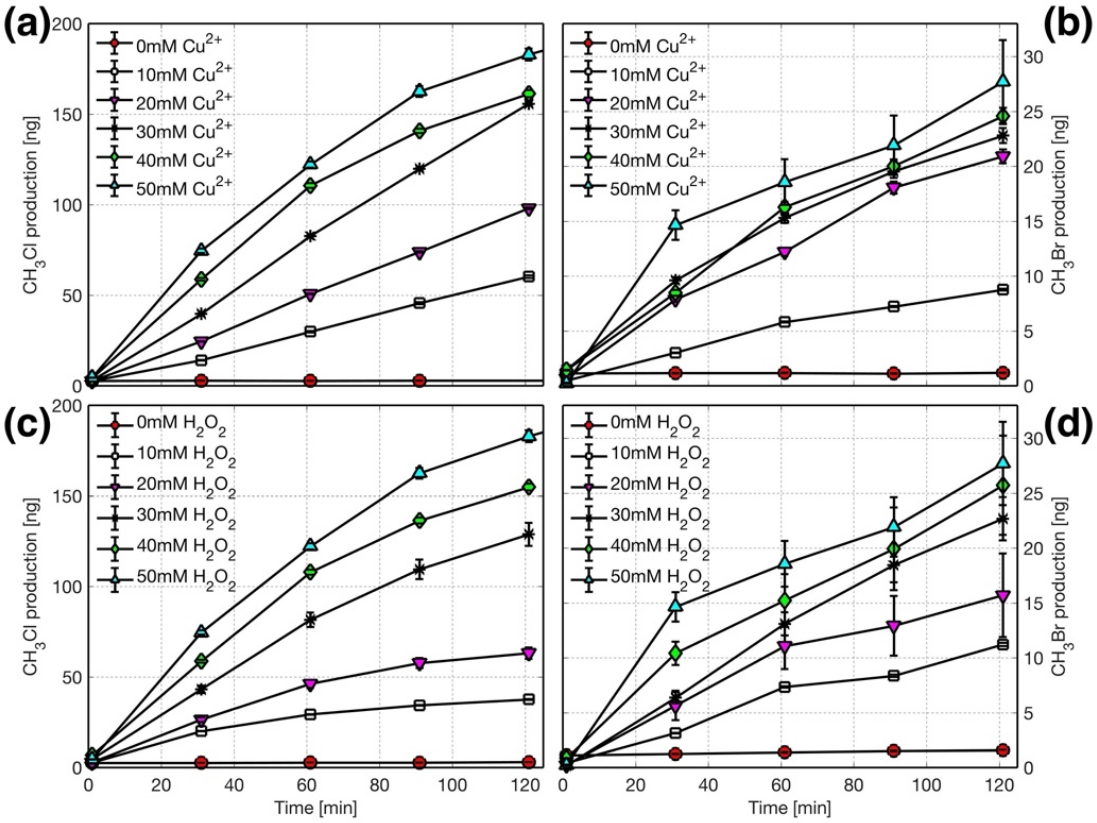

Figure 4.5 Methyl chloride (CH_3Cl) and methyl bromide (CH_3Br) production over time from different chemical mixtures: (a) 10 ml each of 10 mM catechol, 20 mM KCl, 50 mM H_2O_2, and $CuSO_4$ at concentrations of 0 mM, 10 mM, 20 mM, 30 mM, 40 mM and 50 mM; (b) 10 ml each of 10 mM catechol, 20 mM KBr, 50 mM H_2O_2, and $CuSO_4$ at concentrations of 0 mM, 10 mM, 20 mM, 30 mM, 40 mM and 50 mM; (c) 10 ml each of 10 mM catechol, 20 mM KCl, 50 mM $CuSO_4$, and H_2O_2 at concentrations of 0 mM, 10 mM, 20 mM, 30 mM, 40 mM and 50 mM; (d) 10 ml each of 10 mM catechol, 20 mM KBr, 50 mM $CuSO_4$, and H_2O_2 at concentrations

of 0 mM, 10 mM, 20 mM, 30 mM, 40 mM and 50 mM. Each incubation had two replicates (n = 2).

4.4.2 Model reactions with catechol

Catechol (benzene-1,2-diol) is often used as a model substance of monomeric phenols that are commonly formed during the microbial degradation of many naturally occurring and anthropogenic aromatic substances, and it is regarded as a precursor of soil humic substances (Butenschoen et al., 2009). Hence, catechol was used to elucidate abiotic chemical reactions, in the absence of soil microbes, or complex soil organic matter in soils that may be chemically altered during the autoclaving process.

Water solutions containing only catechol (10 mM), KCl or KBr (20 mM), $CuSO_4$ (50 mM) and H_2O_2 (50 mM) produced large amounts of CH_3Cl and CH_3Br (Figure 4.5) associated with abrupt color change from clear to brownish. Emission rates increase with increasing concentrations of $CuSO_4$ (Figure 4.5a and 4.5b) and H_2O_2 (Figure 4.5c and 4.5d). However, the omission of any one of these four species prevented significant formation of CH_3Cl or CH_3Br (Figure 4.5). The solutions change color to a dark brown with the addition of both $CuSO_4$ and H_2O_2 to the catechol/halide mixture, with visible precipitates (Figure 4.7). A range of organic and inorganic compounds are detected in this mixture (Table 4.2).

A series of trace-addition experiments was designed to further test the essentiality of Cu(II) and H_2O_2 in the formation of CH_3Cl and CH_3Br. As shown in Figure 4.6, a mixture of catechol, KCl/KBr, and either $CuSO_4$ or H_2O_2 was incubated for 90 minutes, and at the 91st minute, 1 ml of either 50mM $CuSO_4$ or 50mM H_2O_2 was injected into the mixture, which was further incubated for another 90 minutes. Before the 92nd minute, the clear solution became yellowish. A rapid accumulation of CH_3Cl or CH_3Br was also observed after the injection of the fourth compound, further proving that both Cu(II) and H_2O_2 were involved in this mechanism of methyl halide production.

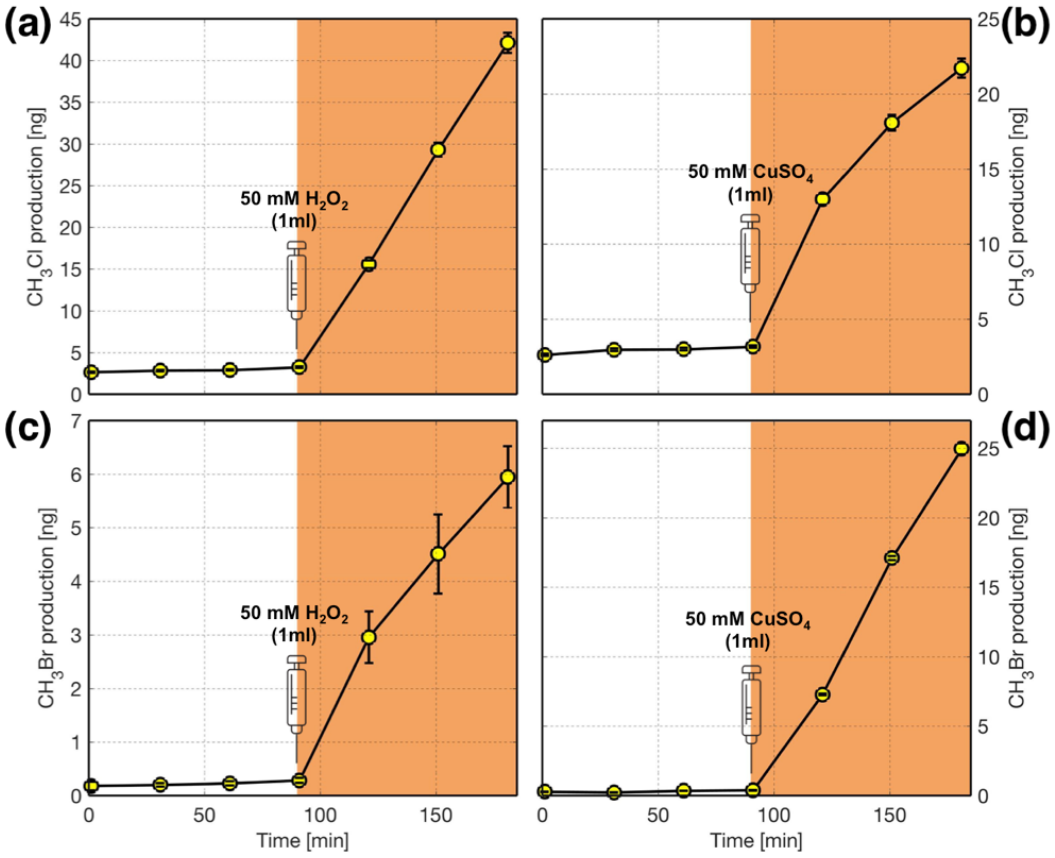

Figure 4.6 Methyl chloride (CH_3Cl) and methyl bromide (CH_3Br) production over time from (a) a mixture of 10 ml each of catechol at 10 mM, KCl at 20 mM, and $CuSO_4$ at 50 mM; (b) a mixture of 10 ml each of catechol at 10 mM, KCl at 20 mM, and H_2O_2 at 50 mM; (c) a mixture of 10 ml each of catechol at 10 mM, KBr at 20 mM, and $CuSO_4$ at 50 mM; (d) a mixture of 10 ml each of catechol at 10 mM, KBr at 20 mM, and H_2O_2 at 50 mM. As indicated in the plot, 1 ml of H_2O_2 or $CuSO_4$ at 50 mM was injected into the mixture at the 91st minute. Each incubation had two replicates (n = 2). The brownish background color also represents the color change of the chemical mixtures.

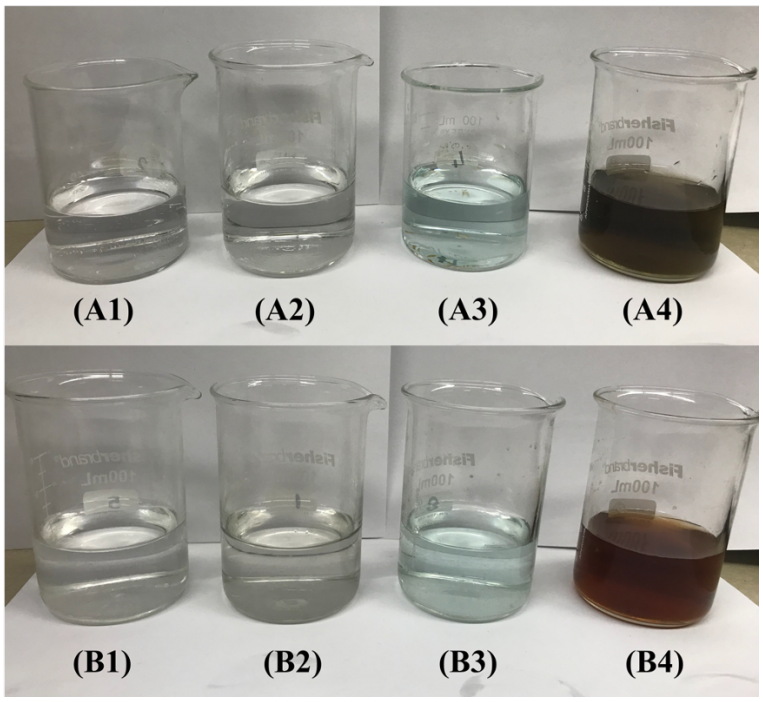

Figure 4.7 Pictures of the chemical mixtures after 2 hours of reaction at room temperature (~20° C). The configurations of the chemical mixtures were: (A1) 10 ml 10 mM catechol (benzene-1,2-diol), 10 ml 20 mM KCl, 20 ml H_2O; (A2) 10 ml 10 mM catechol, 10 ml 20 mM KCl, 10 ml 50 mM H_2O_2, 10 ml H_2O; (A3) 10 ml 10 mM catechol, 10 ml 20 mM KCl, 10 ml 50 mM $CuSO_4$, 10 ml H_2O; (A4) 10 ml 10 mM catechol, 10 ml 20 mM KCl, 10 ml 50 mM H_2O_2, 10 ml 50 mM $CuSO_4$; (B1) 10 ml 10 mM catechol, 10 ml 20 mM KBr, 20 ml H_2O; (B2) 10 ml 10 mM catechol, 10 ml 20 mM KBr, 10 ml 50 mM H_2O_2, 10 ml H_2O; (B3) 10 ml 10 mM catechol, 10 ml 20 mM KBr, 10 ml 50 mM $CuSO_4$, 10 ml H_2O; (B4) 10 ml 10 mM catechol, 10 ml 20 mM KBr, 10 ml 50 mM H_2O_2, 10 ml 50 mM $CuSO_4$.

4.4.3 Sunlight effect

The experiments described so far showed that the addition of $CuSO_4$ invokes a positive methyl halide flux from the soil to the air, indicating possible production of methyl halides from the reaction with $CuSO_4$. However, $CuSO_4$ alone does not drive this reaction forward significantly; rather, Cu(II) works in conjunction with other oxidizing agents, such as H_2O_2, to increase the rate of methyl halide production.

In natural ecosystems, the formation of H_2O_2 in the water or soil results principally from exciting humic substances by UV radiation of sunlight (Clark et al., 2009; Zhang et al., 2012). Therefore, light experiments were conducted with both catechol and guaiacol to test a potential photochemical pathway involving ambient sunlight. Results showed rapid production rates of CH_3Cl and CH_3Br occurred when the chemical solutions with Cu(II)

were exposed to sunlight (Figure 4.8). The omission of either Cu(II) or sunlight exposure yielded little to no production of CH_3Cl and CH_3Br, indicating a likely photochemical production pathway.

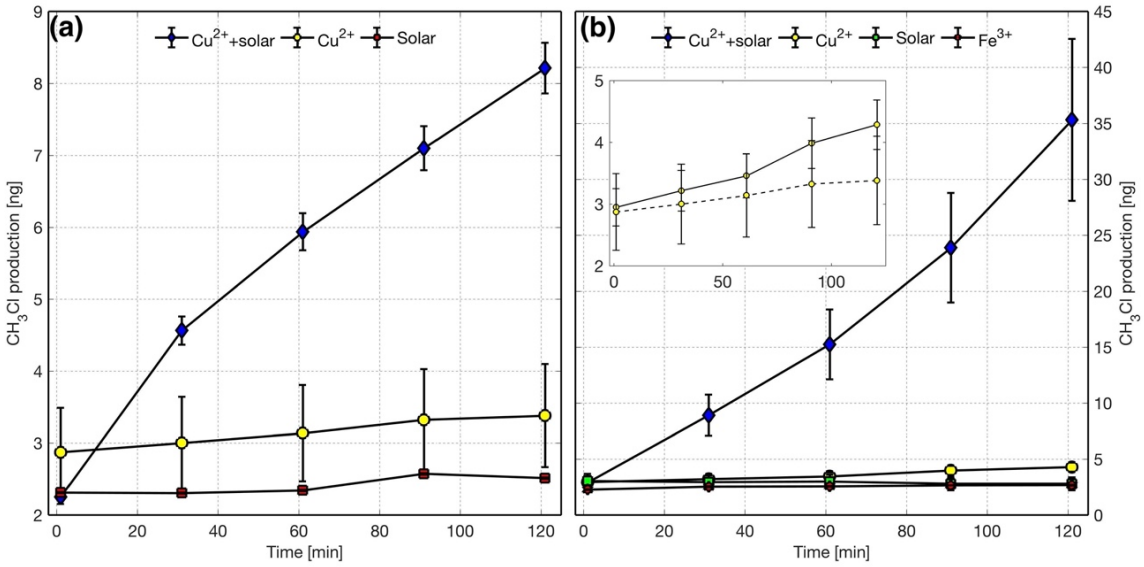

Figure 4.8 Methyl chloride (CH_3Cl) production over time from mixtures of 10 ml each of (a) catechol or (b) guaiacol at 10 mM and KCl at 20 mM. For subsample (i), 10 ml of $CuSO_4$ at 50 mM was added; subsample (ii) was exposed to sunlight for three hours before the start of the incubation; and subsample (iii) was both exposed under sunlight as (ii) and 10 ml of $CuSO_4$ at 50 mM was added. In order to compare the effect between Cu (II) and Fe (III), another subsample of guaiacol had 10 ml of $Fe_2(SO_4)_3$ at 50 mM added. The inset plot in (b) shows the comparison between the effect of Cu (II) on catechol and guaiacol on an enlarged scale. Each incubation had two replicates (n = 2).

4.4.4 Methyl halide production in seawater

Seawater produced relatively small amounts of CH_3Cl or CH_3Br under dark or light conditions, in comparison to the copper addition treatment. The treatment, with both copper sulfate amendment and exposure to ambient sunlight showed the greatest positive average flux for both CH_3Cl and CH_3Br (Figure 4.9), while samples undergoing other treatments displayed relatively smaller fluxes. Similar to the results of model compound incubations, CH_3Cl and CH_3Br productions were contingent upon the presence of both Cu(II) and sunlight.

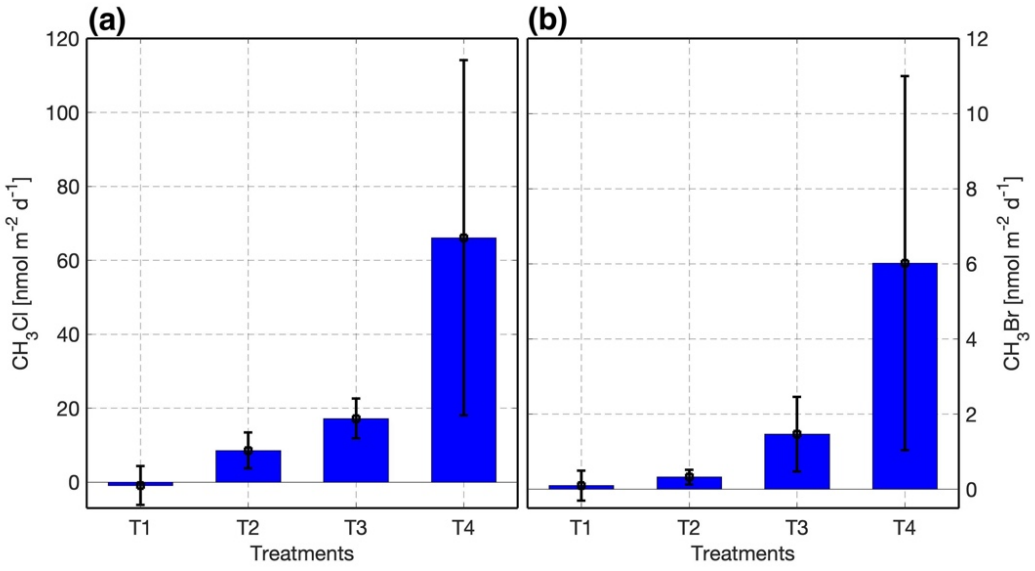

Figure 4.9 (a) Methyl chloride (CH_3Cl) and (b) methyl bromide (CH_3Br) production rates from the ocean water under different treatments: (T1, n = 2) seawater incubated under ambient sunlight; (T2, n = 5) seawater incubated under dark condition; (T3, n= 7) seawater with Cu (II) amendment incubated under dark condition; (T4, n = 4) seawater with Cu (II) amendment incubated under ambient sunlight.

Considering the greater CH_3Cl and CH_3Br flux measurements in samples with copper sulfate and sunlight, the implication of sunlight as a driver for the reaction is highly plausible. Many anthropogenic pathways for copper discharge to the oceans exist, with copper leaching from boat antifouling paint and aquaculture nets, copper residue from automobile brake pads in urban runoff being the primary routes, atmospheric aerosol deposition (Davis et al., 2001; Mahowald et al., 2018). Therefore, this study revealed a previously unaccounted for, primarily anthropogenic driven methyl halide source from the interaction of copper, sunlight and dissolved organic matter.

A few studies have proven the importance of UV irradiation in the production of methyl halides (Liu et al., 2020; Moore, 2008; Richter & Wallace, 2004; Yang et al., 2020). For example, it is reported that UV irradiation can catalyze the reaction between dissolved organic carbon and chlorine in seawater to generate CH_3Cl (Moore, 2008; Yang et al., 2020), based on experiments using artificial ultraviolet irradiation ($\lambda = 254$ nm). However, it is noted that solar UV radiation with such a short wavelength would have been absorbed by stratospheric ozone before it can reach ecosystems on earth's surface. Therefore, the pathway proposed in the previous study (Yang et al., 2020) would be plausible in sewage treatment industries only, instead of natural environments. In our sunlight experiments, the UVB ($280 < \lambda < 315$ nm), UVA ($315 < \lambda < 400$ nm), and photosynthetic active radiation (PAR) were attenuated by about 75%, <1%, and 23%, respectively (Table 4.1) by the glass container, suggesting that emissions may be even higher under natural conditions.

Table 4.1 Temperature, UVA ($315 < \lambda < 400$ nm), UVB ($280 < \lambda < 315$ nm) and photosynthetic active radiation (PAR) intensities inside and outside the Manson jar during the light treatment experiments (n = 10).

Attribute	Outside	Inside	Unit	Ratio [in/out]
Temperature	23.14 ± 2.29	27.05 ± 1.33	[°C]	1.17
Ultraviolet A	19393.2 ± 2.0	19393 ± 1.8	[mW m^{-2}]	1.00
Ultraviolet B	126.6 ± 18.52	31.0 ± 5.8	[mW m^{-2}]	0.24
PAR	1273.0 ± 114.2	985.0 ± 139.3	[µmol m^{-2} s^{-1}]	0.77

4.4.5 Reaction with guaiacol and Fe (III)

It has been established that Fe(III) (Keppler et al., 2000) or UV_{254} irradiation (Yang et al., 2020) can foster the reaction between guaiacol and chloride ions to produce CH_3Cl, and the only byproduct of this reaction was 1,2-benzoquinone. The aromatic ring remained intact in this process (Scheme 4.1).

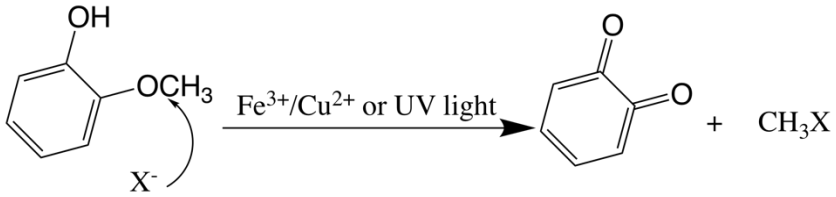

Scheme 4.1 Presumed reaction pathway of guaiacol and halide ions to form methyl halides (Keppler et al., 2000; Yang et al., 2020).

To compare halogenation rates between this study with catechol and Cu (II) and previous studies with guaiacol and Fe (III), parallel experiments were conducted with guaiacol and Fe (III) as well. As shown in the inset plot of Figure 6B, the mixture of guaiacol, KCl, and Cu (II) showed a higher production rate of CH_3Cl than catechol, which may be attributed to the cleavage of $\cdot CH_3$ radical from the methoxy group of guaiacol. The bond dissociation energy (BDE) required to cleave the $\cdot CH_3$ radical from the methoxy group of guaiacol is approximately 247 kJ/mol, the least within the structure. In comparison, the carbon bonds within the aromatic ring could possess up to 611 kJ/mol of BDE. Accordingly, the $\cdot CH_3$ radical from the methoxy group of guaiacol, rather than other aromatic humic substances without methoxy structures, such as catechol, is more readily available to the formation of volatile halogenated compounds through nucleophilic attack of Cl^-.

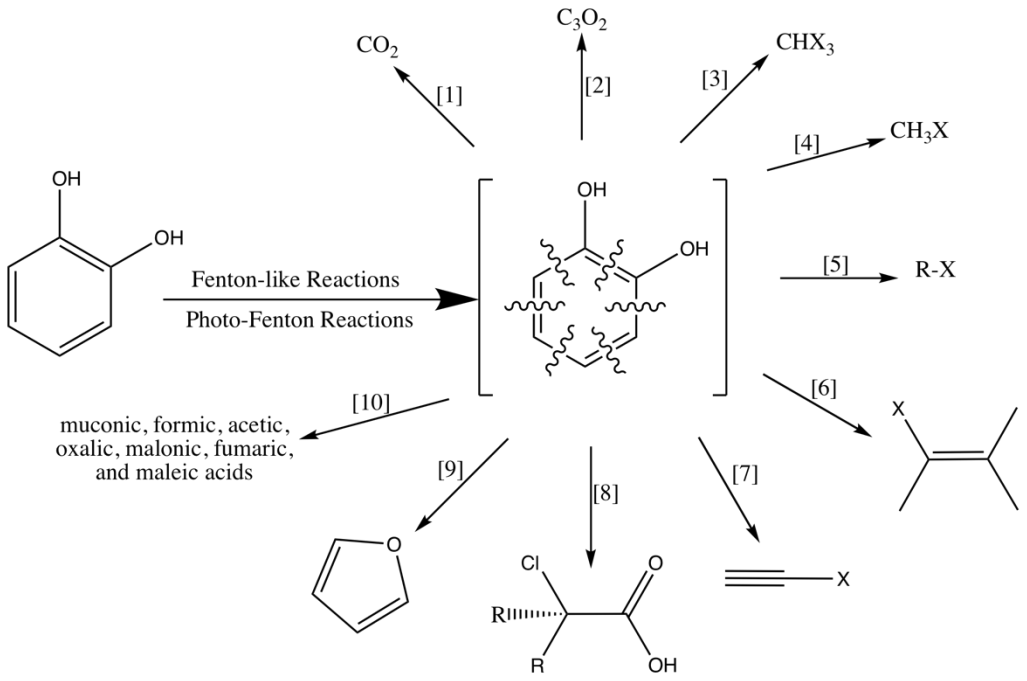

Scheme 4.2 Presumed degradation pathway of catechol in the conditions of Fenton-like or Photo-Fenton reactions to form carbon dioxide (Pracht et al., 2001), carbon suboxide (Huber et al., 2007), trihalomethanes (Huber et al., 2009), methyl halides, chloroethene and other chloroalkanes (Keppler et al., 2002, 2006), chloroethene, chloroethyne (Keppler et al., 2006), chlorinated acetic acid (Althoff et al., 2014; Fahimi et al., 2003), furan (Huber et al., 2010; Krause et al., 2014), and muconic, formic, acetic, oxalic, malonic, fumaric and maleic acids (M'hemdi et al., 2012; Pracht et al., 2001; Studenroth et al., 2013; Zazo et al., 2005). X represent Cl, Br and I (assumed).

To compare halogenation rates between this study with catechol and Cu(II) and previous studies with guaiacol and Fe(III), parallel experiments were conducted with guaiacol and/or Fe(III) as well. As shown in the inset plot of Figure 6B, the mixture of guaiacol, KCl, and Cu(II) actually showed a higher CH_3Cl production rate in comparison to the mixture of guaiacol, KCl, and Fe(III). The mixture of guaiacol, KCl, and Cu(II) also showed a higher production rate of CH_3Cl than the mixture with catechol, which may be attributed to the cleavage of $\cdot CH_3$ radical from the methoxy group of guaiacol. The bond dissociation energy (BDE) required to cleave the $\cdot CH_3$ radical from the methoxy group of guaiacol is approximately 247 kJ/mol (Nowakowska et al., 2018; Yang et al., 2017), the least within the structure. In comparison, the carbon bonds within the aromatic ring could possess up to 611 kJ/mol of BDE. Accordingly, the $\cdot CH_3$ radical from the methoxy group of guaiacol, rather than other aromatic humic substances without methoxy structures, such as catechol, is more readily available to the formation of volatile halogenated compounds through nucleophilic attack of Cl^-.

The mechanism involved in the production of methyl halides from catechol, which has no such methoxy group, must follow a different pathway, whereby the aromatic ring is fractured to provide carbon radicals. Studies have found furans (Huber et al., 2010; Krause et al., 2014), oxalic acid (Studenroth et al., 2013), chloroethyne (Keppler et al., 2006), and other organic acids (M'hemdi et al., 2012) (such as formic acid, muconic acid, maleic acid, malonic acid and acetic acid) as byproducts of the Fenton-like reactions of catechol.

This study found this process also produced chloroform ($CHCl_3$) and CO_2 (Table 4.2), the same as a previous study (Pracht et al., 2001; Huber et al., 2009). The formation of volatile methyl halides suggested this reaction produced $\cdot CH_3$ radicals. While the nature of the intermediates is unknown, it was suggested that Fenton-like or photo-Fenton reactions resulted in multiple ring-opening reactions of catechol (Scheme 4.2), which facilitated the formation of multiple volatile compounds and halogenated organic carbon when halide ions were present.

Table 4.2 Other products detected from the mixture of 10 ml each of 10 mM catechol (benzene-1,2-diol), 20 mM KCl, 50 mM $CuSO_4$ and 50 mM H_2O_2 after 2 hours of reaction, by TOF-MS-ES-, and magnet EI^+. The soluble phase was first extracted by CH_2Cl_2.

Method	**products**	**phase**
laser absorption	CO_2	gaseous
GC/MS	Chloroform ($CHCl_3$)	gaseous
magnet EI^+	furan	soluble
magnet EI^+	tetrahydrofuran	soluble
magnet EI^+	dibutyl phthalate	soluble
magnet EI^+	2-ethyl-1-hexanol	soluble
magnet EI^+	2,4-bis(1,1-dimethylethyl)-phenol	soluble
magnet EI^+	1-(2-hydroxy-6-methoxyphenyl)-ethanone	soluble
magnet EI^+	4'-hydroxy-2,2-dimethylpropiophenone	soluble
magnet EI^+	2,2'-methylenebis[6-(1,1-dimethylethyl)4-ethyl-phenol	soluble
magnet EI^+	7,9-dit-ert-butyl-1-oxaspiro (4,5) deca-6,9-diene-2,8-dione	soluble
TOF MS ES^-	$CuKS_2$	precipitate
TOF MS ES^-	Cu_2S_2	precipitate
TOF MS ES^-	$CuKS_2O_8$	precipitate
TOF MS ES^-	$Cu_2S_2O_8$	precipitate
TOF MS ES^-	$C_7H_6Cu_3K_2S_3$	precipitate
TOF MS ES^-	$C_6H_2O_5Cu_3K_2S_1$	precipitate

This could also potentially help explain the phenomenon observed from the experiments of live and autoclaved soil that the same amount of Cu(II) addition would trigger a higher production rates of methyl halides from the autoclaved soil. The degradation of labile and resistant organic matter respond similarly to increasing temperature (Fang et al., 2005). Thermal decomposition of catechol and other aromatic

compounds also produces a range of C_1–C_6 products, suggesting the existence of thermal-facilitated ring-opening reactions (Furutani et al., 2017; Lomnicki et al., 2008; Ormond et al., 2018). Hence, it is speculated that autoclaved soil had more non-aromatic carbon fragments, which reacted more readily in the production of halogenated volatile compounds.

4.4.6 Implications

This study presents a novel mechanism of methyl halide formation, especially in agricultural fields or water bodies where large amounts of copper pesticides and fungicides were presented. This suggests a strong anthropogenic influence on the abiotic production of methyl halides. Copper sulfate and other copper-based pesticides have been used widely for algal management in rice fields as well as to manage aquatic products in both conventional and organic agriculture (Flemming & Trevors, 1989).

This report suggests that the impact of anthropogenic copper-based applications on atmospheric CH_3Cl, CH_3Br depends on several factors, including sunlight intensity, temperature, soil properties, including organic matter content and structure, and halide content. However, a rough quantification using the molar ratio between Cu(II) amendment and CH_3Cl and CH_3Br produced in the live soil experiments suggests that the global agricultural usage of copper(II) sulfate may yield emissions of CH_3Cl and CH_3Br more than 22.6 ± 6.3 Gg year^{-1} and 6.9 ± 6.2 Gg year^{-1}, respectively. Therefore, the distribution of copper compounds on agricultural fields or copper-containing runoff in coastal or marine systems may have large potential to emit methyl halides. It may alter the local atmospheric composition of methyl halides and account for an important part of the missing global sources of atmospheric methyl halides.

Chapter 5. Conclusion and suggestions for future research

This dissertation presents three case studies investigating and quantifying the emission of halogenated volatile organic compounds (HVOCs) from some natural ecosystems impacted by human activities. Despite the reduced anthropogenic production and emission of the ODS included in the Montreal Protocol, some natural ODS sources, especially those involving ecosystems increased by climate change or anthropogenic activities, may offset some of the achievements on atmospheric halogen load reductions and delay the recovery of stratospheric ozone.

5.1 Major findings of this dissertation

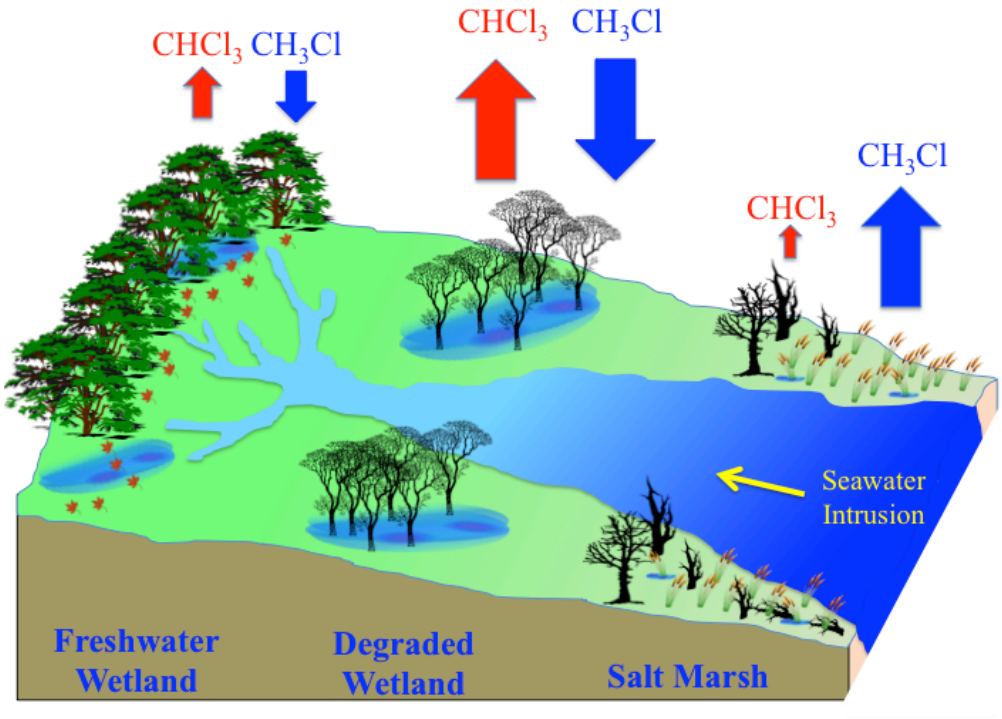

Figure 5.1 A conceptual drawing of chloroform ($CHCl_3$) and methyl chloride (CH_3Cl) fluxes from the gradient of the coastal ecosystems subject to seawater intrusion induced by storm surge and sea level rise.

In the coastal southeastern United States, large areas of tidal freshwater forested wetlands (over 200,000 hectare) represent an intriguing and understudied type of ecosystem. Their position occupying low-lying, coastal areas makes them susceptible to

global climate change phenomena, such as storm surges, sea level rise and associated saltwater intrusion. As a consequence, acute and chronic exposure to different levels of salinity has readily converted some tidal freshwater forested wetlands to degraded forested wetlands, and to salt marshes eventually. Chapter two described a series of HVOC flux measurements along a salinity gradient across the transect of coastal ecosystems in South Carolina: freshwater forested wetland, oligohaline degraded forested wetland and mesohaline salt marshes. The degraded forested wetland showed significant $CHCl_3$ emission rates and remained a net CH_3Cl sink and a negligible CH_3Br source/sink, unlike the saltmarsh which was a significant source for both. Assuming the annually averaged fluxes of $CHCl_3$ (146 ± 129 nmol m^{-2} d^{-1}) and CH_3Cl (-90 ± 61 nmol m^{-2} d^{-1}) observed in this study are representative of coastal degraded forested wetland for the continental United States (1.7×10^{11} m^2), it is estimated that -0.46 ± 0.05 Gg CH_3Cl and 1.06 ± 0.15 Gg $CHCl_3$ are breathed in and out of these ecosystems each year. Sea level rise and frequent storm surges derived from global climate change, in the long term, may increase $CHCl_3$ emissions from coastal degraded forested wetlands and of methyl halides if salt marshes expand, with potential impacts for stratospheric ozone depletion.

Rapeseed (*Brassica napus*) is quantified as the second largest natural terrestrial source of CH_3Br, following salt marshes. In addition, CH_3Cl and CH_3I production rates, two ODS species with shared biogenic production pathways as CH_3Br, had not been measured prior to this work. Increasing demand for canola oil has led to increased cultivation area and harvest mass of *B. napus* globally since 1961. Chapter three describes measured life-cycle fluxes of CH_3Cl, CH_3Br and CH_3I from *B. napus* (cultivar: Empire) with static-chamber enclosures. The results suggested that *B. napus* emitted 5.3 ± 1.3 Gg CH_3Cl $year^{-1}$, 2.8 ± 0.7 Gg CH_3Br $year^{-1}$, and 4.0 ± 0.8 Gg CH_3I $year^{-1}$ as of 2018, which constitute a significant biogenic source of methyl halides to the atmosphere. The geographic distribution of *B. napus* production is mainly in mid-latitudes in the Northern Hemisphere; thus, it represents an important CH_3Br source which probably contributes to the skewed latitudinal profile of atmospheric CH_3Br. Assuming the future global production of *B. napus* follows the same rate of increase as the past 60 years, the atmospheric sources of CH_3Cl, CH_3Br and CH_3I may increase to 13.1 Gg $year^{-1}$, 7.0 Gg $year^{-1}$, and 9.8 Gg $year^{-1}$, respectively by 2050, becoming an ever-larger global source.

In both modern conventional and organic agriculture, copper(II) sulfate is widely used as an active ingredient in fungicides, herbicides and algaecides. Roughly 2.3×10^{11} kg of copper(II) sulfate were used as fungicide, herbicide, or pesticide in 2020 worldwide, in addition to smaller quantities of other copper compounds. Chapter four explored the effect of Cu (II) on CH_3Cl and CH_3Br production from organic matter in soil, ocean water and model organic compounds. The $CuSO_4$, in conjunction with either hydrogen peroxide (H_2O_2) or solar radiation, significantly enhanced CH_3Cl and CH_3Br production rates from the soil or ocean. Thus, this study identifies a new pathway of abiotic methyl halide production occurring in agricultural fields and water bodies that can result from the widespread application of Cu(II)-based pesticides, herbicides and fungicides. A rough quantification suggests this mechanism may yield CH_3Cl and CH_3Br emissions of 22.6 ±

6.3 Gg year^{-1} and 6.9 ± 6.2 Gg year^{-1}, respectively, and account for a significant part of their missing sources. It also suggests that what is currently considered organic produce may have significant atmospheric impacts.

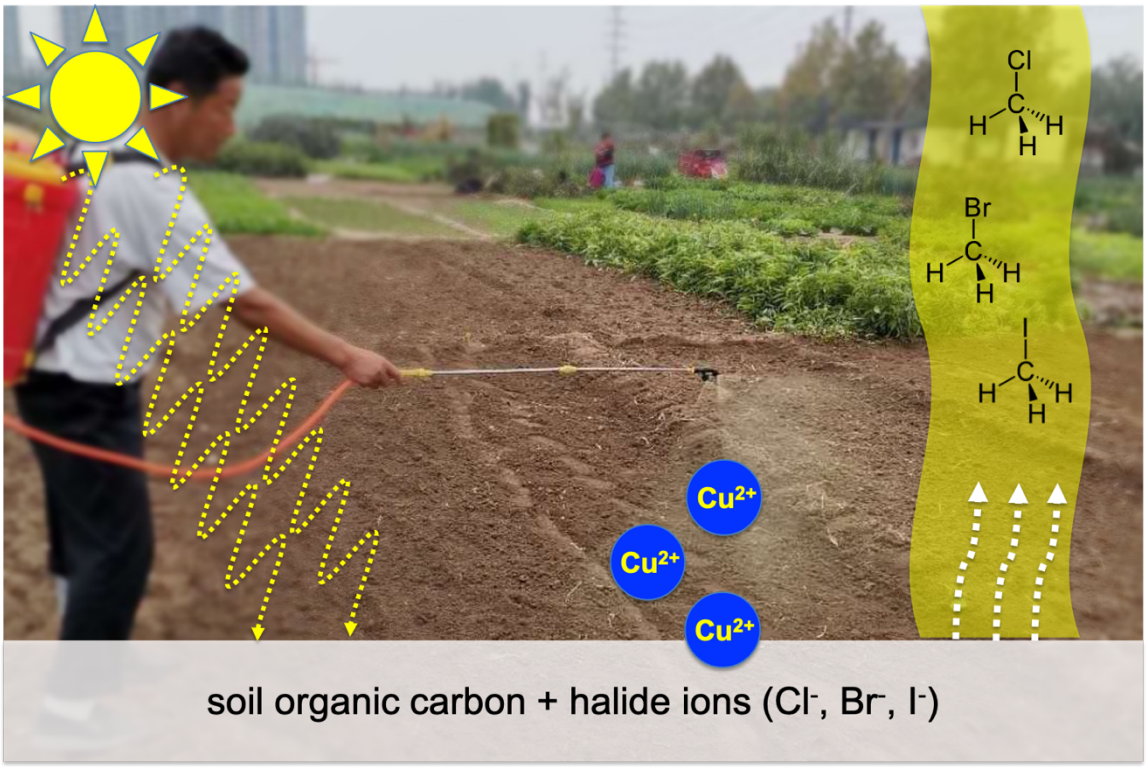

Figure 5.2 A conceptual drawing of potentially ubiquitous production of methyl halide from agricultural soils catalyzed by ambient sunlight and human applied copper-based pesticides, fungicide, and herbicides (photo credit: Yingying Cai, Wanying Zhang).

5.2 Problems unsolved and suggestions for future work

The conclusion of chapter two suffers from the limited number of measurements conducted in coastal forested ecosystems subject to seawater intrusion induced by storm surges and sea level rise. Therefore, a long-term and spatially extended measurement network would better quantify the extent of spiked halocarbon productions and evaluate its impact on atmospheric compositions of halocarbons. Chapter two also proposed an abiotic pathway of $CHCl_3$ production in soil based upon experiments autoclaving soil samples. It is noted that this method may also alter the biogeochemical properties of soil, such as organic matter content and structure, moisture, when deactivating enzymatic and microbial activities. Other sterilization techniques, such as γ-irradiation, NaN_3 addition, should be utilized to completely rule out the microorganisms' roles in $CHCl_3$ production in soil.

In chapter three, life-cycle emissions of methyl halide with respect to *B. napus* was quantified using static-chamber measurements and soil incubations. It captured the variations of methyl halide emission rates associated with the life cycle of *B. napus* and quantified CH_3Cl and CH_3I fluxes for the first time. However, static-chamber enclosures introduce perturbations on microenvironments, such as temperature, sunlight, wind velocity and ambient gases concentration, which may influence biogenic methyl halides emission rates. Relaxed eddy accumulation (REA) or eddy covariance (EC), would provide direct *in situ* methods of flux measurement at ecosystem scales, and would be ideal to reduce these potential uncertainties. In addition to *B. napus*, *Brassica* genus plants in general showed the potential to emit high amounts of methyl halides as suggested by previous *in vitro* studies. Therefore, more measurements of methyl halides flux could be conducted with other *Brassica* species, such as cabbage (*B. rapa*), broccoli and cauliflower (*B. oleracea*), mustard (*B. juncea*), and different cultivars. These vegetables are also under growing demands and may potentially become ever-larger sources of methyl halides.

Chapter four identified a novel and ubiquitous copper(II)-mediated production pathway of methyl halides from organic matter in soil or seawater, which could account for a significant part of their sources. Though the chemicals used in the laboratory incubations (e.g. copper (II) sulfate) are identical to commercially used copper(II) sulfate, this study still lacks field-based measurements to quantify the influence of copper(II) catalyst at actual dosage level and frequency. Field-based long-term measurements of methyl halide emission should be conducted to determine the differences between copper(II) and non-copper(II) amended agricultural fields or water bodies in the future to evaluate its global impact on atmospheric composition of methyl halides. The mechanism at the molecular level for ring-opening of aromatic carbon catalyzed by copper(II) to produce methyl halides is still unknown. It may be unveiled by tracing carbon flows with isotopic labelling studies.

REFERENCES

Albers, C. N., Jacobsen, O. S., Flores, É. M. M., Pereira, J. S. F., & Laier, T. (2011). Spatial variation in natural formation of chloroform in the soils of four coniferous forests. *Biogeochemistry*, *103*(1–3), 317–334.

Albers, C. N., Jacobsen, O. S., Flores, E. M. M., & Johnsen, A. R. (2017). Arctic and subarctic natural soils emit chloroform and brominated analogues by alkaline hydrolysis of trihaloacetyl compounds. *Environmental Science & Technology*, *51*(11), 6131–6138.

Althoff, F., Benzing, K., Comba, P., McRoberts, C., Boyd, D. R., Greiner, S., & Keppler, F. (2014). Abiotic methanogenesis from organosulphur compounds under ambient conditions. *Nature Communications*, *5*(1), 4205.

Amiro, B. D., & Johnston, F. L. (1989). Volatilization of iodine from vegetation. *Atmospheric Environment (1967)*, *23*(3), 533–538.

Andreae, M. O., Atlas, E., Harris, G. W., Helas, G., Kock, A. de, Koppmann, R., Maenhaut, W., Manø, S., Pollock, W. H., Rudolph, J., Scharffe, D., Schebeske, G., & Welling, M. (1996). Methyl halide emissions from savanna fires in southern Africa. *Journal of Geophysical Research: Atmospheres*, *101*(D19), 23603–23613.

Andreae, M. O., & Merlet, P. (2001). Emission of trace gases and aerosols from biomass burning. *Global Biogeochemical Cycles*, *15*(4), 955–966.

Andreae, M. O. (2019). Emission of trace gases and aerosols from biomass burning – an updated assessment. *Atmospheric Chemistry and Physics*, *19*(13), 8523–8546.

Attieh, J. M., Hanson, A. D., & Saini, H. S. (1995). Purification and characterization of a novel methyltransferase responsible for biosynthesis of halomethanes and methanethiol in *Brassica oleracea*. *Journal of Biological Chemistry*, *270*(16), 9250–9257.

Attieh, J., Sparace, S. A., & Saini, H. S. (2000). Purification and properties of multiple isoforms of a novel thiol methyltransferase involved in the production of volatile sulfur compounds from Brassica oleracea. *Archives of Biochemistry and Biophysics*, *380*(2), 257–266.

Bahlmann, E., Keppler, F., Wittmer, J., Greule, M., Schöler, H. F., Seifert, R., & Zetzsch, C. (2019). Evidence for a major missing source in the global chloromethane budget from stable carbon isotopes. *Atmospheric Chemistry and Physics*, *19*(3), 1703–1719.

Baker, J. M., Reeves, C. E., Penkett, S. A., Cardenas, L. M., & Nightingale, P. D. (1998). An estimate of the global emissions of methyl bromide from automobile exhausts. *Geophysical Research Letters*, *25*(13), 2405–2408.

Bárcenas-Moreno, G., García-Orenes, F., Mataix-Solera, J., Mataix-Beneyto, J., & Bååth, E. (2011). Soil microbial recolonisation after a fire in a Mediterranean forest. *Biology and Fertility of Soils*, *47*(3), 261–272.

Bayer, T. S., Widmaier, D. M., Temme, K., Mirsky, E. A., Santi, D. V., & Voigt, C. A. (2009). Synthesis of methyl halides from biomass using engineered microbes. *Journal of the American Chemical Society*, *131*(18), 6508–6515.

Bell, N., Hsu, L., Jacob, D. J., Schultz, M. G., Blake, D. R., Butler, J. H., King, D. B., Lobert, J. M., & Maier-Reimer, E. (2002). Methyl iodide: Atmospheric budget and use as a tracer of marine convection in global models. *Journal of Geophysical Research: Atmospheres*, *107*(D17), ACH-8.

Berns, A. E., Philipp, H., Narres, H.-D., Burauel, P., Vereecken, H., & Tappe, W. (n.d.). Effect of gamma-sterilization and autoclaving on soil organic matter structure as studied by solid state NMR, UV and fluorescence spectroscopy. *European Journal of Soil Science*, *59*(3), 540–550.

Bertram, F. J., & Kolowich, J. B. (2000). A study of methyl bromide emissions from automobiles burning leaded gasoline using standardized vehicle testing procedures. *Geophysical Research Letters*, *27*(9), 1423–1426.

Bie, P., Fang, X., Li, Z., Wang, Z., & Hu, J. (2017). Emissions estimates of carbon tetrachloride for 1992–2014 in China. *Environmental Pollution*, *224*, 670–678.

Blake, N. J., Blake, D. R., Sive, B. C., Chen, T.-Y., Rowland, F. S., Collins, J. E., Sachse, G. W., & Anderson, B. E. (1996). Biomass burning emissions and vertical distribution of atmospheric methyl halides and other reduced carbon gases in the South Atlantic region. *Journal of Geophysical Research: Atmospheres*, *101*(D19), 24151–24164.

Blei, E., Hardacre, C. J., Mills, G. P., Heal, K. V., & Heal, M. R. (2010). Identification and quantification of methyl halide sources in a lowland tropical rainforest. *Atmospheric Environment*, *44*(8), 1005–1010.

Bouttier, C., & Morgan, D. G. (1992). Development of oilseed rape buds, flowers, and pods in vitro. *Journal of Experimental Botany*, *43*(8), 1089–1096.

Breider, F., & Albers, C. N. (2015). Formation mechanisms of trichloromethyl-containing compounds in the terrestrial environment: A critical review. *Chemosphere*, *119*, 145–154.

Breider, F., & Hunkeler, D. (2014a). Mechanistic insights into the formation of chloroform from natural organic matter using stable carbon isotope analysis. *Geochimica et Cosmochimica Acta*, *125*, 85–95.

Breider, F., & Hunkeler, D. (2014b). Investigating chloroperoxidase-catalyzed formation of chloroform from humic substances using stable chlorine isotope analysis. *Environmental Science & Technology*, *48*(3), 1592–1600.

Brown, A. C., Canosa-Mas, C. E., & Wayne, R. P. (1990). A kinetic study of the reactions of OH with CH_3I and CF_3I. *Atmospheric Environment. Part A. General Topics*, *24*(2), 361–367.

Brown, F. S., & Hager, L. P. (1967). Chloroperoxidase. IV. Evidence for an Ionic electrophilic substitution mechanism. *Journal of the American Chemical Society*, *89*(3), 719–720.

Buntin, G. D., Grey, T. L., Harris, G. H., Phillips, D., Prostko, E. P., Raymer, P., Smith, N. B., Sumner, P. E., & Woodruff, J. (2007). *Canola production in Georgia* [Report]. University of Georgia.

Busbee, W. S., Conner, W. H., Allen, D. M., & Lanham, J. D. (2003). Composition and aboveground productivity of three seasonally flooded depressional forested wetlands in coastal South Carolina. *Southeastern Naturalist*, *2*(3), 335–346.

Butenschoen, O., Ji, R., Schäffer, A., & Scheu, S. (2009). The fate of catechol in soil as affected by earthworms and clay. *Soil Biology and Biochemistry*, *41*(2), 330–339.

Butler, J. H. (2000). Atmospheric chemistry: Better budgets for methyl halides? *Nature*, *403*(6767), 260–261.

Butler, J. H., King, D. B., Lobert, J. M., Montzka, S. A., Yvon-Lewis, S. A., Hall, B. D., Warwick, N. J., Mondeel, D. J., Aydin, M., & Elkins, J. W. (2007). Oceanic distributions and emissions of short-lived halocarbons. *Global Biogeochemical Cycles*, *21*(1).

California Department of Pesticide Regulation. (2019). *Summary of pesticide use report data 2017*. California Environmental Protection Agency.

Campos, M. L. a. M., Nightingale, P. D., & Jickells, T. D. (1996). A comparison of methyl iodide emissions from seawater and wet depositional fluxes of iodine over the southern North Sea. *Tellus B*, *48*(1), 106–114.

Carpenter, L. J., Reimann, S., Burkholder, J. B., Clerbaux, C., Hall, B. D., Hossaini, R., Laube, J. C., & Yvon-Lewis, S. A. (2014). *Update on ozone-depleting substances (ODSs) and other gases of interest to the Montreal Protocol*, Chapter 1 in Scientific Assessment of Ozone Depletion: 2014, Global Ozone Research and Monitoring Project – Report No. 55. World Meteorological Organization, Geneva, Switzerland.

Chen, T.-Y., Blake, D. R., Lopez, J. P., & Rowland, F. S. (1999). Estimation of global vehicular methyl bromide emissions: Extrapolation from a case study in Santiago, Chile. *Geophysical Research Letters*, *26*(3), 283–286.

Chen, X., & Wood, A. J. (2004). Purification and characterization of S-adenosyl-L-methionine nicotinic acid-N-methyltransferase from leaves of *Glycine max*. *Biologia Plantarum*, *48*(4), 531–535.

Chipperfield, M. P., Bekki, S., Dhomse, S., Harris, N. R. P., Hassler, B., Hossaini, R., Steinbrecht, W., Thiéblemont, R., & Weber, M. (2017). Detecting recovery of the stratospheric ozone layer. *Nature*, *549*(7671), 211–218.

Chipperfield, M. P., Hossaini, R., Montzka, S. A., Reimann, S., Sherry, D., & Tegtmeier, S. (2020). Renewed and emerging concerns over the production and emission of ozone-depleting substances. *Nature Reviews Earth & Environment*, *1*(5), 251–263.

Chow, A. T., Dai, J., Conner, W. H., Hitchcock, D. R., & Wang, J.-J. (2013). Dissolved organic matter and nutrient dynamics of a coastal freshwater forested wetland in Winyah Bay, South Carolina. *Biogeochemistry*, *112*(1–3), 571–587.

Cicerone, R. J., Stolarski, R. S., & Walters, S. (1974). Stratospheric ozone destruction by man-made chlorofluoromethanes. *Science*, *185*(4157), 1165–1167.

Clark, C. D., De Bruyn, W. J., & Jones, J. G. (2009). Photochemical production of hydrogen peroxide in size-fractionated Southern California coastal waters. *Chemosphere*, *76*(1), 141–146.

Claxton, T., Hossaini, R., Wild, O., Chipperfield, M. P., & Wilson, C. (2019). On the regional and seasonal ozone depletion potential of chlorinated very short-lived substances. *Geophysical Research Letters*, *46*(10), 5489–5498.

Clerbaux, C., Cunnold, D. M., Anderson, J., Engel, A., Fraser, P. J., Mahieu, E., Manning, A., Miller, J., Montzka, S. A., Nassar, R., Prinn, R., Rinsland, C. P., Simmonds, P., Verdonik, D., Weiss, R., Wuebbles, D., & Yokouchi, Y. (2007). *Long-Lived Compounds*, Chapter 1 in Scientific Assessment of Ozone Depletion: 2006. Global Ozone Research and Monitoring Project - Report No. 50, World Meteorological Organization, Geneva, Switzerland.

Cohan, D. S., Sturrock, G. A., Biazar, A. P., & Fraser, P. J. (2003). Atmospheric methyl iodide at Cape Grim, Tasmania, from AGAGE observations. *Journal of Atmospheric Chemistry*, *44*(2), 131–150.

Cormier, N., Krauss, K. W., & Conner, W. H. (2013). Periodicity in stem growth and litterfall in tidal freshwater forested wetlands: Influence of salinity and drought on nitrogen recycling. *Estuaries and Coasts*, *36*(3), 533–546.

Cox, M. L., Sturrock, G. A., Fraser, P. J., Siems, S. T., & Krummel, P. B. (2005). Identification of regional sources of methyl bromide and methyl iodide from AGAGE observations at Cape Grim, Tasmania. *Journal of Atmospheric Chemistry*, *50*(1), 59–77.

Cox, M. L., Sturrock, G. A., Fraser, P. J., Siems, S. T., Krummel, P. B., & O'Doherty, S. (2003). Regional sources of methyl chloride, chloroform and dichloromethane

identified from AGAGE observations at Cape Grim, Tasmania, 1998–2000. *Journal of Atmospheric Chemistry*, *45*(1), 79–99.

Cox, Michelle L, Fraser, P. J., Sturrock, G. A., Siems, S. T., & Porter, L. W. (2004). Terrestrial sources and sinks of halomethanes near Cape Grim, Tasmania. *Atmospheric Environment*, *38*(23), 3839–3852.

Dahl, T. E., & Stedman, S. M. (n.d.). *Status and trends of wetlands in the coastal watersheds of the Conterminous United States 2004 to 2009*. National Oceanic and Atmospheric Administration, National Marine Fisheries Service. Retrieved September 23, 2017, from https://www.fws.gov/wetlands/Documents/Status-and-Trends-of-Wetlands-in-the-Conterminous-United-States-2004-to-2009.pdf

Davis, A. P., Shokouhian, M., & Ni, S. (2001). Loading estimates of lead, copper, cadmium, and zinc in urban runoff from specific sources. *Chemosphere*, *44*(5), 997–1009.

De Leer, E. W. B., Damste, J. S. Sinninghe., Erkelens, Corrie., & De Galan, Leo. (1985). Identification of intermediates leading to chloroform and C-4 diacids in the chlorination of humic acid. *Environmental Science & Technology*, *19*(6), 512–522.

Deventer, M. J., Jiao, Y., Knox, S. H., Anderson, F., Ferner, M. C., Lewis, J. A., & Rhew, R. C. (2018). Ecosystem-scale measurements of methyl halide fluxes from a brackish tidal marsh invaded with perennial pepperweed (*Lepidium latifolium*). *Journal of Geophysical Research: Biogeosciences*, *123*(7), 2104–2120.

Devlin, J. F., & Müller, D. (1999). Field and laboratory studies of carbon tetrachloride transformation in a sandy aquifer under sulfate reducing conditions. *Environmental Science & Technology*, *33*(7), 1021–1027.

Dhomse, S. S., Feng, W., Montzka, S. A., Hossaini, R., Keeble, J., Pyle, J. A., Daniel, J. S., & Chipperfield, M. P. (2019). Delay in recovery of the Antarctic ozone hole from unexpected CFC-11 emissions. *Nature Communications*, *10*(1), 5781.

Dhomse, Sandip S., Kinnison, D., Chipperfield, M. P., Salawitch, R. J., Cionni, I., Hegglin, M. I., Abraham, N. L., Akiyoshi, H., Archibald, A. T., Bednarz, E. M., Bekki, S., Braesicke, P., Butchart, N., Dameris, M., Deushi, M., Frith, S., Hardiman, S. C., Hassler, B., Horowitz, L. W., … Zeng, G. (2018). Estimates of ozone return dates from Chemistry-Climate Model Initiative simulations. *Atmospheric Chemistry and Physics*, *18*(11), 8409–8438.

Diepenbrock, W. (2000). Yield analysis of winter oilseed rape (*Brassica napus* L.): A review. *Field Crops Research*, *67*(1), 35–49.

Dimmer, C. H., Simmonds, P. G., Nickless, G., & Bassford, M. R. (2001). Biogenic fluxes of halomethanes from Irish peatland ecosystems. *Atmospheric Environment*, *35*(2), 321–330.

Donahue, T. M., Cicerone, R. J., Liu, S. C., & Chameides, W. L. (1976). Effect of odd hydrogen on ozone depletion by chlorine reactions. *Geophysical Research Letters*, *3*(2), 105–108.

Doyle, T. W., O'Neil, C. P., Melder, M. P. V., From, A. S., & Palta, M. M. (2007). Tidal freshwater swamps of the southeastern United States: Effects of land use, hurricanes, sea-level Rise, and climate change. In *Ecology of Tidal Freshwater Forested Wetlands of the Southeastern United States* (pp. 1–28). Springer, Dordrecht.

Drewer, J., Heal, M. R., Heal, K. V., & Smith, K. A. (2006). Temporal and spatial variation in methyl bromide flux from a salt marsh. *Geophysical Research Letters*, *33*(16), L16808.

Elkins, J. W., Thompson, T. M., Swanson, T. H., Butler, J. H., Hall, B. D., Cummings, S. O., Fishers, D. A., & Raffo, A. G. (1993). Decrease in the growth rates of atmospheric chlorofluorocarbons 11 and 12. *Nature*, *364*(6440), 780–783.

Emmerich, M., Bhansali, A., Lösekann-Behrens, T., Schröder, C., Kappler, A., & Behrens, S. (2012). Abundance, distribution, and activity of Fe(II)-oxidizing and Fe(III)-reducing microorganisms in hypersaline sediments of lake Kasin, southern Russia. *Applied and Environmental Microbiology*, *78*(12), 4386–4399.

Engel, A., Rigby, M., Burkholder, J. B., Fernandez, R. P., Froidevaus, L., Hall, B. D., Hossaini, R., Saito, T., Vollmer, M. K., & Yao, B. (2018). *Update on ozone-depleting substances (ODSs) and other gases of interest to the Montreal Protocol*, Chapter 1 in Scientific Assessment of Ozone Depletion: 2018, Global Ozone Research and Monitoring Project – Report No. 58. World Meteorological Organization, Geneva, Switzerland.

Epstein, L., & Bassein, S. (2001). Pesticide applications of copper on perennial crops in California, 1993 to 1998. *Journal of Environmental Quality*, *30*(5), 1844–1847.

Fahimi, I. J., Keppler, F., & Schöler, H. F. (2003). Formation of chloroacetic acids from soil, humic acid and phenolic moieties. *Chemosphere*, *52*(2), 513–520.

Fang, C., Smith, P., Moncrieff, J. B., & Smith, J. U. (2005). Similar response of labile and resistant soil organic matter pools to changes in temperature. *Nature*, *433*(7021), 57–59.

Fang, X., Park, S., Saito, T., Tunnicliffe, R., Ganesan, A. L., Rigby, M., Li, S., Yokouchi, Y., Fraser, P. J., Harth, C. M., Krummel, P. B., Mühle, J., O'Doherty, S., Salameh, P. K., Simmonds, P. G., Weiss, R. F., Young, D., Lunt, M. F., Manning, A. J., … Prinn, R. G. (2019). Rapid increase in ozone-depleting chloroform emissions from China. *Nature Geoscience*, *12*(2), 89.

Fang, X., Pyle, J. A., Chipperfield, M. P., Daniel, J. S., Park, S., & Prinn, R. G. (2019). Challenges for the recovery of the ozone layer. *Nature Geoscience*, *12*(8), 592–596.

Farman, J. C., Gardiner, B. G., & Shanklin, J. D. (1985). Large losses of total ozone in Antarctica reveal seasonal ClOx /NOx interaction. *Nature*, *315*(6016), 207–210.

Ferek, R. J., Reid, J. S., Hobbs, P. V., Blake, D. R., & Liousse, C. (1998). Emission factors of hydrocarbons, halocarbons, trace gases and particles from biomass burning in Brazil. *Journal of Geophysical Research: Atmospheres*, *103*(D24), 32107–32118.

Fernandez, R. P., Kinnison, D. E., Lamarque, J.-F., Tilmes, S., & Saiz-Lopez, A. (2017). Impact of biogenic very short-lived bromine on the Antarctic ozone hole during the 21st century. *Atmospheric Chemistry and Physics*, *17*(3), 1673–1688.

Fernandez-Cornejo, J., Nehring, R. F., Osteen, C., Wechsler, S., Martin, A., & Vialou, A. (2014). *Pesticide use in U.S. agriculture: 21 selected crops, 1960-2008*. Social Science Research Network.

Flemming, C. A., & Trevors, J. T. (1989). Copper toxicity and chemistry in the environment: A review. *Water, Air, and Soil Pollution*, *44*(1), 143–158.

Flury, M., & Papritz, A. (1993). Bromide in the natural environment: Occurrence and toxicity. *Journal of Environmental Quality*, *22*(4), 747–758.

Frank, H., Frank, W., & Thiel, D. (1989). C_1- and C_2-halocarbons in soil-air of forests. *Atmospheric Environment (1967)*, *23*(6), 1333–1335.

Frank, H.. (1991). Airborne chlorocarbons, photooxidants, and forest decline. *Ambio*, *20*(1), 13–18.

Furutani, Y., Dohara, Y., Kudo, S., Hayashi, J., & Norinaga, K. (2017). Theoretical study on the kinetics of thermal decomposition of guaiacol and catechol. *The Journal of Physical Chemistry A*, *121*(44), 8495–8503.

Gan, J., Yates, S. R., Ohr, H. D., & Sims, J. J. (1998). Production of methyl bromide by terrestrial higher plants. *Geophysical Research Letters*, *25*(19), 3595–3598.

Gebhardt, S., Colomb, A., Hofmann, R., Williams, J., & Lelieveld, J. (2008). Halogenated organic species over the tropical South American rainforest. *Atmospheric Chemistry and Physics*, *8*(12), 3185–3197.

Geilfus, C.-M. (2019). Chloride in soil: From nutrient to soil pollutant. *Environmental and Experimental Botany*, *157*, 299–309.

Graziosi, F., Arduini, J., Bonasoni, P., Furlani, F., Giostra, U., Manning, A. J., McCulloch, A., O'Doherty, S., Simmonds, P. G., Reimann, S., Vollmer, M. K., & Maione, M. (2016). Emissions of carbon tetrachloride from Europe. *Atmospheric Chemistry and Physics*, *16*(20), 12849–12859.

Guenther, A. B., Jiang, X., Heald, C. L., Sakulyanontvittaya, T., Duhl, T., Emmons, L. K., & Wang, X. (2012). The model of emissions of gases and aerosols from nature version 2.1 (MEGAN2.1): An extended and updated framework for modeling biogenic emissions. *Geoscientific Model Development*, *5*(6), 1471–1492.

Hamilton, J. T. G., McRoberts, W. C., Keppler, F., Kalin, R. M., & Harper, D. B. (2003). Chloride methylation by plant pectin: An efficient environmentally significant process. *Science*, *301*(5630), 206–209.

Hardacre, C. J., Blei, E., & Heal, M. R. (2009). Growing season methyl bromide and methyl chloride fluxes at a sub-arctic wetland in Sweden. *Geophysical Research Letters*, *36*(12).

Haselmann, K. F., Ketola, R. A., Laturnus, F., Lauritsen, F. R., & Grøn, C. (2000). Occurrence and formation of chloroform at Danish forest sites. *Atmospheric Environment*, *34*(2), 187–193.

Haselmann, K. F., Laturnus, F., & Grøn, C. (2002). Formation of chloroform in soil. A year-round study at a Danish spruce forest site. *Water, Air, and Soil Pollution*, *139*(1–4), 35–41.

Haselmann, K. F., Laturnus, F., Svensmark, B., & Grøn, C. (2000). Formation of chloroform in spruce forest soil – results from laboratory incubation studies. *Chemosphere*, *41*(11), 1769–1774.

Hellén, H., Hakola, H., Pystynen, K.-H., Rinne, J., & Haapanala, S. (2006). C_2-C_{10} hydrocarbon emissions from a boreal wetland and forest floor. *Biogeosciences*, *3*(2), 167–174.

Herbert, E. R., Boon, P., Burgin, A. J., Neubauer, S. C., Franklin, R. B., Ardón, M., Hopfensperger, K. N., Lamers, L. P. M., & Gell, P. (n.d.). A global perspective on wetland salinization: Ecological consequences of a growing threat to freshwater wetlands. *Ecosphere*, *6*(10), 1–43.

Hines, M. E., Crill, P. M., Varner, R. K., Talbot, R. W., Shorter, J. H., Kolb, C. E., & Harriss, R. C. (1998). Rapid consumption of low concentrations of methyl bromide by soil bacteria. *Applied and Environmental Microbiology*, *64*(5), 1864–1870.

Hoekstra, E. J., de Leer, E. W. B., & Brinkman, U. A. Th. (1998). Natural formation of chloroform and brominated trihalomethanes in soil. *Environmental Science & Technology*, *32*(23), 3724–3729.

Hoekstra, E. J., Duyzer, J. H., de Leer, E. W. B., & Brinkman, U. A. T. (2001). Chloroform – concentration gradients in soil air and atmospheric air, and emission fluxes from soil. *Atmospheric Environment*, *35*(1), 61–70.

Hoekstra, E. J., Lassen, P., van Leeuwen, J. G., de Leer, E. W., & Carlsen, L. (1995). Formation of organic chlorine compounds of low molecular weight in the chloroperoxidase-mediated reaction between chloride and humic material. In Naturally-produced organohalogens (pp. 149-158). Springer, Dordrecht.

Hossaini, R., Chipperfield, M. P., Montzka, S. A., Leeson, A. A., Dhomse, S. S., & Pyle, J. A. (2017). The increasing threat to stratospheric ozone from dichloromethane. *Nature Communications*, *8*(1), 15962.

Hossaini, R., Chipperfield, M. P., Saiz-Lopez, A., Harrison, J. J., Glasow, R. von, Sommariva, R., Atlas, E., Navarro, M., Montzka, S. A., Feng, W., Dhomse, S., Harth, C., Mühle, J., Lunder, C., O'Doherty, S., Young, D., Reimann, S., Vollmer, M. K., Krummel, P. B., & Bernath, P. F. (2015). Growth in stratospheric chlorine from short-lived chemicals not controlled by the Montreal Protocol. *Geophysical Research Letters*, *42*(11), 4573–4580.

Howard, P. H., & Hanchett, A. (1975). Chlorofluorocarbon sources of environmental contamination. *Science*, *189*(4198), 217–219.

Hu, L. (2012). *The role of the ocean in the atmospheric budgets of methyl bromide, methyl chloride and methane* [Ph.D. Dissertation, Texas A&M University]. https://search.proquest.com/docview/1221291140/abstract/C35C0833D6A140C5PQ/1

Hu, L., Montzka, S. A., Miller, B. R., Andrews, A. E., Miller, J. B., Lehman, S. J., Sweeney, C., Miller, S. M., Thoning, K., Siso, C., Atlas, E. L., Blake, D. R., Gouw, J. de, Gilman, J. B., Dutton, G., Elkins, J. W., Hall, B., Chen, H., Fischer, M. L., … Tans, P. (2016). Continued emissions of carbon tetrachloride from the United States nearly two decades after its phaseout for dispersive uses. *Proceedings of the National Academy of Sciences*, *113*(11), 2880–2885.

Hu, L., Yvon-Lewis, S. A., Butler, J. H., Lobert, J. M., & King, D. B. (2013). An improved oceanic budget for methyl chloride. *Journal of Geophysical Research: Oceans*, *118*(2), 715–725.

Huber, S. G., Kilian, G., & Schöler, H. F. (2007). Carbon suboxide, a highly reactive intermediate from the abiotic degradation of aromatic compounds in soil. *Environmental Science & Technology*, *41*(22), 7802–7806.

Huber, S. G., Kotte, K., Schöler, H. F., & Williams, J. (2009). Natural abiotic formation of trihalomethanes in soil: Results from laboratory studies and field samples. *Environmental Science & Technology*, *43*(13), 4934–4939.

Huber, S. G., Wunderlich, S., Schöler, H. F., & Williams, J. (2010). Natural abiotic formation of furans in soil. *Environmental Science & Technology*, *44*(15), 5799–5804.

Jat, R. S., Singh, V. V., Sharma, P., & Rai, P. K. (2019). Oilseed brassica in India: Demand, supply, policy perspective and future potential. *OCL*, *26*, 8.

Jiao, Y., Acdan, J., Xu, R., Deventer, M. J., Zhang, W., & Rhew, R. C. (2020). Global methyl halide emissions from rapeseed (*Brassica napus*) using life cycle measurements. *Geophysical Research Letters*, *47*(19), e2020GL089373.

Jiao, Y., Ruecker, A., Deventer, M. J., Chow, A. T., & Rhew, R. C. (2018). Halocarbon emissions from a degraded forested wetland in coastal South Carolina impacted by sea level rise. *ACS Earth and Space Chemistry*, *2*(10), 955–967.

Johnsen, A. R., Jacobsen, O. S., Gudmundsson, L., & Albers, C. N. (2016). Chloroform emissions from arctic and subarctic ecosystems in Greenland and Northern Scandinavia. *Biogeochemistry*, *130*(1–2), 53–65.

Jones, C. E., Hornsby, K. E., Sommariva, R., Dunk, R. M., Glasow, R. von, McFiggans, G., & Carpenter, L. J. (2010). Quantifying the contribution of marine organic gases to atmospheric iodine. *Geophysical Research Letters*, *37*(18).

Jurburg, S. D., Nunes, I., Brejnrod, A., Jacquiod, S., Priemé, A., Sørensen, S. J., Van Elsas, J. D., & Salles, J. F. (2017). Legacy effects on the recovery of soil bacterial communities from extreme temperature perturbation. *Frontiers in Microbiology*, *8*.

Keene, William. C., Khalil, M. A. K., Erickson III, David. J., McCulloch, A., Graedel, T. E., Lobert, J. M., Aucott, M. L., Gong, S. L., Harper, D. B., Kleiman, G., Midgley, P., Moore, R. M., Seuzaret, C., Sturges, W. T., Benkovitz, C. M., Koropalov, V., Barrie, L. A., & Li, Y. F. (1999). Composite global emissions of reactive chlorine from anthropogenic and natural sources: Reactive chlorine emissions inventory. *Journal of Geophysical Research: Atmospheres*, *104*(D7), 8429–8440.

Keppler, F., Eiden, R., Niedan, V., Pracht, J., & Schöler, H. F. (2000). Halocarbons produced by natural oxidation processes during degradation of organic matter. *Nature*, *403*(6767), 298–301.

Keppler, F., Harper, D. B., Röckmann, T., Moore, R. M., & Hamilton, J. T. G. (2005). New insight into the atmospheric chloromethane budget gained using stable carbon isotope ratios. *Atmospheric Chemistry and Physics*, *5*(9), 2403–2411.

Keppler, F., Borchers, R., Elsner, P., Fahimi, I., Pracht, J., & Schöler, H. F. (2003). Formation of volatile iodinated alkanes in soil: Results from laboratory studies. *Chemosphere*, *52*(2), 477–483.

Keppler, F., Borchers, R., Hamilton, J. T. G., Kilian, G., Pracht, J., & Schöler, H. F. (2006). De novo formation of chloroethyne in soil. *Environmental Science & Technology*, *40*(1), 130–134.

Keppler, F., Borchers, R., Pracht, J., Rheinberger, S., & Schöler, H. F. (2002). Natural formation of vinyl chloride in the terrestrial environment. *Environmental Science & Technology*, *36*(11), 2479–2483.

Keppler, F., Röhling, A. N., Jaeger, N., Schroll, M., Hartmann, S. C., & Greule, M. (2020). Sources and sinks of chloromethane in a salt marsh ecosystem: Constraints from concentration and stable isotope measurements of laboratory incubation experiments. *Environmental Science: Processes & Impacts*, *22*(3), 627–641.

Khalil, M. A. K., Rasmussen, R. A., Shearer, M. J., Chen, Z.-L., Yao, H., & Yang, J. (1998). Emissions of methane, nitrous oxide, and other trace gases from rice fields in China. *Journal of Geophysical Research: Atmospheres*, *103*(D19), 25241–25250.

Khalil, M. A. K., & Rasmussen, R. A. (2000). Soil-atmosphere exchange of radiatively and chemically active gases. *Environmental Science and Pollution Research*, *7*(2), 79–82.

Khan, M. A. H., Rhew, R. C., Whelan, M. E., Zhou, K., & Deverel, S. J. (2011). Methyl halide and chloroform emissions from a subsiding Sacramento–San Joaquin Delta island converted to rice fields. *Atmospheric Environment*, *45*(4), 977–985.

Khan, M. A. H., Rhew, R. C., Zhou, K., & Whelan, M. E. (2013). Halogen biogeochemistry of invasive perennial pepperweed (*Lepidium latifolium*) in a peatland pasture. *Journal of Geophysical Research: Biogeosciences*, *118*(1), 239–247.

Khan, M. A. H., Whelan, M. E., & Rhew, R. C. (2012). Effects of temperature and soil moisture on methyl halide and chloroform fluxes from drained peatland pasture soils. *Journal of Environmental Monitoring*, *14*(1), 241–249.

Krause, T., Tubbesing, C., Benzing, K., & Schöler, H. F. (2014). Model reactions and natural occurrence of furans from hypersaline environments. *Biogeosciences*, *11*(10), 2871–2882.

Krauss, K. W., Duberstein, J. A., Doyle, T. W., Conner, W. H., Day, R. H., Inabinette, L. W., & Whitbeck, J. L. (2009). Site condition, structure, and growth of baldcypress along tidal/non-tidal salinity gradients. *Wetlands*, *29*(2), 505–519.

Kuttippurath, J., Kumar, P., Nair, P. J., & Pandey, P. C. (2018). Emergence of ozone recovery evidenced by reduction in the occurrence of Antarctic ozone loss saturation. *Npj Climate and Atmospheric Science*, *1*(1), 1–8.

Laturnus, F., Fahimi, I., Gryndler, M., Hartmann, A., Heal, M., Matucha, M., Schöler, H. F., Schroll, R., & Svensson, T. (2005). Natural formation and degradation of chloroacetic acids and volatile organochlorines in forest soil. Challenges to understanding (12 pp). *Environmental Science and Pollution Research*, *12*(4), 233–244.

Laube, J. C., Newland, M. J., Hogan, C., Brenninkmeijer, C. A. M., Fraser, P. J., Martinerie, P., Oram, D. E., Reeves, C. E., Röckmann, T., Schwander, J., Witrant, E., & Sturges, W. T. (2014). Newly detected ozone-depleting substances in the atmosphere. *Nature Geoscience*, *7*(4), 266–269.

Lee-Taylor, J. M., Brasseur, G. P., & Yokouchi, Y. (2001). A preliminary three-dimensional global model study of atmospheric methyl chloride distributions. *Journal of Geophysical Research: Atmospheres*, *106*(D24), 34221–34233.

Lee-Taylor, J. M., Doney, S. C., Brasseur, G. P., & Müller, J.-F. (1998). A global three-dimensional atmosphere-ocean model of methyl bromide distributions. *Journal of Geophysical Research: Atmospheres*, *103*(D13), 16039–16057.

Lee-Taylor, J. M., & Holland, E. A. (2000). Litter decomposition as a potential natural source of methyl bromide. *Journal of Geophysical Research: Atmospheres*, *105*(D7), 8857–8864.

Lee-Taylor, J. M., & Redeker, K. R. (2005). Reevaluation of global emissions from rice paddies of methyl iodide and other species. *Geophysical Research Letters*, *32*(15).

Leri, A. C., Mayer, L. M., Thornton, K. R., Northrup, P. A., Dunigan, M. R., Ness, K. J., & Gellis, A. B. (2015). A marine sink for chlorine in natural organic matter. *Nature Geoscience*, *8*(8), ngeo2481.

Levine, J. G., Braesicke, P., Harris, N. R. P., Savage, N. H., & Pyle, J. A. (2007). Pathways and timescales for troposphere-to-stratosphere transport via the tropical tropopause layer and their relevance for very short lived substances. *Journal of Geophysical Research: Atmospheres*, *112*(D4), D04308.

Li, S., Park, M.-K., Jo, C. O., & Park, S. (2017). Emission estimates of methyl chloride from industrial sources in China based on high frequency atmospheric observations. *Journal of Atmospheric Chemistry*, *74*(2), 227–243.

Liang, Q., Newman, P. A., Reimann, S., & Reimann, S. (2016). SPARC report on the mystery of carbon tetrachloride. *SPARC Report No. 7*, *WCRP-13/2016*.

Liang, Q., Strahan, S. E., & Fleming, E. L. (2017). Concerns for ozone recovery. *Science*, *358*(6368), 1257–1258.

Liss, P. S., & Slater, P. G. (1974). Flux of gases across the air-sea interface. *Nature*, *247*(5438), 181.

Liu, H., Pu, Y., Tong, T., Zhu, X., Sun, B., & Zhang, X. (2020). Photochemical generation of methyl chloride from humic aicd: Impacts of precursor concentration, solution pH, solution salinity and ferric ion. *International Journal of Environmental Research and Public Health*, *17*(2), 503.

Liu, H., Tong, T., Pu, Y., Sun, B., Zhu, X., & Yan, Z. (2020). Insight into the formation paths of methyl bromide from syringic acid in aqueous bromide solutions under simulated sunlight irradiation. *International Journal of Environmental Research and Public Health*, *17*(6), 2081.

Liu, J., Wang, J., Wang, H., Wang, W., Zhou, R., Mei, D., Cheng, H., Yang, J., Raman, H., & Hu, Q. (2016). Multigenic control of pod shattering resistance in Chinese Rapeseed Germplasm revealed by genome-wide association and linkage analyses. *Frontiers in Plant Science*, *7*, 1058.

Liu, J.-Z., & Wang, M. (2007). Improvement of activity and stability of chloroperoxidase by chemical modification. *BMC Biotechnology*, *7*(1), 1-8.

Lobert, J. M., Keene, W. C., Logan, J. A., & Yevich, R. (1999). Global chlorine emissions from biomass burning: Reactive chlorine emissions inventory. *Journal of Geophysical Research: Atmospheres*, *104*(D7), 8373–8389.

Lomnicki, S., Truong, H., & Dellinger, B. (2008). Mechanisms of product formation from the pyrolytic thermal degradation of catechol. *Chemosphere*, *73*(4), 629–633.

Lu, K., Xiao, Z., Jian, H., Peng, L., Qu, C., Fu, M., He, B., Tie, L., Liang, Y., Xu, X., & Li, J. (2016). A combination of genome-wide association and transcriptome analysis reveals candidate genes controlling harvest index-related traits in *Brassica napus*. *Scientific Reports*, *6*(1), 1–13.

Lunt, M. F., Park, S., Li, S., Henne, S., Manning, A. J., Ganesan, A. L., Simpson, I. J., Blake, D. R., Liang, Q., O'Doherty, S., Harth, C. M., Mühle, J., Salameh, P. K., Weiss, R. F., Krummel, P. B., Fraser, P. J., Prinn, R. G., Reimann, S., & Rigby, M. (2018). Continued emissions of the ozone-depleting substance carbon tetrachloride from Eastern Asia. *Geophysical Research Letters*, *45*(20), 11,423-11,430.

Luo, T., Zhang, J., Khan, M. N., Liu, J., Xu, Z., & Hu, L. (2018). Temperature variation caused by sowing dates significantly affects floral initiation and floral bud differentiation processes in rapeseed (*Brassica napus* L.). *Plant Science*, *271*, 40–51.

Macdonald, M. L., Wadham, J. L., Young, D., Lunder, C. R., Hermansen, O., Lamarche-Gagnon, G., & O'Doherty, S. (2020). Consumption of CH_3Cl, CH_3Br, and CH_3I and emission of $CHCl_3$, $CHBr_3$, and CH_2Br_2 from the forefield of a retreating Arctic glacier. *Atmospheric Chemistry and Physics*, *20*(12), 7243–7258.

Mahowald, N. M., Hamilton, D. S., Mackey, K. R., Moore, J. K., Baker, A. R., Scanza, R. A., & Zhang, Y. (2018). Aerosol trace metal leaching and impacts on marine microorganisms. *Nature communications*, 9(1), 1–15.

Manley, S. L., & Dastoor, M. N. (1988). Methyl iodide (CH_3I) production by kelp and associated microbes. *Marine Biology*, *98*(4), 477–482.

Manley, S. L., & Cuesta, J. L. de la. (1997). Methyl iodide production from marine phytoplankton cultures. *Limnology and Oceanography*, *42*(1), 142–147.

Manley, S. L., & Dastoor, M. N. (1987). Methyl halide (CH_3X) production from the giant kelp, Macrocystis, and estimates of global CH_3X production by kelp1. *Limnology and Oceanography*, *32*(3), 709–715.

Manley, S. L., Goodwin, K., & North, W. J. (1992). Laboratory production of bromoform, methylene bromide, and methyl iodide by macroalgae and distribution in nearshore southern California waters. *Limnology and Oceanography*, *37*(8), 1652–1659.

Manley, S. L., Wang, N.-Y., Walser, M. L., & Cicerone, R. J. (2006). Coastal salt marshes as global methyl halide sources from determinations of intrinsic production by marsh plants. *Global Biogeochemical Cycles*, *20*(3), GB3015.

Manley, S. L., Wang, N.-Y., Walser, M. L., & Cicerone, R. J. (2007). Methyl halide emissions from greenhouse-grown mangroves. *Geophysical Research Letters*, *34*(1).

Matucha, M., Gryndler, M., Schröder, P., Forczek, S. T., Uhlířová, H., Fuksová, K., & Rohlenová, J. (2007). Chloroacetic acids—Degradation intermediates of organic matter in forest soil. *Soil Biology and Biochemistry*, *39*(1), 382–385.

McCormick, M. L., Bouwer, E. J., & Adriaens, P. (2002). Carbon tetrachloride transformation in a model iron-reducing culture: Relative kinetics of biotic and abiotic reactions. *Environmental Science & Technology*, *36*(3), 403–410.

McCulloch, A. (2003). Chloroform in the environment: Occurrence, sources, sinks and effects. *Chemosphere*, *50*(10), 1291–1308.

McCulloch, A., Aucott, M. L., Benkovitz, C. M., Graedel, T. E., Kleiman, G., Midgley, P. M., & Li, Y.-F. (1999). Global emissions of hydrogen chloride and chloromethane from coal combustion, incineration and industrial activities: Reactive chlorine emissions inventory. *Journal of Geophysical Research: Atmospheres*, *104*(D7), 8391–8403.

Mead, M. I., Khan, M. A. H., White, I. R., Nickless, G., & Shallcross, D. E. (2008). Methyl halide emission estimates from domestic biomass burning in Africa. *Atmospheric Environment*, *42*(21), 5241–5250.

Mead, M. I., White, I. R., Nickless, G., Wang, K.-Y., & Shallcross, D. E. (2008). An estimation of the global emission of methyl bromide from rapeseed (*Brassica napus*) from 1961 to 2003. *Atmospheric Environment*, *42*(2), 337–345.

M'hemdi, A., Dbira, B., Abdelhedi, R., Brillas, E., & Ammar, S. (2012). Mineralization of catechol by Fenton and photo-Fenton processes. *CLEAN – Soil, Air, Water*, *40*(8), 878–885.

Molina, M. J., & Rowland, F. S. (1974). Stratospheric sink for chlorofluoromethanes: Chlorine atom-catalysed destruction of ozone. *Nature*, *249*(5460), 810–812.

Montelius, M., Svensson, T., Lourino-Cabana, B., Thiry, Y., & Bastviken, D. (2016). Chlorination and dechlorination rates in a forest soil—A combined modelling and experimental approach. *Science of The Total Environment*, *554–555*, 203–210.

Montzka, S. A., Butler, J. H., Hall, B. D., Mondeel, D. J., & Elkins, J. W. (2003). A decline in tropospheric organic bromine. *Geophysical Research Letters*, *30*(15).

Montzka, S. A., Butler, J. H., Myers, R. C., Thompson, T. M., Swanson, T. H., Clarke, A. D., Lock, L. T., & Elkins, J. W. (1996). Decline in the tropospheric abundance of halogen from halocarbons: Implications for stratospheric ozone depletion. *Science*, *272*(5266), 1318–1322.

Montzka, S. A., Dutton, G. S., Portmann, R. W., Chipperfield, M. P., Davis, S., Feng, W., Manning, A. J., Ray, E., Rigby, M., Hall, B. D., Siso, C., Nance, J. D., Krummel, P. B., Mühle, J., Young, D., O'Doherty, S., Salameh, P. K., Harth, C. M., Prinn, R. G., … Theodoridi, C. (2021). A decline in global CFC-11 emissions during 2018−2019. *Nature*, *590*(7846), 428–432.

Montzka, S. A., Dutton, G. S., Yu, P., Ray, E., Portmann, R. W., Daniel, J. S., Kuijpers, L., Hall, B. D., Mondeel, D., Siso, C., Nance, J. D., Rigby, M., Manning, A. J., Hu, L., Moore, F., Miller, B. R., & Elkins, J. W. (2018). An unexpected and persistent increase in global emissions of ozone-depleting CFC-11. *Nature*, *557*(7705), 413–417.

Montzka, S. A., Reimannander, S., Engel, A., Kruger, K., Simon, O., Sturges, W. T., Blake, D. R., Dorf, M. D., Fraser, P. J., Froidevaux, L., Jucks, K., Kreher, K., Iii, M. J. K., Mellouki, A., Miller, J., Nielsen, O. J., Orkin, V. L., Prinn, R. G., Rhew, R., … Verdonik, D. P. (2011). *Ozone-depleting substances (ODSs) and related chemicals*, Chapter 1 in Scientific Assessment of Ozone Depletion: 2010, Global Ozone Research and Monitoring Project – Report No. 52. World Meteorological Organization, Geneva, Switzerland.

Moore, R. M. (2000). The solubility of a suite of low molecular weight organochlorine compounds in seawater and implications for estimating the marine source of methyl chloride to the atmosphere. *Chemosphere - Global Change Science*, *2*(1), 95–99.

Moore, R. M. (2008). A photochemical source of methyl chloride in saline waters. *Environmental Science & Technology*, *42*(6), 1933–1937.

Moore, R. M., & Groszko, W. (1999). Methyl iodide distribution in the ocean and fluxes to the atmosphere. *Journal of Geophysical Research: Oceans*, *104*(C5), 11163–11171.

Morrison, M. J., Stewart, D. W., & McVetty, P. B. E. (1992). Maximum area, expansion rate and duration of summer rape leaves. *Canadian Journal of Plant Science*, *72*(1), 117–126.

Müller, G., Spassovski, M., & Henschler, D. (1972). Trichloroethylene exposure and trichloroethylene metabolites in urine and blood. *Archiv Für Toxikologie*, *29*(4), 335–340.

Muramatsu, Y., & Yoshida, S. (1995). Volatilization of methyl iodide from the soil-plant system. *Atmospheric Environment*, *29*(1), 21–25.

Neumann, C. S., Fujimori, D. G., & Walsh, C. T. (2008). Halogenation strategies in natural product biosynthesis. *Chemistry & Biology*, *15*(2), 99–109.

Newchurch, M. J., Yang, E.-S., Cunnold, D. M., Reinsel, G. C., Zawodny, J. M., & Russell, J. M. (2003). Evidence for slowdown in stratospheric ozone loss: First stage of ozone recovery. *Journal of Geophysical Research: Atmospheres*, *108*(D16).

Ni, X., & Hager, L. P. (1998). cDNA cloning of *Batis maritima* methyl chloride transferase and purification of the enzyme. *Proceedings of the National Academy of Sciences*, *95*(22), 12866–12871.

Ni, X., & Hager, L. P. (1999). Expression of *Batis maritima* methyl chloride transferase in *Escherichia coli*. *Proceedings of the National Academy of Sciences*, *96*(7), 3611–3615.

Nowakowska, M., Herbinet, O., Dufour, A., & Glaude, P. A. (2018). Kinetic study of the pyrolysis and oxidation of guaiacol. *The Journal of Physical Chemistry A*, *122*(39), 7894–7909.

O'Doherty, S., Simmonds, P. G., Cunnold, D. M., Wang, H. J., Sturrock, G. A., Fraser, P. J., Ryall, D., Derwent, R. G., Weiss, R. F., Salameh, P., Miller, B. R., & Prinn, R. G. (2001). *In situ* chloroform measurements at Advanced Global Atmospheric Gases Experiment atmospheric research stations from 1994 to 1998. *Journal of Geophysical Research: Atmospheres*, *106*(D17), 20429–20444.

Oman, L. D., Plummer, D. A., Waugh, D. W., Austin, J., Scinocca, J. F., Douglass, A. R., Salawitch, R. J., Canty, T., Akiyoshi, H., Bekki, S., Braesicke, P., Butchart, N., Chipperfield, M. P., Cugnet, D., Dhomse, S., Eyring, V., Frith, S., Hardiman, S. C., Kinnison, D. E., … Ziemke, J. R. (2010). Multimodel assessment of the factors driving stratospheric ozone evolution over the 21st century. *Journal of Geophysical Research: Atmospheres*, *115*(D24).

Oram, D. E., Ashfold, M. J., Laube, J. C., Gooch, L. J., Humphrey, S., Sturges, W. T., Leedham-Elvidge, E., Forster, G. L., Harris, N. R. P., Mead, M. I., Samah, A. A., Phang, S. M., Ou-Yang, C.-F., Lin, N.-H., Wang, J.-L., Baker, A. K., Brenninkmeijer, C. A. M., & Sherry, D. (2017). A growing threat to the ozone layer from short-lived anthropogenic chlorocarbons. *Atmospheric Chemistry and Physics*, *17*(19), 11929–11941.

Ordóñez, C., Lamarque, J.-F., Tilmes, S., Kinnison, D. E., Atlas, E. L., Blake, D. R., Sousa Santos, G., Brasseur, G., & Saiz-Lopez, A. (2012). Bromine and iodine chemistry in a global chemistry-climate model: Description and evaluation of very short-lived oceanic sources. *Atmospheric Chemistry and Physics*, *12*(3), 1423–1447.

Ormond, T. K., Baraban, J. H., Porterfield, J. P., Scheer, A. M., Hemberger, P., Troy, T. P., Ahmed, M., Nimlos, M. R., Robichaud, D. J., Daily, J. W., & Ellison, G. B. (2018). Thermal decompositions of the lignin model compounds: Salicylaldehyde and catechol. *The Journal of Physical Chemistry A*, *122*(28), 5911–5924.

Page, S. E., Sander, M., Arnold, W. A., & McNeill, K. (2012). Hydroxyl radical formation upon oxidation of reduced humic acids by oxygen in the dark. *Environmental Science & Technology*, *46*(3), 1590–1597.

Park, S., Li, S., Mühle, J., O'Doherty, S., Weiss, R. F., Fang, X., Reimann, S., & Prinn, R. G. (2018). Toward resolving the budget discrepancy of ozone-depleting carbon tetrachloride (CCl_4): An analysis of top-down emissions from China. *Atmospheric Chemistry and Physics*, *18*(16), 11729–11738.

Park, S., Western, L. M., Saito, T., Redington, A. L., Henne, S., Fang, X., Prinn, R. G., Manning, A. J., Montzka, S. A., Fraser, P. J., Ganesan, A. L., Harth, C. M., Kim, J., Krummel, P. B., Liang, Q., Mühle, J., O'Doherty, S., Park, H., Park, M.-K., … Rigby, M. (2021). A decline in emissions of CFC-11 and related chemicals from eastern China. *Nature*, *590*(7846), 433–437.

Perez-Benito, J. F. (2001). Copper(II)-catalyzed decomposition of hydrogen peroxide: Catalyst activation by halide ions. *Monatshefte Für Chemie / Chemical Monthly*, *132*(12), 1477–1492.

Pickard, M. A., & Hashimoto, A. (1988). Stability and carbohydrate composition of chloroperoxidase from *Caldariomyces fumago* grown in a fructose–salts medium. *Canadian Journal of Microbiology*, *34*(8), 998–1002.

Pickering, L., Black, T. A., Gilbert, C., Jeronimo, M., Nesic, Z., Pilz, J., Svensson, T., & Öberg, G. (2013). Portable chamber system for measuring chloroform fluxes from terrestrial environments – methodological challenges. *Environmental Science & Technology*, *47*(24), 14298–14305.

Pracht, J., Boenigk, J., Isenbeck-Schröter, M., Keppler, F., & Schöler, H. F. (2001). Abiotic Fe(III) induced mineralization of phenolic substances. *Chemosphere*, *44*(4), 613–619.

Rasmussen, R. A., Khalil, M. a. K., Gunawardena, R., & Hoyt, S. D. (1982). Atmospheric methyl iodide (CH_3I). *Journal of Geophysical Research: Oceans*, *87*(C4), 3086–3090.

Redeker, K. R., Andrews, J., Fisher, F., Sass, R., & Cicerone, R. J. (2002). Interfield and intrafield variability of methyl halide emissions from rice paddies. *Global Biogeochemical Cycles*, *16*(4), 1125.

Redeker, K. R., & Cicerone, R. J. (2004). Environmental controls over methyl halide emissions from rice paddies. *Global Biogeochemical Cycles*, *18*(1), GB1027.

Redeker, K. R., Wang, N.-Y., Low, J. C., McMillan, A., Tyler, S. C., & Cicerone, R. J. (2000). Emissions of methyl halides and methane from rice paddies. *Science*, *290*(5493), 966–969.

Reifenhäuser, W., & Heumann, K. G. (1992). Determinations of methyl iodide in the Antarctic atmosphere and the south polar sea. *Atmospheric Environment. Part A. General Topics*, *26*(16), 2905–2912.

Rhew, R. C., Whelan, M. E., & Min, D.-H. (2014). Large methyl halide emissions from south Texas salt marshes. *Biogeosciences*, *11*(22), 6427–6434.

Rhew, R. C., & Mazéas, O. (2010). Gross production exceeds gross consumption of methyl halides in northern California salt marshes. *Geophysical Research Letters*, *37*(18), L18813.

Rhew, R. C., & Abel, T. (2007). Measuring simultaneous production and consumption fluxes of methyl chloride and methyl bromide in annual temperate grasslands. *Environmental Science & Technology*, *41*(22), 7837–7843.

Rhew, R. C., Aydin, M., & Saltzman, E. S. (2003). Measuring terrestrial fluxes of methyl chloride and methyl bromide using a stable isotope tracer technique. *Geophysical Research Letters*, *30*(21), 2103.

Rhew, R. C., Chen, C., Teh, Y. A., & Baldocchi, D. (2010). Gross fluxes of methyl chloride and methyl bromide in a California oak-savanna woodland. *Atmospheric Environment*, *44*(16), 2054–2061.

Rhew, R. C., Miller, B. R., Bill, M., Goldstein, A. H., & Weiss, R. F. (2002). Environmental and biological controls on methyl halide emissions from southern California coastal salt marshes. *Biogeochemistry*, *60*(2), 141–161.

Rhew, R. C., Miller, B. R., Vollmer, M. K., & Weiss, R. F. (2001). Shrubland fluxes of methyl bromide and methyl chloride. *Journal of Geophysical Research: Atmospheres*, *106*(D18), 20875–20882.

Rhew, R. C., Miller, B. R., & Weiss, R. F. (2000). Natural methyl bromide and methyl chloride emissions from coastal salt marshes. *Nature*, *403*(6767), 292.

Rhew, R. C., Miller, B. R., & Weiss, R. F. (2008a). Chloroform, carbon tetrachloride and methyl chloroform fluxes in southern California ecosystems. *Atmospheric Environment*, *42*(30), 7135–7140.

Rhew, R. C., Østergaard, L., Saltzman, E. S., & Yanofsky, M. F. (2003). Genetic control of methyl halide production in Arabidopsis. *Current Biology*, *13*(20), 1809–1813.

Rhew, R. C., Teh, Y. A., & Abel, T. (2007). Methyl halide and methane fluxes in the northern Alaskan coastal tundra. *Journal of Geophysical Research: Biogeosciences*, *112*(G2), G02009.

Rhew, R. C., Teh, Y. A., Abel, T., Atwood, A., & Mazéas, O. (2008b). Chloroform emissions from the Alaskan Arctic tundra. *Geophysical Research Letters*, *35*(21), L21811.

Richter, U., & Wallace, D. W. R. (2004). Production of methyl iodide in the tropical Atlantic Ocean. *Geophysical Research Letters*, *31*(23).

Rigby, M., Park, S., Saito, T., Western, L. M., Redington, A. L., Fang, X., Henne, S., Manning, A. J., Prinn, R. G., Dutton, G. S., Fraser, P. J., Ganesan, A. L., Hall, B. D., Harth, C. M., Kim, J., Kim, K.-R., Krummel, P. B., Lee, T., Li, S., … Young, D. (2019). Increase in CFC-11 emissions from eastern China based on atmospheric observations. *Nature*, *569*(7757), 546–550.

Roehl, C. M., Burkholder, J. B., Moortgat, G. K., Ravishankara, A. R., & Crutzen, P. J. (1997). Temperature dependence of UV absorption cross sections and atmospheric

implications of several alkyl iodides. *Journal of Geophysical Research: Atmospheres*, *102*(D11), 12819–12829.

Rowland, F. S. (1996). Stratospheric ozone depletion by chlorofluorocarbons (Nobel Lecture). *Angewandte Chemie International Edition in English*, *35*(16), 1786–1798.

Rudolph, J., Khedim, A., Koppmann, R., & Bonsang, B. (1995). Field study of the emissions of methyl chloride and other halocarbons from biomass burning in Western Africa. *Journal of Atmospheric Chemistry*, *22*(1–2), 67–80.

Ruecker, A., Weigold, P., Behrens, S., Jochmann, M., Laaks, J., & Kappler, A. (2014). Predominance of biotic over abiotic formation of halogenated hydrocarbons in hypersaline sediments in Western Australia. *Environmental Science & Technology*, *48*(16), 9170–9178.

Rueffer, M., Zumstein, G., & Zenk, M. H. (1990). Partial purification and properties of S-adenosyl-l-methionine: (S)-tetrahydroprotoberberinecis-N-methyltransferase from suspension-cultured cells of Eschscholtzia and Corydalis. *Phytochemistry*, *29*(12), 3727–3733.

Saini, H. S., Attieh, J. M., & Hanson, A. D. (1995). Biosynthesis of halomethanes and methanethiol by higher plants via a novel methyltransferase reaction. *Plant, Cell & Environment*, *18*(9), 1027–1033.

Saito, T., Yokouchi, Y., Kosugi, Y., Tani, M., Philip, E., & Okuda, T. (2008). Methyl chloride and isoprene emissions from tropical rain forest in Southeast Asia. *Geophysical Research Letters*, *35*(19).

Serça, D., Guenther, A., Klinger, L., Helmig, D., Hereid, D., & Zimmerman, P. (1998). Methyl bromide deposition to soils. *Atmospheric Environment*, *32*(9), 1581–1586.

Sherry, D., McCulloch, A., Liang, Q., Reimann, S., & Newman, P. A. (2018). Current sources of carbon tetrachloride (CCl_4) in our atmosphere. *Environmental Research Letters*, *13*(2), 024004.

Shigeoka, S., Ishiko, H., Nakano, Y., & Mitsunaga, T. (1992). Isolation and properties of γ-tocopherol methyltransferase in Euglena gracilis. *Biochimica et Biophysica Acta (BBA) - Lipids and Lipid Metabolism*, *1128*(2), 220–226.

Shorter, J. H., Kolb, C. E., Crill, P. M., Kerwin, R. A., Talbot, R. W., Hines, M. E., & Harriss, R. C. (1995). Rapid degradation of atmospheric methyl bromide in soils. *Nature*, *377*(6551), 717–719.

Singh, H. B., Salas, L. J., & Stiles, R. E. (1983). Methyl halides in and over the eastern Pacific (40°N–32°S). *Journal of Geophysical Research: Oceans*, *88*(C6), 3684–3690.

Sive, B. C., Varner, R. K., Mao, H., Blake, D. R., Wingenter, O. W., & Talbot, R. (2007). A large terrestrial source of methyl iodide. *Geophysical Research Letters*, *34*(17).

Smythe-Wright, D., Boswell, S. M., Breithaupt, P., Davidson, R. D., Dimmer, C. H., & Eiras Diaz, L. B. (2006). Methyl iodide production in the ocean: Implications for climate change. *Global Biogeochemical Cycles*, *20*(3), GB3003.

Solomon, S. (1988). The mystery of the Antarctic ozone "hole." *Reviews of Geophysics*, *26*(1), 131–148.

Solomon, S., Garcia, R. R., Rowland, F. S., & Wuebbles, D. J. (1986). On the depletion of Antarctic ozone. *Nature*, *321*(6072), 755–758.

Solomon, S., Ivy, D. J., Kinnison, D., Mills, M. J., Neely, R. R., & Schmidt, A. (2016). Emergence of healing in the Antarctic ozone layer. *Science*, *353*(6296), 269–274.

Stemmler, I., Hense, I., Quack, B., & Maier-Reimer, E. (2014). Methyl iodide production in the open ocean. *Biogeosciences*, *11*(16), 4459–4476.

Stolarski, R. S., & Cicerone, R. J. (1974). Stratospheric chlorine: A possible sink for ozone. *Canadian Journal of Chemistry*.

Stone, K. A., Solomon, S., & Kinnison, D. E. (2018). On the identification of ozone recovery. *Geophysical Research Letters*, *45*(10), 5158–5165.

Strahan, S. E., Douglass, A. R., & Damon, M. R. (2019). Why do Antarctic ozone recovery trends vary? *Journal of Geophysical Research: Atmospheres*, *124*(15), 8837–8850.

Studenroth, S., Huber, S. G., Kotte, K., & Schöler, H. F. (2013). Natural abiotic formation of oxalic acid in soils: Results from aromatic model compounds and soil samples. *Environmental Science & Technology*, *47*(3), 1323–1329.

Tebaldi, C., Strauss, B. H., & Zervas, C. E. (2012). Modelling sea level rise impacts on storm surges along US coasts. *Environmental Research Letters*, *7*(1), 014032.

Teh, Y. A., Mazéas, O., Atwood, A. R., Abel, T., & Rhew, R. C. (2009). Hydrologic regulation of gross methyl chloride and methyl bromide uptake from Alaskan Arctic tundra. *Global Change Biology*, *15*(2), 330–345.

Teh, Y. A., Rhew, R. C., Atwood, A., & Abel, T. (2008). Water, temperature, and vegetation regulation of methyl chloride and methyl bromide fluxes from a shortgrass steppe ecosystem. *Global Change Biology*, *14*(1), 77–91.

Van Schijndel, J. W. P. M., Barnett, P., Roelse, J., Vollenbroek, E. G. M., & Wever, R. (1994). The stability and steady-state kinetics of vanadium chloroperoxidase from the fungus *Curvularia Inaequalis*. *European Journal of Biochemistry*, *225*(1), 151–157.

Varner, R. K., Crill, P. M., & Talbot, R. W. (1999). Wetlands: A potentially significant source of atmospheric methyl bromide and methyl chloride. *Geophysical Research Letters*, *26*(16), 2433–2435.

Varner, R. K., White, M. L., Mosedale, C. H., & Crill, P. M. (2003). Production of methyl bromide in a temperate forest soil. *Geophysical Research Letters*, *30*(10).

Velders, G. J. M., Andersen, S. O., Daniel, J. S., Fahey, D. W., & McFarland, M. (2007). The importance of the Montreal Protocol in protecting climate. *Proceedings of the National Academy of Sciences*, *104*(12), 4814–4819.

Vollmer, M. K., Mühle, J., Henne, S., Young, D., Rigby, M., Mitrevski, B., Park, S., Lunder, C. R., Rhee, T. S., Harth, C. M., Hill, M., Langenfelds, R. L., Guillevic, M., Schlauri, P. M., Hermansen, O., Arduini, J., Wang, R. H. J., Salameh, P. K., Maione, M., … Steele, L. P. (2021). Unexpected nascent atmospheric emissions of three ozone-depleting hydrochlorofluorocarbons. *Proceedings of the National Academy of Sciences*, *118*(5).

Wagner, C., El Omari, M., & König, G. M. (2009). Biohalogenation: Nature's way to synthesize halogenated metabolites. *Journal of Natural Products*, *72*(3), 540–553.

Walter, B., & Ballschmiter, K. (1992). Formation of C_1/C_2-bromo-/chloro-hydrocarbons by haloperoxidase reactions. *Fresenius' Journal of Analytical Chemistry*, *342*(10), 827–833.

Wang, J.-J., Jiao, Y., Rhew, R. C., & Chow, A. T. (2016). Haloform formation in coastal wetlands along a salinity gradient at South Carolina, United States. *Environmental Chemistry*, *13*(4), 745–756.

Warwick, N. J., Pyle, J. A., & Shallcross, D. E. (2006). Global modelling of the atmospheric methyl bromide budget. *Journal of Atmospheric Chemistry*, *54*(2), 133–159.

Watling, R., & Harper, D. B. (1998). Chloromethane production by wood-rotting fungi and an estimate of the global flux to the atmosphere. *Mycological Research*, *102*(7), 769–787.

Weigold, P., El-Hadidi, M., Ruecker, A., Huson, D. H., Scholten, T., Jochmann, M., Kappler, A., & Behrens, S. (2016). A metagenomic-based survey of microbial (de)halogenation potential in a German forest soil. *Scientific Reports*, *6*, srep28958.

Weinberg, I., Bahlmann, E., Eckhardt, T., Michaelis, W., & Seifert, R. (2015). A halocarbon survey from a seagrass dominated subtropical lagoon, Ria Formosa (Portugal): Flux pattern and isotopic composition. *Biogeosciences*, *12*(6), 1697–1711.

Westerling, A. L., Hidalgo, H. G., Cayan, D. R., & Swetnam, T. W. (2006). Warming and earlier spring increase Western U.S. forest wildfire activity. *Science*, *313*(5789), 940–943.

Wishkerman, A., Gebhardt, S., McRoberts, C. W., Hamilton, J. T. G., Williams, J., & Keppler, F. (2008). Abiotic methyl bromide formation from vegetation, and its strong dependence on temperature. *Environmental Science & Technology*, *42*(18), 6837–6842.

Worton, D. R., Sturges, W. T., Schwander, J., Mulvaney, R., Barnola, J.-M., & Chappellaz, J. (2006). 20th century trends and budget implications of chloroform and related tri- and dihalomethanes inferred from firn air. *Atmospheric Chemistry and Physics*, *6*(10), 2847–2863.

Wright, G. C., Smith, C. J., & Woodroofe, M. R. (1988). The effect of irrigation and nitrogen fertilizer on rapeseed (*Brassica napes*) production in South-Eastern Australia. *Irrigation Science*, *9*(1), 1–13.

Wuosmaa, A. M., & Hager, L. P. (1990). Methyl chloride transferase: A carbocation route for biosynthesis of halometabolites. *Science*, *249*(4965), 160–162.

Xiao, X., Prinn, R. G., Fraser, P. J., Simmonds, P. G., Weiss, R. F., O'Doherty, S., Miller, B. R., Salameh, P. K., Harth, C. M., Krummel, P. B., Porter, L. W., Mühle, J., Greally, B. R., Cunnold, D., Wang, R., Montzka, S. A., Elkins, J. W., Dutton, G. S., Thompson, T. M., … Yokouchi, Y. (2010). Optimal estimation of the surface fluxes of methyl chloride using a 3-D global chemical transport model. *Atmospheric Chemistry and Physics*, *10*(12), 5515–5533.

Yang, E.-S., Cunnold, D. M., Newchurch, M. J., Salawitch, R. J., McCormick, M. P., Russell, J. M., Zawodny, J. M., & Oltmans, S. J. (2008). First stage of Antarctic ozone recovery. *Journal of Geophysical Research: Atmospheres*, *113*(D20).

Yang, L., Seshan, K., & Li, Y. (2017). A review on thermal chemical reactions of lignin model compounds. *Catalysis Today*, *298*, 276–297.

Yang, Q., Guo, Y., E, Y., Zhang, S., Blatchley, E. R., & Li, J. (2020). Methyl chloride produced during UV_{254} irradiation of saline water. *Journal of Hazardous Materials*, *384*, 121263.

Yokouchi, Y., Ikeda, M., Inuzuka, Y., & Yukawa, T. (2002). Strong emission of methyl chloride from tropical plants. *Nature*, 416(6877), 163-165.

Yokouchi, Y., Noijiri, Y., Barrie, L. A., Toom-Sauntry, D., Machida, T., Inuzuka, Y., Akimoto, H., Li, H.-J., Fujinuma, Y., & Aoki, S. (2000). A strong source of methyl chloride to the atmosphere from tropical coastal land. *Nature*, *403*(6767), 295–298.

Yokouchi, Y., Nojiri, Y., Barrie, L. A., Toom-Sauntry, D., & Fujinuma, Y. (2001). Atmospheric methyl iodide: High correlation with surface seawater temperature and its implications on the sea-to-air flux. *Journal of Geophysical Research: Atmospheres*, *106*(D12), 12661–12668.

Yokouchi, Y., Saito, T., Ishigaki, C., & Aramoto, M. (2007). Identification of methyl chloride-emitting plants and atmospheric measurements on a subtropical island. *Chemosphere*, *69*(4), 549–553.

Yoshida, Y., Wang, Y., Zeng, T., & Yantosca, R. (2004). A three-dimensional global model study of atmospheric methyl chloride budget and distributions. *Journal of Geophysical Research: Atmospheres*, *109*(D24).

Zazo, J. A., Casas, J. A., Mohedano, A. F., Gilarranz, M. A., & Rodríguez, J. J. (2005). Chemical pathway and kinetics of phenol oxidation by Fenton's reagent. *Environmental Science & Technology*, *39*(23), 9295–9302.

Zhang, J., Wuebbles, D. J., Kinnison, D. E., & Saiz-Lopez, A. (2020). Revising the ozone depletion potentials metric for short-lived chemicals such as CF_3I and CH_3I. *Journal of Geophysical Research: Atmospheres*, *125*(9), e2020JD032414.

Zhang, W., Jiao, Y., Zhu, R., & Rhew, R. C. (2020). Methyl chloride and methyl bromide production and consumption in coastal Antarctic tundra soils subject to sea animal activities. *Environmental Science & Technology*, *54*(20), 13354–13363.

Zhang, Y., Del Vecchio, R., & Blough, N. V. (2012). Investigating the mechanism of hydrogen peroxide photoproduction by humic substances. *Environmental Science & Technology*, *46*(21), 11836–11843.

Ziska, F., Quack, B., Abrahamsson, K., Archer, S. D., Atlas, E., Bell, T., Butler, J. H., Carpenter, L. J., Jones, C. E., Harris, N. R. P., Hepach, H., Heumann, K. G., Hughes, C., Kuss, J., Krüger, K., Liss, P., Moore, R. M., Orlikowska, A., Raimund, S., … Yokouchi, Y. (2013). Global sea-to-air flux climatology for bromoform, dibromomethane and methyl iodide. *Atmospheric Chemistry and Physics*, *13*(17), 8915–8934.

Zlamal, J. E., Raab, T. K., Little, M., Edwards, R. A., & Lipson, D. A. (2017). Biological chlorine cycling in the Arctic Coastal Plain. *Biogeochemistry*, *134*(3), 243–260.